TAMPERE UNIVERSITY OF TECHNOLOGY

Ásgeir Bjarnason

Development of Implantable Pulse Oxygen Saturation Meter for Dairy-Cattle Respiratory Monitoring

Master of Science Thesis

Examiners: Professor Jari Hyttinen
and Timo Vuorela, D.Sc. (Eng.)
Examiners and topic approved in the
Science and Environmental Engineering
Faculty Council meeting
on 09.11.2011

ABSTRACT

TAMPERE UNIVERSITY OF TECHNOLOGY
Master's Degree Programme in Biomedical Engineering
BJARNASON , ÁSGEIR : Development of Implantable Pulse Oxygen Saturation Meter for Dairy-Cattle Respiratory Monitoring
Master of Science Thesis, 82 pages, 4 Appendix pages
January 2012
Major: Medical Instrumentation
Examiners: Professor Jari Hyttinen, D.Sc. Timo Vuorela
Keywords: Pulse Oximetry, Implantable Medical Device, Biocompatability

This master of science thesis introduces an implantable measurement device that can be used to measure oxygen saturation (SpO_2) with pulse oximetry methods. The device is intended to be incorporated into a implantable measurement device developed earlier at Tampere University of Technology (TUT). Two prototype devices were built and tested externally on a human subject with number of different measurement setups to determine how it would function *in vivo*.

Respiratory diseases are the cause of approximately 50 % of all mortality in cattle. They can be hard to diagnose in early stages since there are no obvious external symptoms, this can cause outbreaks in groups of cattle. SpO_2 gives a good measurement on how the respiratory system is functioning in the cattle by measuring the amount of oxygenated hemoglobin versus deoxygenated hemoglobin.

The developed device measures the SpO_2 with a probe made out of two light emitting diodes (LED) and a photosensor. In the thesis two types of coating methods where used to seal the probe, 3.5mm layer of medical grade epoxy and 15 μm layer of Parylene-C. The effect of these coatings on the probe components and signals where determined with measurements prior to coating and after. Parylene-C coating had much less effect on the signal acquisition than the epoxy coating, where the amplitude of the non-pulsatile signal increased on average over 1V and the pulsatile part decreased in amplitude. For Parylene-C there was a minor decrease in the amplitude of the non-pulsatile part but the pulsatile part had similar amplitude to non-coated probe. This difference is partially explained with the fact that thicker layer of coating creates internal scattering of light inside the coating. This light hits the photosensor before being absorbed by tissue and thus increases the DC level.

A signal processing script was written in MATLAB to calculate the uncalibrated SpO_2 from the raw signal. The noise level in all measurements was estimated with the standard deviation since the signal is unambigous and it was concluded that with a moving average filter of 4- or 8-points it is possible to reduce the noise significantly.

Thermal radiation of the probe was estimated with test measurement of two different LED drive currents and theoretical calculations, neither case showed any

significant increase in temperature. The effect of fat tissue that will surround the implant was also tested in a practical way with cow fat from a local supermarket. According to theory, light penetrates well through fat tissue and this was confirmed with measurements where the increased thickness of fat tissue decreased the amplitude of the signal. By applying a 8-point moving average filter it was possible to acquire a signal through ∼1cm thick layer of tissue with no perfusion. Number of other minor topics were solved some theoretically and others practically.

The output of the thesis is a novel device that could be easily implanted in a dairy-cow as well as other mammals. The thesis also presents new information on the effects of coating SpO_2 probes and the effects of fat tissue in cattle on the SpO_2 signal. Pulse oxygen saturation measurements have not been conducted with an implantable meter before in any type of animal and thus certain uncertainty of measurements can only be eliminated with an implantation of a real device.

PREFACE

The work presented in this thesis has been carried out in the Department of Biomedical Engineering at Tampere University of Technology (TUT), between May 2011 and December 2011. The initial idea of the project comes from the author and is based on earlier work that he conducted for the Icelandic based instrumentation company Star-Oddi in the summer of 2009.

This project is meant as an un-official expansion to the Removel project, that is funded by Agrifood Research of Finland (MTT). Removel focuses on presenting new welfare technologies for remote monitoring of animal welfare the author has been working in that project as a research assistant during the writing of this thesis.

There are number of people that I would like to thank for making this thesis possible. I would like to thank my supervisors, first Professor Jari Hyttinen for good guidance and allowing my the freedom I had when conducting this thesis. Secondly Dr. Timo Vuorela for great feedback and help several times in the process of the thesis. Another person is Raimo Peurakoski for good ideas and help in the probe manufacturing. I would also like to thank Jarno Riistama and Juha Väisänen for giving me the initial opportunity to work in the Removel project.

Sigmar Guðbjörnsson and Hákon Guðmundsson at Star-Oddi that initially hired my to work on implantable measurement devices and had the first idea for this thesis topic though it was meant for other application, thank you for your motivation and help through the years.

Last but not least I would like to thank my family in Iceland and my dear girlfriend Paula that always gives good support.

Tampere, December 14th, 2011

Ásgeir Bjarnason

CONTENTS

1 Introduction **1**
1.1 Implantable oxygen saturation meter 1
1.2 Problem statement 2

2 Background **4**
2.1 Theory of oxygen saturation measurements 4
2.1.1 Skin and tissue properties 10
2.1.2 Photoplethysmograph 11
2.1.3 Reflectance pulse oximetry 14
2.2 History of pulse oxygen saturation meters 16
2.2.1 Animal meters 17
2.2.2 Implantable meters 18
2.3 Noise and errors in oximetry measurements 20
2.4 Oxygen saturation meters in cattle monitoring 23
2.4.1 Diagnostic purpose 25
2.4.2 Placement of meter in tissue 26
2.5 Coating materials 29
2.6 Signal processing of oxygen saturation signals 30
2.6.1 Analog to digital conversion 31
2.6.2 Filtering 31
2.6.3 SpO_2 calculation 32
2.7 Power consumption 34

3 Methods **37**
3.1 Device : design and components selection 37
3.1.1 Transimpedance amplifier 38
3.1.2 Filters 39
3.1.3 AGC and switching circuit 39
3.2 Probe design 41
3.2.1 Coating process 42
3.2.2 Temperature effect 44
3.3 Signal processing implementation 45
3.4 Experimental testing of the device 47

4 Results **50**
4.1 Measurement system 50
4.2 Measurement of the thermal radiation of probe and coating 54

4.3 Measurement of the effect of coating on the probe 56
4.3.1 Epoxy coating 56
4.3.2 Parylene-C coating 59
4.4 Measurement of the effect of cattle fat tissue 60

5 Discussion **65**
5.1 Measurement system 65
5.2 Interpretation of measurement result 66
5.2.1 Measurement of the thermal radiation of the probe 66
5.2.2 Measurement of the effect of coating on the probe 67
5.2.3 Measurement of the effect of cattle fat tissue 68
5.3 Future considerations 68
5.3.1 Future developments and improvements 69
5.3.2 Future impact 70

6 Conclusion **72**

References **74**

A Appendix: MATLAB code **83**

B Appendix: Schematics of the Device **86**

ABBREVIATIONS AND NOTATIONS

c	Concentration of substance
d	Optical path length through the medium
δ	Penetration depth
$\varepsilon(\lambda)$	Extinction coefficient
$\varepsilon_{HbO_2}(\lambda)$	Extinction coefficient of HbO_2
$\varepsilon_{Hb}(\lambda)$	Extinction coefficient of Hb
f_s	Sampling frequency
H_e	Surface radiant exposure
I_0	Incident light intensity
I	Transmitted light intensity
λ	Wavelength
$mSpO_2$	Mean oxygen saturation
μ_a	Absorption coefficient
P_O	Radiant flux
PO_2	Partial pressure of oxygen
R	Relative absorbance between wavelengths
R_{OS}	Ratio-of-ratios
SaO_2	Arterial oxygen saturation
σ	Standard deviation
SpO_2	Oxygen saturation as measured by the pulse oximeter; usually measured in percent
SvO_2	Mixed venous oxygen saturation
V_f	Forward voltage
AC	Alternating Current
ADC	Analog-to-Digital converter
AGC	Automatic-Gain-Control
bpm	Beats-Per-Minute
BRD	Bovine Respiratory Disease
BRSV	Bovine Respiratory Syncytial Virus
DC	Direct Current
DSP	Digital-Signal-Processor
ECG	Electrocardiograph
FDA	Food and Drug Administration
FOM	Figure of Merit

Hb	Deoxyhemoglobin, functional hemoglobin unbound to oxygen
HbCO	Carboxyhemoglobin
HbO_2	Oxyhemoglobin, oxygenated hemoglobin
Hi	Methemoglobin
HR	Heart Rate
IR	Infra-Red
LED	Light Emitting Diode
LSB	Least Significant Bit
MCU	Microcontroller Unit
PCB	Printed Circuit Board
POM	Polyoxymethylene
PPG	Photoplethysmograph
PSD	Power Spectral Density
PWM	Pulse-Width-Modulation
RMS	Root Mean Square
RMSD	Root Mean Square Difference
SMT	Surface Mount Technology
SNR	Signal-to-Noise Ratio
T	Transmittance
TUT	Tampere University of Technology

1. INTRODUCTION

Animal welfare has become a growing issue in the recent years. We can categorize the role of the animals in our environment in a number of different ways such as animals used for food production, animals used for toxicology studies, as pets and for sports. With the growing number of earth population it is important that we keep the animals healthy, thus maximizing their food production and reducing their death ratio caused by lack of welfare.

This thesis aims to develop an oxygen saturation (SpO_2) meter that can be easily integrated into the implantable measurement device monitoring well-being of dairy-cattle. Current device developed prior to this thesis at Tampere University of Technology (TUT) records temperature, single-channel electrocardiograph (ECG) and activity of the animal with accelerometers [1]. The current device is built on existing knowledge from number of previous implants that where mainly focused on recording the ECG [2, 3].

The oxygen saturation meter will employ a technique called *pulse oximetry* that is a standard non-invasive external monitoring method used in number of human clinical applications as well as in some veterinarian applications [4]. The oxygen saturation gives a good measure of how the respiratory system of the dairy-cow is functioning. This can help in early detection of Bovine respiratory diseases (BRD) that are a major health problem in cattle worldwide and the most common cause of mortality in dairy-cattle [5]. The detection of Bovine respiratory diseases is very hard at early stages but important since they can be easily transmitted between cattle [6]. The method is a novel approach to that problem since first, there is no kind of continuous measurement device existing for respiratory monitoring of dairy-cattle. And second, there is no implantable oxygen saturation meter existing as a commercial product and very little research exists about such a device.

1.1 Implantable oxygen saturation meter

The standard commercial pulse oximeter uses a pair of light emitting diodes (LED), one red (wavelength ($\lambda \approx 660nm$)) and one Infra-Red (IR) ($\lambda \approx 940nm$). The diode pair is located so that it emits light through a reasonable thin tissue which has good perfusion underneath. A photodiode is placed opposite to the light emitters. The absorption of the wavelengths differs, since oxygenated hemoglobin (HbO_2) absorbs

more IR light than red light and the deoxygenated hemoglobin (Hb) absorbs more red light than IR light. The oxygen saturation can then be calculated by utilizing the ratio of those two wavelengths, RED/IR, and comparing that value to calibrated values or empirical tables [7].

The oxygen saturation meter presented in this thesis uses the reflection of the light. Reflectance pulse oximetry has been initially described by Brinkman and Zijlstra in 1949 [8] and later implemented by Zijlstra and Mook in 1962 [9]. Further developments where made by A.Cohen and N.Wadsworth in 1972 [10]. Its main purpose was to increase the ease of placing or acquiring oxygen saturation measurement from subject since earlier meters where restricted to either through tissue, such as finger or ear lobe, or reflection from the blood stream using intra venous fibre optic catheter [11, 12]. With reflectance oxygen saturation measurement it is possible to acquire signal from almost any place on the skin surface as long as there is some perfusion.

In this thesis the reflectance oximeter is taken one step further by implanting it under the skin of the dairy-cattle. This thesis will present the theory behind measurements of SpO_2 as as well as discussion on how most noise factors effecting the external pulse oxygen saturation signal such as motion artifacts, ambient light, skin pigmentation and skin thickness and hairs of cattle will effect the implantable signal. Implantable pulse oximeters have not been tested clinically apart from a pacemaker developed by Medtronics that used the principles of pulse oxygen saturation measurement to measure the mixed venous oxygen saturation (SvO_2) from a lead placed in the right ventricular apex of a human subjects [13]. Two publications from 2008, one journal paper [14] and one conference paper [15], also propose implantable oxygen saturation measurements for human measurements.

1.2 Problem statement

There are number of problems that have to be faced when developing a successful implantable pulse oximeter, some of them can be solved before implantation but some of them will only be concluded *in vivo*. This thesis works on a solution to a number of problems, the main focus was set on problems that have little or no publications such as the biocompatability of the probe that includes the LEDs and the photosensor, due to tissue response electronic devices have to be sealed or coated before implantation. Another biocompatability problem is how the implants thermal radiation effects the tissue. There are very limited number of publications about this topic, specially about the coating effect on the photosensor. Another problem faced is the place of implantation and how different tissues effect the signal acquisition specially fat tissue that will surround the implant.

The main focus of the thesis is still to design a prototype device that can mea-

sure the SpO_2 and can be incorporated in the well-being monitoring device. This creates a number of problems by itself since the device has to be able to measure ideally for months so the power consumption is an important factor, the device also has to have few components since size is a real issue. It should be able to adapt the brightness of the LEDs depending on the tissue surrounding it, since the mammalian tissue is not uniform. Then there are number of problems regarding the noise effecting the measurements and how it is possible to filter the signal to enhance the quality. Grosenbough *et al.* concluded that SpO_2 meters designed for human measurements and that utilize signal processing algorithms designed for human SpO_2 signals, should be compatible to cattle monitoring [16] and thus we base our technology on human meter design.

All of these topics mentioned will be discussed in the thesis and a full practical solution presented to some of them. Other topics are reasoned and a partially solved which gives space for future improvements of the device.

2. BACKGROUND

This chapter reviews the basic principals needed to conduct SpO_2 measurements in all relevant applications. The aim of this chapter is to give the reader a broad understanding of the different topics this thesis covers.

The structure of this background chapter is the following: Section 2.1 gives a brief theoretical background on the physical properties of oxygen saturation measurements, it covers the skin and tissue properties as well as theoretical measurement principals. Section 2.2 makes a brief history review of oximeters both for human and animal measurements as well as implantable meters. Section 2.3 discusses the noise factors affecting external SpO_2 measurements as well as expected noise in implantable SpO_2 measurements. Section 2.4 discusses the purpose of measuring oxygen saturation in dairy-cattle as well as different issues with measuring oxygen saturation *in vivo* and externally in dairy-cattle. Then there are sections that give background information on some of the challenging technological issues that are faced in this thesis. Those are coating materials of the implant in Section 2.5, signal processing methods for the SpO_2 signal, in Section 2.6 and power consumption of the implantable meter in Section 2.7.

2.1 Theory of oxygen saturation measurements

The mammalian body does not function without oxygen. Oxygen delivery to cells is a combined process of the respiratory system and the circulatory system. In this process the respiratory system takes care of the ventilation and gas exchange that occurs in the lungs. In the lungs oxygen is diffused into the blood in exchange of carbon dioxide that is created as a by-product from the mitochondria, also known as cellular respiration [17]. Ventilation is the process of moving air in and out of the lungs. It has both involuntary components and voluntary components. The involuntary control is controlled by the respiratory centers in the medulla oblongata and pons that excite motor neurons that cause movement of respiratory muscles. The motor neurons are generally controlled by this involuntary respiratory reflex but it can also be controlled voluntary through commands delivered by the corticospinal pathway [17]. The gas exchange that occurs in the lungs is driven by diffusion. Diffusion is defined as the distribution process of atoms or molecules from an area of higher concentration to an area of lower concentration [17]. The diffusion takes place

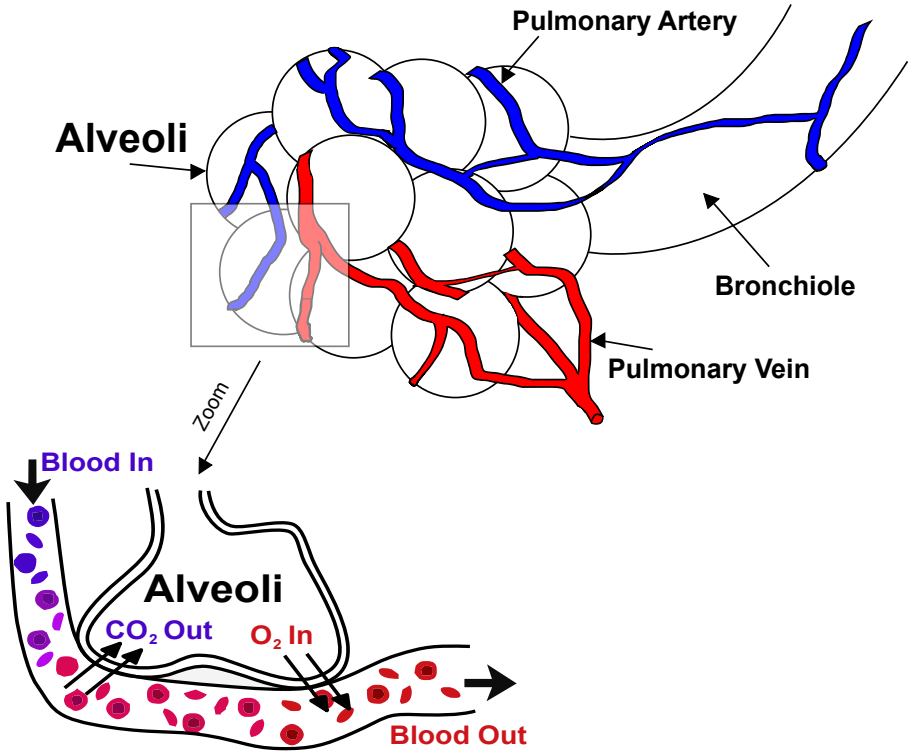

Figure 2.1: *Alveoli structure shown as multiple beads and in detail how the gas exchange occurs in a single alveoli. Figure is adapted from [18, 19].*

in the alveoli of the lungs which are small beds in the end of the bronchi structure of the lungs surrounded by a capillary network, see Figure 2.1 for clarification.

The blood of the mammalian body is composed mostly of water and thus gas is not particularly soluble. As an example, for every 100 mL of blood that leaves the alveolar capillaries roughly 20 mL is oxygen. Of that amount only about 0.3 mL are oxygen molecules in the solution [17]. The rest of the oxygen is bound to hemoglobin (Hb) molecules that account for more then 95 percent of the intracellular protein structure of red blood cells. The structure of a single hemoglobin is complex but can be described with consisting of four heme units and four globin units. Heme being a non-protein pigment that contains iron and is able to interact with oxygen molecules and then globin being a polypetide chain. Each heme and globin unit can carry one molecule of oxygen forming oxyhemoglobin (HbO_2). Furthermore hemoglobin molecule whose iron is unbound is called deoxyhemoglobin (Hb). Figure 2.2 shows a simplified structure of hemoglobin where the heme and globin units are simply shown as a uniform medium able to bind to four oxygen molecules. One red blood cell contains about 280 million Hb molecules, meaning that each red blood cell can carry over a billion oxygen molecules [17, 20].

Pulse oximetry measures only the group known as functional hemoglobins which is

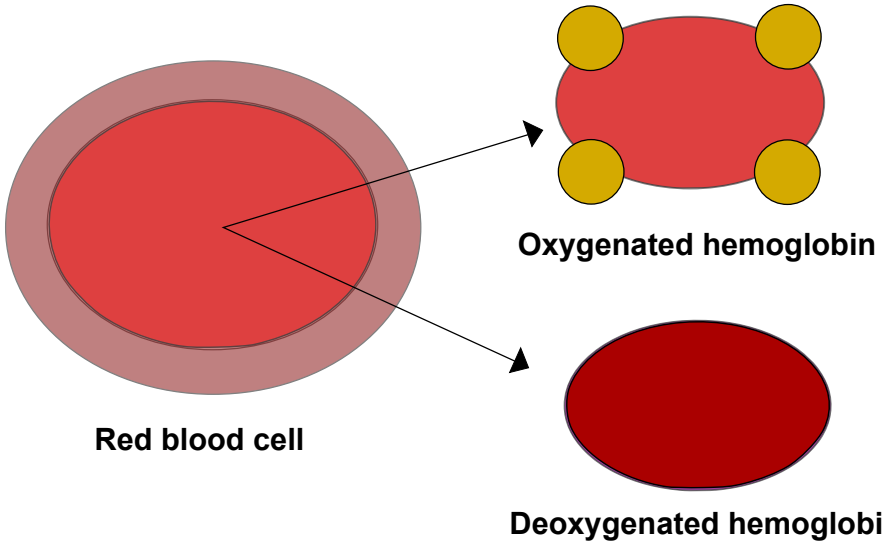

Figure 2.2: *Simplified figure of oxygenated and deoxygenated hemoglobin as part of a red blood cell. Adapted from [20].*

the hemoglobin that is able to bind reversibly with molecular oxygen. Dysfunctional hemoglobins are hemoglobins that are either not able to bind reversibly to oxygen or they distrupt the normal function of oxyhemoglobins. The four most common dysfunctional hemoglobins are methemoglobin (Hi), carboxyhemoglobin (HbCO), sulfhemoglobin and carboxysulfurhemoglobin [21].

Deoxygenated Hb molecule is dark red while HbO_2 is bright red. This color change enables measuring the hemoglobin oxygen saturation with pulse oximetry by utilizing a releationship between the absorption of red and IR light in the blood [20].

Beer's law also known as Beer-Lambert's law presented in equation (2.1) describes absorption of a single wavelength through a uniform tissue as a measure of intensity of light [21].

$$I = I_0 e^{-\varepsilon(\lambda)cd} \tag{2.1}$$

In the equation (2.1), I is the transmitted light, I_0 is the incident light, $\varepsilon(\lambda)$ is the extinction coefficient or the absorptivity at a given wavelength of the absorbing substance (measured in $L \cdot mmol^{-1} \cdot cm^{-1}$), c is the concentration of the substance and d is the optical path length through the medium. Beer's law does not account for reflection of light at the surface or scattering inside the medium nor any photochemical reactions or reaction between absorbent and solvent.

From Beer's law it is possible to define the transmittance T of a light travelling

through a medium, see equation (2.2) and the unscattered absorbance (A) of that process, see equation (2.3) [21].

$$T = \frac{I}{I_0} = e^{-\varepsilon(\lambda)cd} \tag{2.2}$$

$$A = -ln(T) = \varepsilon(\lambda)cd \tag{2.3}$$

Then expanding the unscattered absorbance quantity to count for more then one substance in the medium by superposition of the individual absorbing processes. This is defined as total absorbance (A_t).

$$A_t = \varepsilon_1(\lambda)c_1d_1 + \varepsilon_2(\lambda)c_2d_2 + ... + \varepsilon_n(\lambda)c_nd_n = \sum_{i=1}^{n} \varepsilon_i(\lambda)c_id_i \tag{2.4}$$

Where $\varepsilon_i(\lambda)$ and c_i represent the extinction coefficient and concentration of the substance i, d_i represents the optical path through that substance. It may differ from substance to substance in the medium.

We apply this principle to the blood, making the assumption that majority of the hemoglobin is Hb and HbO_2 and that the optical path length is the same for Hb and HbO_2 see equation (2.5) [21].

$$A_t = [\varepsilon_{HbO_2}(\lambda)c_{HbO_2} + \varepsilon_{Hb}(\lambda)c_{Hb}]d \tag{2.5}$$

Where $\varepsilon_{HbO_2}(\lambda)$ and $\varepsilon_{Hb}(\lambda)$ are the extinction coefficients , c_{HbO_2} and c_{Hb} the concentrations and d the optical path length for Hb and HbO_2. Zijlstra *et al.* measured the extinction coefficient of Hb and HbO_2, for the wavelength from 450nm to 1000nm in humans, Table 2.1 shows the extinction coefficients for the wavelengths $660nm$ and $880nm$ that are the wavelengths of the LEDs used in our device [22]. The choice of the wavelengths will be justified in Section 3.2. The extinction coefficients can be visualized as a function of wavelength as shown in Figure 2.3, the isobestic point marked on the figure represents the point where $\varepsilon_{HbO_2}(\lambda)$ and $\varepsilon_{Hb}(\lambda)$ are equal [23].

Table 2.1: *Extinction coefficients for Hb and HbO_2 for the specific wavelengths $660nm$ and $880nm$ [22].*

λ	$\varepsilon_{Hb}(\lambda)$	$\varepsilon_{HbO_2}(\lambda)$
660	0.81	0.08
880	0.20	0.29

The functional arterial oxygen saturation can be shown as functional hemoglobin saturation. It is common to ignore the effect of dysfunctional hemoglobins since their amount is only around 2 % of the total amount of hemoglobins [16]. It is

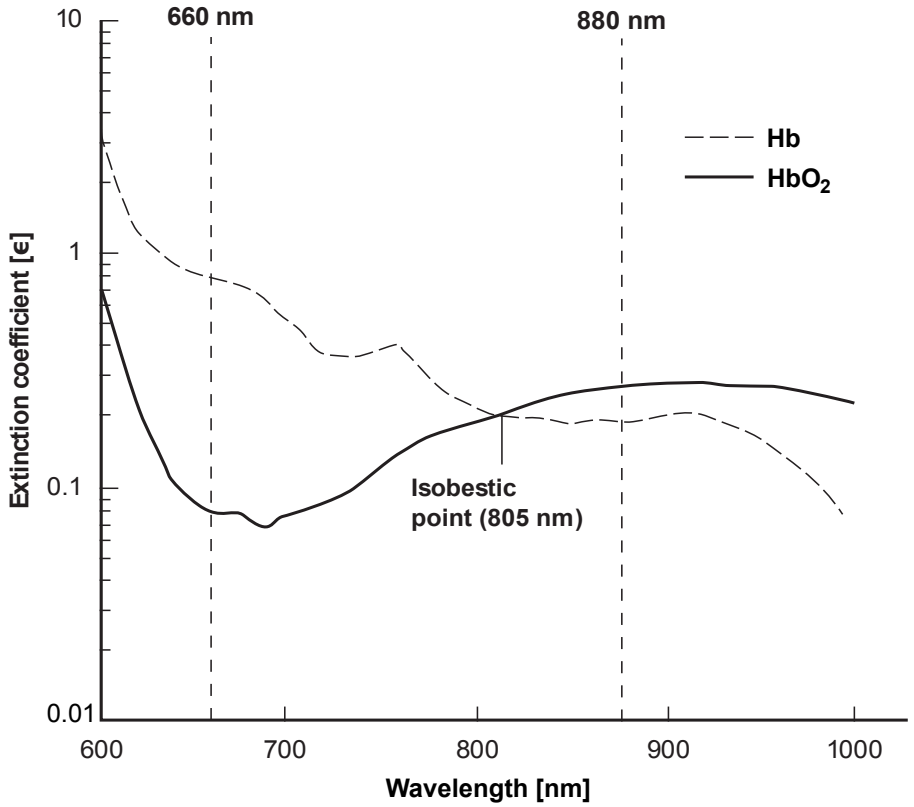

Figure 2.3: *Extinction coefficients of Hb and HbO_2 at wavelengths from 600nm to 1000nm with wavelengths 660nm and 880nm highlighted. Figure is adapted from [7].*

possible to include the effect of dysfunctional hemoglobins with meters that utilize multiple wavelengths and then we refer to fractional oxygen saturation. In this thesis the term oxygen saturation (SpO_2) is used when referring to the functional arterial oxygen saturation as measured by the pulse oximeter defined with equation 2.6 [24, 21].

$$SpO_2 = \frac{HbO_2}{Hb + HbO_2} \cdot 100\% = \frac{c_{HbO_2}}{c_{HbO_2} + c_{Hb}} \cdot 100\% \tag{2.6}$$

The oxygen saturation of arterial blood is usually around 95-98% where the oxygen saturation of venous blood is usually 60-80% [25]. The oxygen saturation in venous blood is referred to as mixed venous oxygen saturation (SvO_2). It gives a measure of the saturation in pulmonary arteries after venous effluents have been mixed and they return to the left ventricle. The biggest difference between SpO_2 and SvO_2 is the pulsation of SpO_2, as well as the factor that SvO_2 represents the amount of oxygen that can be utilized in periods of increased demands. There is an interesting relationship between SpO_2 and partial pressure of oxygen (PO_2) in blood as seen in Figure 2.4. The curve like shape of the figure is caused by increased affin-

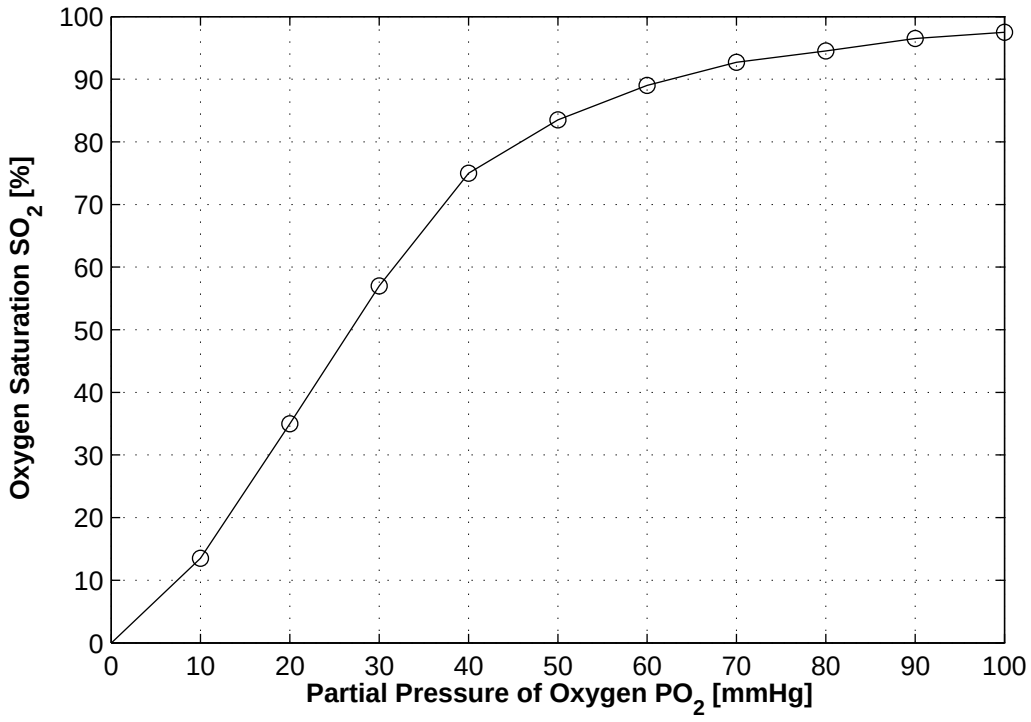

Figure 2.4: *Oxygen saturation of hemoglobin in human blood as a function of partial pressure of oxygen. Determined under normal conditions, with pH of 7.4 and tempereature of* 37^oC*. Figure is created from data presented in [17].*

ity of hemoglobin towards oxygen as it binds to more and more molecules. PO_2 in air is roughly 20.9 % of the gases in atmosphere which is approximately 159 mmHg [17].

Normal alveolar pressure is considered $PO_2 \approx 100$ mmHg, which gives a hemoglobin saturation level of 97.5 %. Complete saturation occurs at the high level of $PO_2 \approx$ 250 mmHg. Difference in PO_2 thus affects venous blood much more than arterial. Inactive tissue has $PO_2 \approx 40$ mmHg, that is about 75 % of maximum saturation. This means that tissue of a resting individual uses around 25% of available oxygen, leaving the rest as a reserve. It is obvious from Figure 2.4 that small changes in venous blood and thus lower level of PO_2 induce large changes in the oxygen saturation, indicating any respiratory problems that reduce the oxygen saturation and the PO_2. The regulation mechanism of the body for oxygen transport in arterial and venous blood is quite complex and is out of the scope of this thesis, but it should be noted that temperature and pH value of the blood as well as age of the mammal affects the saturation-pressure curve [17].

A device called CO-oximeter measures the absorption with multiple wavelengths, to measure the part of dysfunctional hemoglobins in arterial oxygen saturation. This measurement is called arterial oxygen saturation (SaO_2) and is sometimes referred

to as the "gold standard" of the reference measurement for SpO_2 since it is slightly more accurate [24]. This measurement can also be performed with a blood gas analyser.

2.1.1 Skin and tissue properties

The properties of skin and tissue play an important role in the measurement of oxygen saturation since different layers of tissue have different amount of perfusion that directly affects the SpO_2 signal that is aquired. Equation (2.2) shows the transmittance of light through a non-turbid sample according to Beer-Lambert law, it can be represented in a different way as shown by equation (2.7).

$$T = e^{-\mu_a d} \tag{2.7}$$

Where μ_a is known as the absorption coefficient. According to Vogel and Venugopalan [26] it is typical in the biomedical optics community to use the μ_a when expressing optical absorption properties in tissue and $\varepsilon(\lambda)$ when expressing the optical absorption properties for a specific isolated biomolecule. The absorption properties of tissue for wavelengths in the visible spectra (400-780nm) are dominated by Hb, HbO_2 and Melanin that is the cause for skin pigmentation. Figure 2.5 shows the absorption coefficient as a function of wavelength from 0.1μm to 12μm. As shown in Figure 2.5, Hb has its highest absorption peak around λ = 433nm and HbO_2 around 414nm which is in the violet region. Then other peaks for HbO_2 are around λ = 542nm and 576nm and for Hb around λ = 556nm that is in the green region [26]. The reason why SpO_2 measurements are usually conducted with wavelengths in the red and IR region is that all biomolecules have very little absorption there, thus Hb and HbO_2 contribute significantly.

When scattering is absent or negligible such as in Beer-Lamberts law then it is possible to define a quantity of penetration depth (δ) as the reciprocal of the absorption coefficient as shown in equation (2.8).

$$\delta = \frac{1}{\mu_a} \tag{2.8}$$

The penetration depth is defined as the point where the transmitted light is reduced to 37 % of the incident light. This quantity is usually smaller at wavelengths that are sensitive to scattering such as visible and near IR wavelengths ($\lambda \approx$ 400nm-1200nm) [27].

Between 600nm - 1200nm there is a lack of strongly absorbing tissue chromphores. According to Welch and van Gemert collimated light in this wavelength region can penetrate several millimetres in tissue and the associated scattered light several centimetres [28]. Kim and Wilson list the fundamental optical properties for *ex vivo*

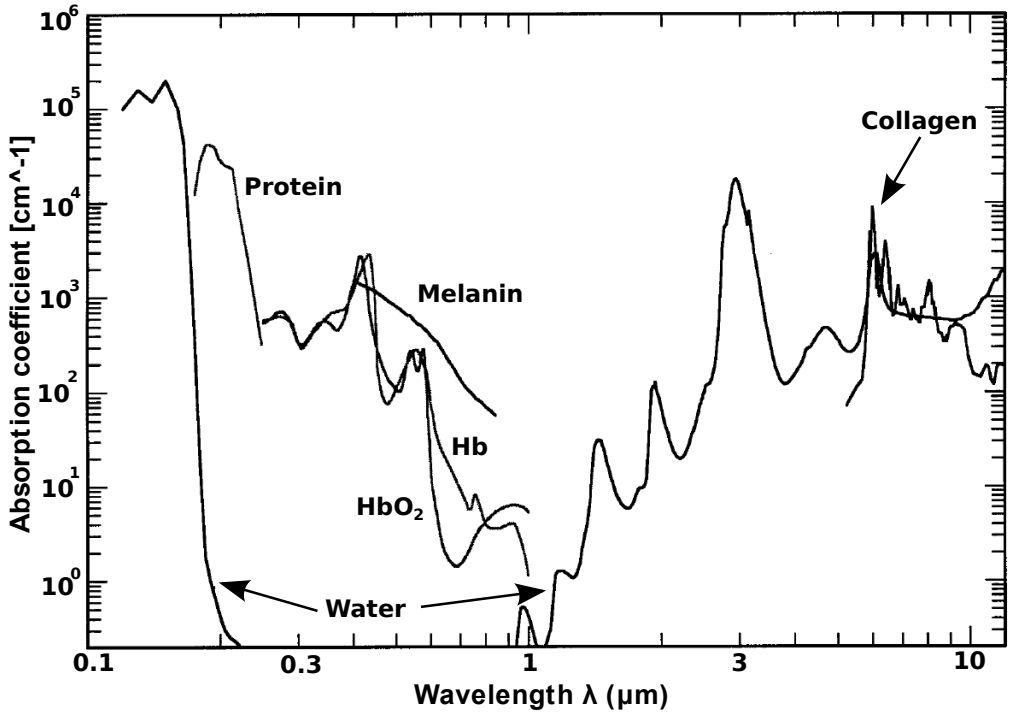

Figure 2.5: *The figure shows absorption coefficient (μ_a) of the principal tissue chromophores as a function of wavelength from 0.1 μm to 12μm. The figure is adapted from [26].*

and *in vivo* tissue measurements as μ_a, scattering coefficient (μ_s), total attenuation coefficient ($\mu_t = \mu_a + \mu_s$), scattering phase function ($p(cos\theta)$, scattering anisotropy (g), reduced scattering coefficient ($\mu'_s = \mu_s(1-g)$) and the tissue refractive index (n) [29]. In this thesis we limit the theory to the absorption coefficient and consider other parameters to be out of our scope.

2.1.2 Photoplethysmograph

The transmitted light is absorbed by different absorbing substances inside the biological tissue. The key substances are skin pigmentation, bones as well as arterial and venous blood [21]. The pulse oximeter utilizes so called arterial pulsation that can be explained with Figure 2.6, which shows how the transmitted light is absorbed by different tissues creating a non pulsatile part noted as DC and pulsatile part noted as AC part of the signal. In the cardiac cycle the arteries contain more blood in systole than in diastole, this directly influences the diameter of the veins [21]. In systole the diameter of the veins increases and larger quantity of hemoglobin increases the absorbance, on Figure 2.6 this relates to point L meaning the intensity of the light that passes through the tissue is low. In diastole the point is marked as H for the high intensity of light that passes through the tissue. This pulsating signal is called Photoplethysmograph (PPG) [30].

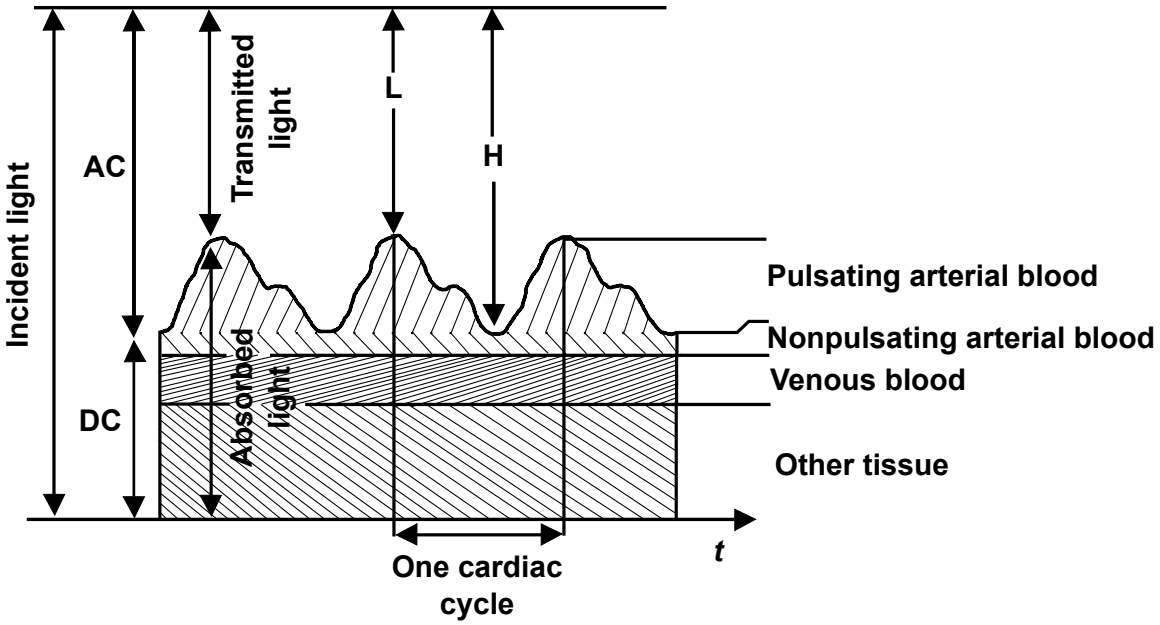

Figure 2.6: *Photoplethysmograph signal showed in an intuitive way. Incident light representing all light coming from the LEDs and striking the surface. Transmitted light being the light sensed by the photosensor that is not absorbed by tissue. Figure is adapted from [21].*

We can apply Beer's law to the transmitted light for systolic and diastolic part of the signal. When the intensity is at its maximum the arteries have a thickness of d_{min} and thickness of d_{max} when the intensity is the lowest, see equation (2.9) and equation (2.10) below:

$$I_H = I_0 \exp[-\varepsilon_{DC} c_{DC} d_{DC}] \exp[-[\varepsilon_{Hb}(\lambda) c_{Hb} + \varepsilon_{HbO_2}(\lambda) c_{HbO_2}] d_{min}] \tag{2.9}$$

$$I_L = I_0 \exp[-\varepsilon_{DC} c_{DC} d_{DC}] \exp[-[\varepsilon_{Hb}(\lambda) c_{Hb} + \varepsilon_{HbO_2}(\lambda) c_{HbO_2}] d_{max}] \tag{2.10}$$

To eliminate the DC part of the signal the equation can be simplified by taking the ratio of the two intensities and then we can make simplification on the equation by substituting Δd for the variation in thickness $d_{max} - d_{min}$ see equation (2.11).:

$$\begin{aligned} \frac{I_H}{I_L} &= \frac{I_0 \exp[-\varepsilon_{DC} c_{DC} d_{DC}] \exp[-[\varepsilon_{Hb}(\lambda) c_{Hb} + \varepsilon_{HbO_2}(\lambda) c_{HbO_2}] d_{min}]}{I_0 \exp[-\varepsilon_{DC} c_{DC} d_{DC}] \exp[-[\varepsilon_{Hb}(\lambda) c_{Hb} + \varepsilon_{HbO_2}(\lambda) c_{HbO_2}] d_{max}]} \\ &= \exp[(\varepsilon_{Hb}(\lambda) c_{Hb} + \varepsilon_{HbO_2}(\lambda) c_{Hb0_2}) \Delta d] \end{aligned} \tag{2.11}$$

The unscattered absorbance or in more detail the relative absorbance of the blood can be defined from equation (2.11) in a similar way as in equation (2.3):

$$ln\left(\frac{I_H}{I_L}\right) = +(\varepsilon_{Hb}(\lambda)c_{Hb} + \varepsilon_{HbO_2}(\lambda)c_{HbO_2})\Delta d \tag{2.12}$$

Sarpeshkar [31] states that it is possible to make the assumption that the modulated signal output from the receiving photoreceptor, i_{ac} is much smaller then the absolute level I_{DC}. Further stating that this is a good assumption in practice where the modulation depth in pulse oximetry noted as $A_{rlt-bld} \approx i_{ac}/I_{DC}$ is usually $0.5 - 2.0\%$.

Equation (2.12) then can be further simplified as:

$$\begin{aligned} ln\left(\frac{I_{DC} + \frac{i_{ac}}{2}}{I_{DC} - \frac{i_{ac}}{2}}\right) &= (\varepsilon_{Hb}(\lambda)c_{Hb} + \varepsilon_{HbO_2}(\lambda)c_{HbO_2})\Delta d \\ A_{rlt-bld} \approx \frac{i_{ac}}{I_{DC}} &= (\varepsilon_{Hb}(\lambda)c_{Hb} + \varepsilon_{HbO_2}(\lambda)c_{HbO_2})\Delta d \end{aligned} \tag{2.13}$$

In the final step we must realize that relative absorbance of the blood will differ between the red and infrared wavelengths. That is the fundamental point in pulse oximetry measurements, that is if we define the ratio (R) of relative absorbance between the wavelengths. Then these absorbances only depend on the light absorbed in the arterial blood, since the optical path lengths for the red LED and the IR LED can be considered equal:

$$\begin{aligned} R = \frac{ln(i_{H,R}/i_{L,R})}{ln(i_{H,IR}/i_{L,IR})} &\approx \frac{(i_{ac}^R/I_{DC}^R)}{i_{ac}^{IR}/I_{DC}^{IR})} \\ &= \frac{(\varepsilon_{Hb}(\lambda_R)c_{Hb} + \varepsilon_{HbO_2}(\lambda_R)c_{HbO_2})\Delta d_R}{(\varepsilon_{Hb}(\lambda_{IR})c_{Hb} + \varepsilon_{HbO_2}(\lambda_{IR})c_{HbO_2})\Delta d_{IR}} \\ &= \frac{(\varepsilon_{Hb}(\lambda_R)c_{Hb} + \varepsilon_{HbO_2}(\lambda_R)c_{HbO_2})}{(\varepsilon_{Hb}(\lambda_{IR})c_{Hb} + \varepsilon_{HbO_2}(\lambda_{IR})c_{HbO_2})} \end{aligned} \tag{2.14}$$

With some simple algebraic manipulation and the relationship introduced in equation (2.6) we can show the SpO_2 as function of R [21]:

$$SpO_2 = \frac{\varepsilon_{Hb}(\lambda_R) - \varepsilon_{Hb}(\lambda_{IR})R}{\varepsilon_{Hb}(\lambda_R) - \varepsilon_{HbO_2}(\lambda_R) + [\varepsilon_{HbO_2}(\lambda_{IR}) - \varepsilon_{Hb}(\lambda_{IR})]R} \cdot 100\% \tag{2.15}$$

Using the extinction coefficients from Table 2.1 the relationship becomes:

$$SpO_2 = \frac{0.81 - 0.20R}{0.73 + 0.09R} \tag{2.16}$$

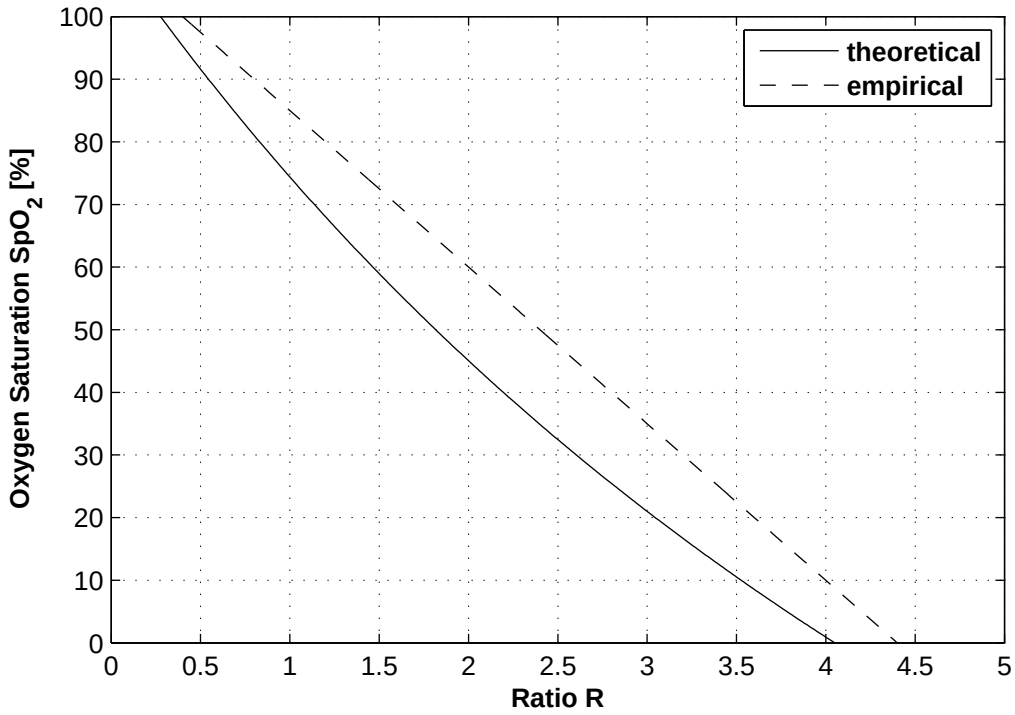

Figure 2.7: *Theoretical curve showing Beer-Lamberts law created from equation (2.16) and empirical curve as suggested by Sarpeshkar [31], created from equation (2.17).*

Sarpeshkar mentions in [31] that since Beer's law does not account for reflection of light at the surface of skin or the scattering of light inside human tissue, the ratio R can be approximated with equation (2.17).

$$SpO_2 = 110 - 25R \tag{2.17}$$

Figure 2.7 shows graphical interpretation of equation (2.16) and equation (2.17).

2.1.3 Reflectance pulse oximetry

Reflectance pulse oximetry as the name implies measures the reflected light that is scattered back from the tissue. Figure 2.8 shows the difference of through finger and reflectance oximetry probes as presented by Webster [21]. The figure is a simplified version of the process as it does not show any scattering that occurs from the tissue itself but only light that is scattered back from bone. A more accurate representation of a reflectance measurement setup is shown in Figure 2.9. Both through tissue and reflectance meters utilize the same theoretical principles but as Figure 2.8 and 2.9 suggests, differ slightly in probe structure and calibration.

As mentioned earlier Beer-Lambert law (presented earlier with equation (2.1)),

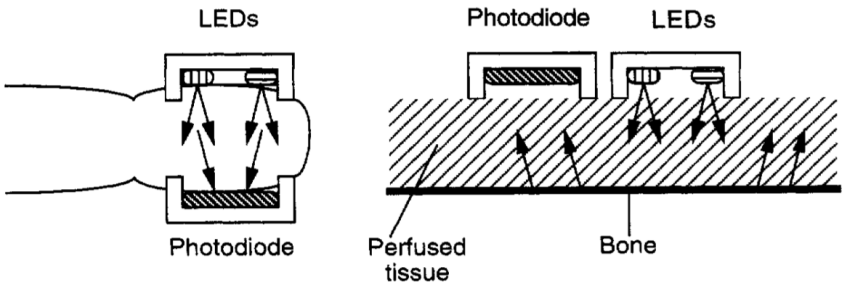

Figure 2.8: *The figure shows two pulse oximeters, the one on left side measures the absorption through finger and the one on right measures the scattering from the tissue. Figure is adapted from [21]*

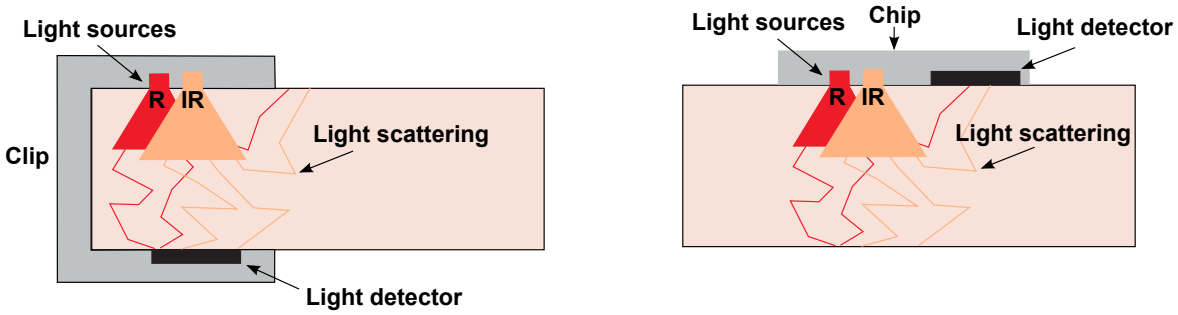

Figure 2.9: *The figure shows two meters just as Figure 2.8. The one on the left measures absorption thorough finger and the one on right measures the scattering from tissue. The figure is adapted from [32]*

does not account for any scattering inside the tissue, which is not true with whole blood [21]. Scattering occurs from objects that are similar in size as the wavelength used and red blood cells are approximately 700nm in diameter. In humans the cells also play a role since they have a diameter of 10 μm to 30 μm and many of their internal parts are in the range of 50 nm - 1000 nm, such as ribosomes, lysosomes, mitochondrion and the nucleus [17]. Yet another factor contributing to the scattering is a discontinuity in index of refraction between plasma and red blood cells. Thus light scatters multiple times inside the tissue and this increases the optical path length and thus the absorbance [33]. Steinke and Shepart showed that the relationship between oxygen saturation and the total scattering effects is approximately linear so that the accuracy of the oximeter should not be affected in a negative way [33, 21]. Marjoron and Nelson [34], presented data combined from few publications where the absorption coefficient for whole blood is presented at 100% (arterial) and 70% (venous) oxygen saturation, Table 2.2 shows this data. The table shows clearly how the penetration depth of red wavelength ($\lambda = 600$nm) is affected in a more negative way by venous blood then IR wavelength ($\lambda = 1064$).

Table 2.2: *The table shows the absorption coefficient (μ_a) and the penetration depth (δ) for two wavelengths λ=600nm and λ = 1064nm, at two saturation percentages namely 100% SpO_2 and at 70% SpO_2 [34].*

	Absorption Coefficient μ_a (mm^{-1})		Penetration depth δ (mm)	
λ (nm)	SpO_2 (100%)	SpO_2 (70%)	SpO_2 (100%)	SpO_2 (70%)
600	2.5	4.0	0.4	0.025
1064	0.5	0.22	2	4.55

Number of theoretical methods exist that describe optical properties of tissue as multiple layers with respect to light propagation, absorption and scattering. Such methods include analytics using Maxwell's equations and Monte Carlo simulations [32]. Some of the more commonly known theories are transport theory, Twersky's multiple scattering theory and Kubelka-Munk theory [21, 28]. Such theories and modelling are considered out of the scope of this thesis due to complexity and their failure to replace the empirical calibration curves for SpO_2 meters.

There are multiple interesting parameters regarding the design of reflectance pulse oximeter. Mendelson and Ochs [35] studied number of them such as spacing between LEDs and photodetector, effect of skin temperature and effect of hypoxemia. They discovered a possibility to increase the signal-to-noise ratio (SNR) with certain trait-off consisting of increasing distance between LEDs and the photodetector to acquire larger plethysmographs with the cost of higher LED driving current. Their tests where done on separation distances of 4-11 mm. For constant LED intensity, the detected light decreases exponentially with increasing distance [35].

2.2 History of pulse oxygen saturation meters

The first commercial oximeter that can be compared to the commercial pulse oximeters, was the Hewlett-Packard ear oximeter in 1970. It used a fiber optic light guide that transmitted eight different wavelength. The arterial oxygen saturation was then calculated from these eight wavelengths. The Hewlett-Packard ear oximeter utilized the Beer-Lambert law published in 1851 by August Beer as an expansion of a principle theory between the absorption of light and the amount of absorbent described by Johann Heinrich Lambert and published 1760 [36]. Takuo Aoyagi influenced greatly the transition from the Hewlett-Packard oximeter to the general commercial pulse oximeter as we know it today. First in 1971 he acknowledged the pulsatile arterial part of the PPG and used it to separate the absorption due to arteries from other tissues. And later in 1974 he developed a prototype pulse oximeter that divided the energy received into two filters centered at 650nm and 805nm the isobestic point for hemoglobin as seen in Figure 2.3. Aoyagis meter was far from perfect but it laid the foundations for the first commercially available pulse oximeter in the year 1975

[36]. As mentioned previously in Section 1.1, reflectance pulse oximetry was first described by Brinkman and Zijlstra in 1949 [8] and later implementations by Zijlstra and Mook in 1962 [9] provided the first commercial device that utilized reflectance pulse oximetry in the eighties.

2.2.1 Animal meters

Pulse oximetry has been used to some extend in animal measurements most common being external measurements of rodents such as mice and rats where a number of commercial products exist. Nellcor and Nonin the biggest producer of oxygen saturation meters, both have their veterinarian line of meters for both rodents as well as domesticated animals such as horses, cats and dogs [37, 38]. Another company SurgiVet specializes in only veterinarian meters and has a big catalog of products, both oximeters and probes [39]. Grosenbaugh *et al.* studied the absorbance spectra over the wavelength of 600nm to 1000nm, for different animals (dog, cat, horse, cow and pig) [16]. Their conclusion was that there where minor differences in the absorbance of both HbO_2 and Hb between human and different animals. However they make the statement that corrections for the presence of Hi, light scattering by impurities in the solution and technical error renderes these differences statistically insignificant. Thus pulse oximeters that are designed for human measurements and utilize signal processing algorithms designed for human PPG signals, should be compatible with the animal species they studied [16].

Starr Life Sciences Inc. introduced their first commercial meter for rodents in 2006 and today has built up a complete series of external SpO_2 meters called $MouseOX^{TM}$ [40]. Starr Life states to this date on their company homepage that they "manufactured the world's first and only patented non-invasive vital signs monitor specifically designed for small laboratory animals". The probes they offer are all through tissue available for thigh, foot, throat and collar measurements. Their meters have been used in total of 101 publications as of January 2011 in research ranging from pulmonary, respiratory and cardiovascular to pharmacology and toxicology studies. Number of other meters exist today such as the $MouseSTAT^{TM}$ from Kent Scientific [41] that offers unique through skin probes. Another meter is the *CANL-425SV-A* from Med Associates Inc. that offers both standard through skin probes as well as transreflectance sensors [42]. All the companies offer the classic Y shaped probe, Nellcor offering a miniaturized transreflectance probe as well and SurgiVet offering a reflectance probe that can also be used rectally for cats and dogs as well as a C-shaped probe specially good for the legs and tails of cats, dogs and horses since it does not deflect the angle of the photosensor. Figure 2.10a-c shows an example of Y- and C-shaped probes as well as a rectal probe.

Matthews *et al.* [44] made a comparison study published in 2003 using 5 different

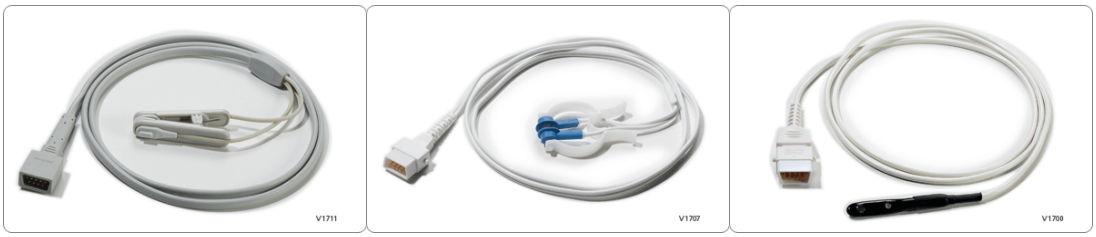

(a) *V1711* **(b)** *V1707* **(c)** *V1700*

Figure 2.10: *List of probes manufactured by SurgiVet. Probe V1711 is an example of a classic Y-shaped probe. Probe V1707 has a special C-shape that is considered specially good for measurement on cats, dogs and horses. Since it can be fitted more easily to wider diameter such as a tail or a leg without deflecting the angle of the photosensor and LEDs too much . Probe V1700 is a transreflectance probe that can also be used rectally for cats and dogs [43].*

oximeters commercially available, both meters specially designed for human measurements and meters designed for animal use. Four of them from Nellcor and one from SurgiVet. The oximeters where tested on five animals of each species (dogs, cats and horses). Five different measurement placements where used the tongue, toe, ear, lip and the prepuce or vulva depending on the gender of the animal. The animals where anaesthetized and SpO_2 was measured in parallel with a CO-oximeter. In horses the root-mean-square difference (RMSD) for all the devices was between $\pm 2 - 5\%$ and the Nellcor devices had a failure rate from 0% to 21%. The tongue and the ear produced the best signal. Big differences between meters where mostly blamed on differences in probes as well as internal detection algorithms and filters inside the measurements devices. For horses, pulse oximetry is considered a method when standard arterial blood gas analysis is not available since it is affected by perfusion deficits, location of the device, pigmented skin, and type of transducer. It can on the other hand have a great value as a rough assessment of respiratory function and to assess response to therapy [45, 46].

Two papers published in 1999 and 2000 by Uysterpruyst and Coghe *et al.* [47], [48], assessed pulse oximetry in cattle as well as the accuracy in newborn calves. These papers will be further addressed in Chapter 2.4.

2.2.2 Implantable meters

Implantable pulse oximeter does not exist on the market for animals or human. The closest thing to implantable pulse oximeter that has been developed and tested clinically is a pacemaker developed in the 90's by Medtronics Inc. model number 8007 that came with a special pacing lead numbered 4327A [13, 49]. The combination used the principles of pulse oxygen saturation to measure the SvO_2 from a lead that was placed inside the right ventricular apex with standard implantation techniques.

The oxygen sensor part was sealed inside a sapphire capsule (see Figure 2.11), 3cm from the lead tip. The sensor has two LEDs (red (660nm) and IR (880nm)), a photo-detector and an integrated circuit. A microprocessor inside the pacemakers capsule samples the SvO_2 data every 4s as the pacemaker synchronizes the sample to the R-wave of the heart with a piezoelectric crystal that is mounted on the inside of the pacemaker. The pacemaker can pace with rate response using either the piezoelectric crystal or the SvO_2 detector. Both the activity and the SvO_2 levels can be accessed with real-time telemetry as well as storing the SvO_2 values in the pacemakers memory [13, 49].

Kjellström *et al.* published a paper in 2004 where they had done a six year follow up on 9 patients implanted with the Medtronics model 8007 and 4327A combo [50]. Their conclusion was that the oxygen saturation levels correlated well between implantable sensor and SvO_2 obtained with optical Swan-Ganz catheters or blood samples. Kjellström also concluded that long-term stability determined with comparison of resting values and responses to sub-maximal exercise was reproducible over the follow up period.

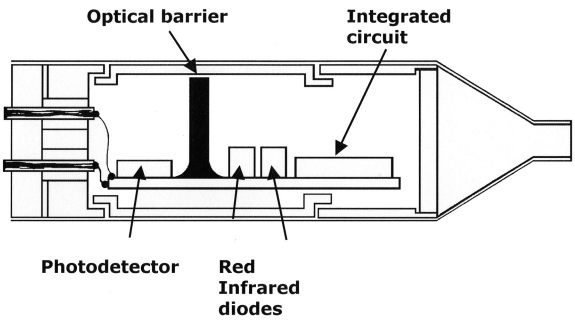

Figure 2.11: *Medtronics Model 4327A Oxygen sensing lead [51].*

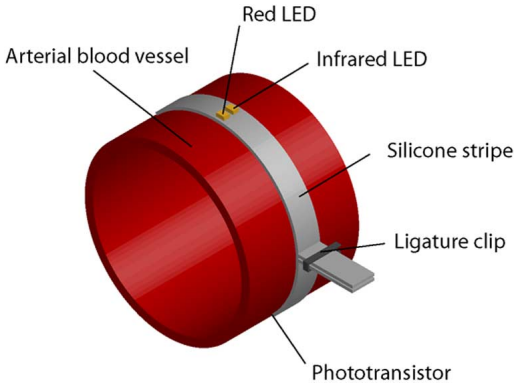

Figure 2.12: *A implantable cuff probe as proposed by Reichelt et al. [14].*

A paper by Reichelt *et al.* from 2008 describes a development of implantable pulse oximeter [14]. Their design proposes a meter to be used for long term surveillance of patients in critical care. They list several clinical situations in which the meter could be useful such as cardiac insufficiency and pulmonary hypertension for high-risk cardiovascular patients, chronic hypoxemia, surveillance of premature infants as well as surveillance and optimization of surgery timing for children with congenital heart defects. It utilizes an optically transparent cuff that includes the LEDs as well as a photosensor and is wrapped directly around an artery. Figure 2.12 shows the proposed probe. In the proposed solution there is a certain trade-off between the complexity of the surgery and the acquired AC signal straight from artery. They made an experimental setup where blood was pumped through an extracted animal

artery and their AC to DC ratio ranged from 20% to 40% compared to 1% to 10% in normal through finger human oximetry and around 1% for standard reflectance pulse oximetry [21]. The LEDs used an operating current of 20mA.

A conference paper also dated from 2008 describes an implantable telemetry capsule that measures oxygen saturation with reflectance pulse oximetry [15]. The purpose of the capsule is to measure fetal vital signs from the uterus of the mother specially in and after surgery that might be needed on the fetus. The paper is mainly a technical paper for a complete system of wireless transmitter, oxygen saturation and a continuous power supply system. It does not discuss any problems that can occur during measurements or the material used for sealing the implant. The implant is tested by measuring a signal from a human finger inside a water tank.

Although non-implantable but certainly related are so called intrapartum oxygen saturation meters used in labour for fetal SpO_2 measurements. Studies dated back to 1989 [52] introduce such a devise and continuous research in the 90's introduce a fully functional intrapartum reflectance pulse oximeter that uses a suction fixation [53]. This led to the first fetal oxygen saturation monitoring system to be approved by the Food and Drug Administration (FDA) in 2000 [54] named $OxiFirst^{TM} Fetal\ Oxygen\ Saturation\ Monitoring\ System$ and was manufactured by Mallinckrodt and Nellcor Perinatal Business.

2.3 Noise and errors in oximetry measurements

Webster [55] states three major sources of noise and errors in SpO_2 measurements. Motion artifacts, reduced saturation levels ($<$80%) and peripheral vasoconstriction (low perfusion) that all can severely affect the PPG signal. Other sources of noise and errors are probe placement, dyshemoglobins, ambient light, intravascular dyes, nail polish and skin pigmentation. It is quite obvious that some of these sources do not apply to implantable meters. Figure 2.13 shows an example of the most common noise artifacts as presented by Jubran [56].

The most important noise source, specially for implantable meters and moving subjects would be motion artifacts. Trivedi *et al.* [57] tested five different commercial meters with motion generator at 2Hz and 4Hz where the subject hands where moved 10cm to generate an artificial shivering. Their conclusion was that there is a significant difference in commercial meters where the failure rates range from 5% to 50% depending on meters. What is interesting about their study is that the error rate for detecting heart rate (HR) is much greater than for the detection of SpO_2 that ranges from 2% to 10% in 2Hz vibration, this is evident from Figure 2.13c and 2.13d since SpO_2 utilizes the ratio of two PPG signals instead of a single PPG signal, meaning the waveform is not as important. It's possible to decrease motion artifacts by avoiding all relative motion between sensor and the subject but this also

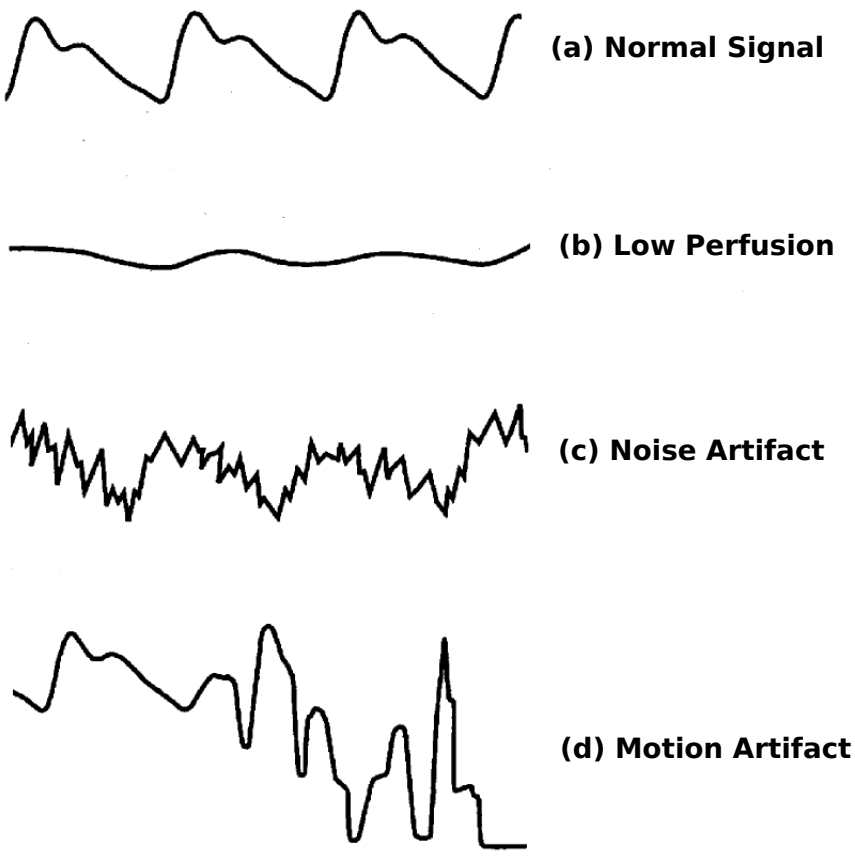

Figure 2.13: *The most common type of noise sources affecting SpO_2 measurements. The figure is adapted from [56].*

reveals a sensitive relationship between applied pressure of sensor and the received signal. There also exists filtering methods that compensate for movement artifacts that will be discussed in Section 2.6.

A study by Dassel *et al.* [58] showed that it is possible to increase the SNR by applying pressure to reflectance oximeter placed on the forehead of a measurement subject. The study proposes that applying pressure to the probe forces venous blood out of the area under the probe reducing disturbing influences of non pulsitile venous blood. Another effect of pressure to probe is the relationship between increase in flow velocities that cause an increase in pulse size. One method in neonatal care to use suction probe on the forehead of infants to record the SpO_2. This also reduces noise created with movements since it reduces the movement between the subject and the meter used.

Several studies [59, 60, 61] have shown the relationship between peripheral vasoconstriction and effect of SpO_2. Kelleher *et al.* [59] were the first to describe this effect. It is considered as a fact from these studies that oxygen saturation values measured with pulse oximetry increase during hypothermia induced peripheral vaso-

constriction and decreases during hyperthermia induced peripheral vasodilation. It was thought that skin/limb temperature was the main trigger of this mechanism but as Talke *et al.* [61] pointed out in 2006 this effect also happens when temperature is kept constant and peripheral vasoconstrictors where administered to the subjects. The mechanism for this change in perfusion remains speculative and unproven until this day. It is still important to realize that adequate arterial pulsation is required since a significant decrease in peripheral vasoconstriction such as in a shock or severe hypotension might lead to very low SNR.

Since oximeters estimate the functional saturation but not the fractional saturation, effects by abnormal haemoglobins, HbCO and other dyshemoglobins can affect the measurement data as well as any substance that absorbs light in the same wavelength as the LEDs of the probe. HbCO having the most effect since the oximeter detects them as HbO_2 and thus overestimates the concentration [62].

Ambient light coming from sources such as surgical lamps , infrared xenon lights and fluorescent lamps has been studied greatly. With strong amount of light its possible to saturate the light photosensor of the measurement device. Trivedi *et al.* made a study how an ambient light in a clinical scenario effects the oximetry measurements of five commercial devices. Their setup was to perform oximetry measurement of a distance of $\approx 1.2m$ from a standard surgical lamp. The error in SpO_2 varied from 6% to 60%. Another more recent study by Fluck *et al.* states that ambient light has no statistical significance [63]. They studied five different types of lights but distance from the subject is unclear. Both studies utilized the same probe the Nellcor N-200. Rusch *et al.* states that reflectance probes provide better shielding to ambient light then probes that work through finger [64].

Other noise sources such as intravascular dyes, nail polish and skin pigmentation are considered minor and unrelated for this thesis topic. It is good to keep in mind that Dairy-Cattle move much less and slower than for example cats, dogs and horses and that can help us estimate the effect of noise in the acquired signal.

Though currently being unpublished data we know from previous implants done in the Remowel project that noise effecting the ECG comes mainly from movement of the animal, see Figure 2.14a for accelerometer data and how it affects the ECG data in Figure 2.14b. When the cow is still as the first 20 minutes indicate all signals are very stable but as soon as the cow starts moving the noise increases in correlation to the amount of movement. As seen in Figure 2.14c the HR of the cow is around 75 beats-per-minute (bpm) when the cow is at rest and goes up to 100 bpm when the cow is active. Our unpublished data shows a range from 60 bpm to 120 bpm that can also be related to the size and age of the cow, this indicates a HR extracted from a PPG signal would be around 1-2 Hz.

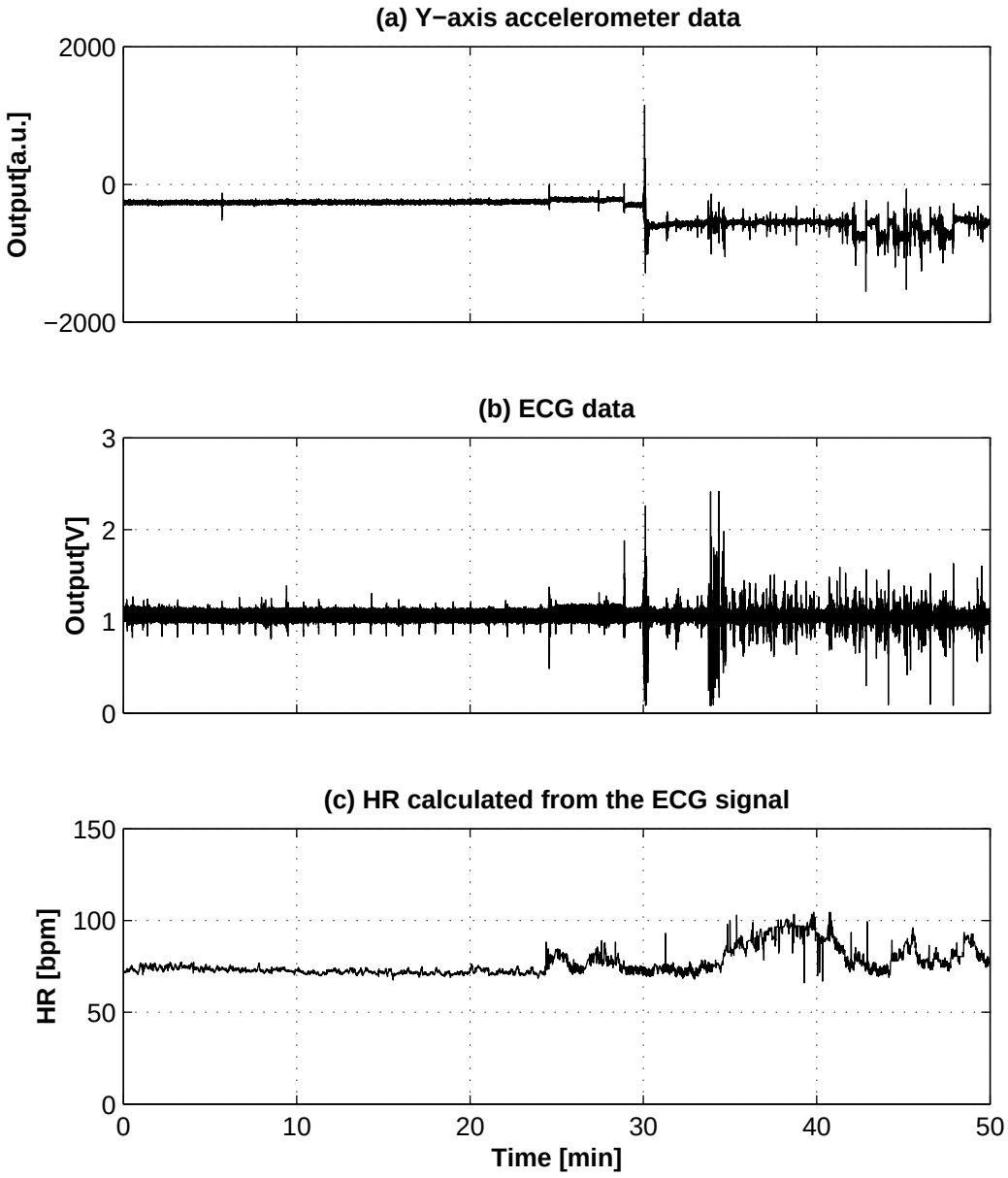

Figure 2.14: *The figure shows a 50min part of a signal recorded with previous implants from the Remowel group. (a) shows data from the Y-axis of the accelerometer inside the implant, it is sampled at 16Hz and gives good indication if the animal is resting or if it is active. (b) shows the ECG data sampled at 341.3Hz for the exact same period of time. (c) shows the HR calculated from the ECG signal where the noise spikes have been averaged out.*

2.4 Oxygen saturation meters in cattle monitoring

No commercial pulse oximeter exist specific for cattle monitoring, but as reviewed earlier in Section 2.2.1 there are some meters on the market focused on large animal

measurements such as horses. Some studies have also been made with both external pulse oximeters [47, 48] and near infrared spectroscopy [65] mostly to asses if the instrumentation technique is useful for diagnosis. Coghe *et al.* [47] showed that pulse oximeters placed on the shaved, non-pigmented tail of a cattle gives no significant difference of measurements done with pulse oximetry SpO_2 and with blood gas analyser SaO_2. In their study they measured 46 cattle where they where able to get a clear signal from 38 by placing the probe on the fourth or fifth verebra of the tail. Thickness of tail was considered the cause of the three non-signals and in five cases the whole tail was darkly pigmented. They pointed out that earlier studies in humans had shown that hair and pigmentation affects greatly the availability of a good signal. It is considered a disadvantage that they don't describe the oximeter they used or the probes. However, it is evident from Figure 1 in their publication that it's a through tissue probe. The second paper the group released described the pulse oximeter being a Nellcor N-3000 with Vet Sat Sensor that was covered with black rubber to shield them from ambient light [48]. The Vet Sat Sensor has a Y-shape as can be seen in Figure 2.15a-b.

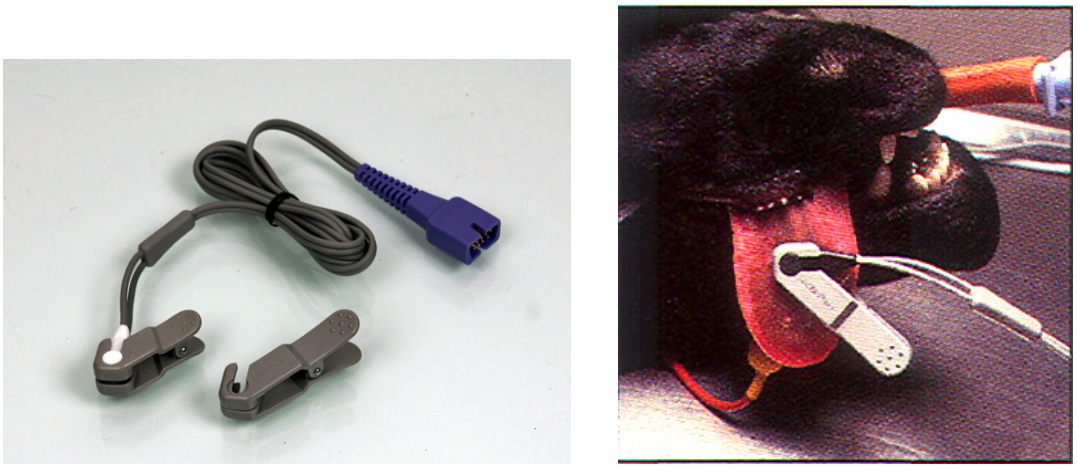

(a) **(b)**

Figure 2.15: *Nellcor Vet Sat Sensor probe (Figure 2.15a) shown in practice measuring on the tongue of a dog (Figure 2.15b) [37]*

Even though Coghe and Ustepruyst *et al.* confirmed the possibility of SpO_2 measurement in cattle, with a oxygen saturation meter designed for humans. We can validate the case even further by comparing two properties of blood in human and cattle. The weight of hemoglobin, is typically around 14 g Hb/100 mL in human blood [20] while compared to that of dairy-cattle it is typically around 11 g Hb/100 mL blood [66]. Another characteristic is the absorbance spectra which Grosenbaugh *et al.* [16] showed that difference between human and cattle is statistically insignificant as stated earlier in Section 2.2.1. The coefficients they measured are shown in

Table 2.3. They also measured the fractional amounts of both methemoglobin and carboxyhemoglobin as shown in Table 2.4

Table 2.3: *Extinction coefficients for Hb and HbO_2 for the specific wavelengths 660nm and 940nm in humans and cattle as measured by Grosenbaugh et al. [16].*

λ	$\varepsilon_{Hb}(\lambda)$ *Human*	$\varepsilon_{Hb}(\lambda)$ *Cattle*	$\varepsilon_{HbO_2}(\lambda)$ *Human*	$\varepsilon_{HbO_2}(\lambda)$ *Cattle*
660	0.84 ± 0.2	0.89 ± 0.06	0.096 ± 0.01	0.12 ± 0.03
940	0.20 ± 0.01	0.25 ± 0.03	0.26 ± 0.01	0.29 ± 0.03

Table 2.4: *Fractional amount of Hi and HbCO in the hemoglobin solution subject to spectral analysis as published by Grosenbaugh et al. [16].*

Species	Hi(%)	HbCO(%)
Human	0.67 ± 0.1	1.0 ± 0.5
Cattle	0.68 ± 0.1	1.2 ± 0.1

2.4.1 Diagnostic purpose

There are multiple respiratory problems that can effect dairy-cattle, Divers and Peek *et al.* [67] made an extensive book covering all diseases that affect dairy cattle. They list eight groups of respiratory diseases:

1. Mechanical or Obstructive Diseases
2. Inflammatory Diseases
3. Bacterial Bronchopneumonia
4. Diseases of the lower airway
5. Viral Diseases of Respiratory Tract
6. Parasitic Pneumonia
7. Noninfectious Causes of Acute Respiratory Distress in Cattle
8. Other less common causes of Respiratory Distress

Even though all of those diseases can be indicated with pulse oximetry, we are specially interested in types 3 to 8 which are all categorized as diseases of the lower airway. Those types of diseases can be hard to diagnose in early stage, causing a spread among the cattle. The most notorious of these diseases are number of viruses and bacteria that induce bovine respiratory diseases (BRD).

The impact of respiratory diseases can be categorized as mortality (death loss) or morbidity (sickness). Smith published a paper in 1998 where he states that cost of morbidity can be even higher than mortality due to expenses related to medication, labour of treatment, premature culling and reduced performance during and after the illness. Smith collected studies of mortality and morbidity in feedlot cattle where morbidity due to respiratory diseases was estimated to be 72% of total disorders and mortality due to respiratory diseases around 47.4 % [68]. The economical impact of BRD has not been studied greatly but Griffin published a study in 1997 where he estimated that cost in the USA of $ 750 millions annually for farmers with indirect cost of treatments and prevention to be even close to $ 3 billion [69]. National Animal Disease Information Service (NADIS) in the UK, publishes data that respiratory diseases in feedlot- and dairy-cattle account for about £60 million annually [70].

The specific causes and symptoms of those viral and bacterial pathogens is out of the scope of this thesis but a study from 2004 indicates that in Finland parainfluenza virus-3 (PIV-3), bovine respiratory syncytial virus (BRSV), bovine coronavirus (BCV), bovine adenovirus-3 (BAV-3) and bovine adenovirus-7 (BAV-7) are the most common [71]. Of the different BRD viral and bacterial pathogens, BRSV has in the last 20 years become one of the most important respiratory pathogen in dairy cattle as it invades the cell lining of the trachea and lungs and is commonly found in BRD cases. It shows high morbidity in several days to one week after infection, signs of infection include increased temperature as high as $40C$ to $42.22C$, depression, anorexia, decreased milk production, salivation as well as increased respiratory rate from forty to hundred breaths per. min. Each cow has to be diagnosed by a specialist to determine infection. The drug treatment to BRSV can include broad-spectrum antibiotics, non steroidal anti inflammatory drugs (NSAID), corticosteroids, antihistamine, atropine, furosemide and dexamethasone [67]. Intranasal oxygen also helps with decreasing the respiratory rate. The cost of each treatment of BRD was estimated $ 15.57 according to Faber *et al.* in 1999 [72]. Schneider *et al.* included indirect costs in feedlot cattle such as reduction of average daily gains (ADG) and less carcass value due to quality grade to amplify the cost to $ 15.76, $ 22.09 or $ 46.70 depending on number of treatments given [73].

When writing this thesis the pharmaceutical giant Merck announced a new antibiotic drug for some BRD pathogens, this shows the constant work that is being done on fighting BRD. This also shows that implantable pulse oximeter could be used for clinical drug trials in a obvious active market [74].

2.4.2 Placement of meter in tissue

The placement of the implantable meter is an important factor for a successful measurement. External measurements have been conducted on cattle from various

places such as the ear, the scrotum, the tongue, the tail, the nasal septum and the lip of the vulva. With external meters the cattle shows signs of stress when meters were placed on the ear, tongue or nasal septum inducing too much noise for a stable reading [47]. Coghe *et al.* paper still showed that pulse oximetry measurements can be conducted anywhere on the cattle where there is a possibility to shine through skin. No studies measuring the oxygen saturation in cattle with a transreflectance meter have been published according to the author of this thesis, those kind of measurements should be conducted prior to implantation at least on the tail of the cattle.

As stated earlier in Section 2.1.3, backscatter is an important factor when deciding the placement of the meter since it enhances the acquired signal. Placement near the ribs of the cattle could be sufficient for a nice backscatter and stronger PPG signal. The lower part of the rib is the widest according to Figure 2.16 that shows a suggested placement of implant. This is a very similar placement as has been used in earlier implants of the Remowel group, for recordings of ECG, temperature and activity of the cattle [1].

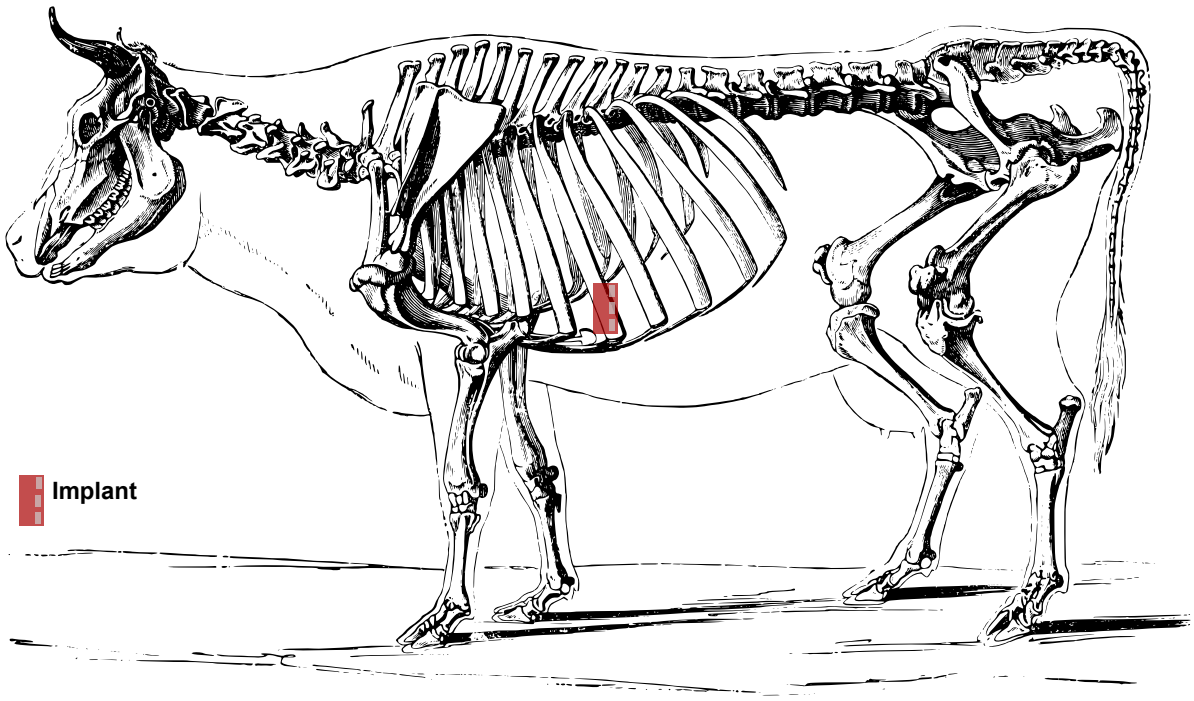

Figure 2.16: *The figure shows the skeleton of a cow drawn by Fred V. Theobald [75]*

Unpublished knowledge from those implantations gives information that considerable amount of fat tissue exist in those areas. Another thing that should be studied prior to implant, is how much the fat tissue degrades the PPG signal since very limited amount of studies have been performed on mammalian fat. One study by Veen *et al.* used clear purified oil obtained from pig lard, their result was presented

in a conference paper [76] and their data is freely available online and was used to create Figure 2.17, the processing steps of the oil are also explained online in detail [77].

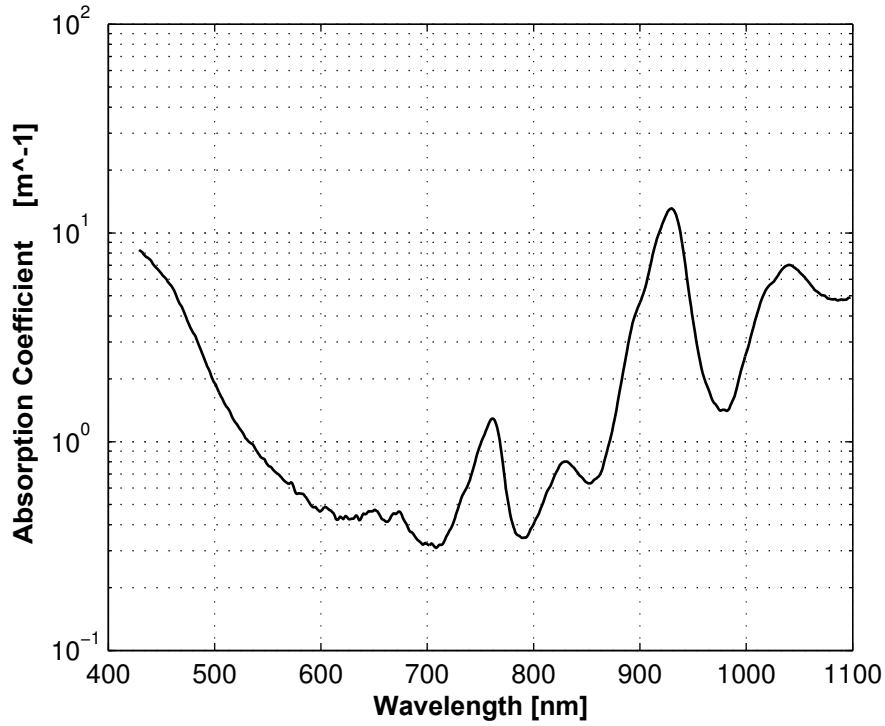

Figure 2.17: *The figure shows the absorption coefficient for purified oil obtained from pig lard as a function of wavelength. The figure is constructed from data available at [77].*

When measuring the PPG signal with reflectance pulse oximetry it is usually the movement of the bone relative to the meter that causes motion artifacts as well as skin to meter movements. It is important that the backscattered light of the red and IR LEDs does not change significantly when conducting measurements. If meter is placed near the ribs there is a possibility that some motion artifacts due to breathing occur though it is not evident from the acceleration data shown in Figure 2.14c.

Since the PPG signal can also be measured from the internally scattered light such as shown in Figure 2.9 the perfusion of the tissue near the meter is important. Figure 2.18 shows how the perfusion in the layers of the skin is represented with black dots. The perfusion is very high where the epidermis and dermis meet, this is because the skin is used for thermal regulation and thus has higher perfusion then other tissue [78]. A more interesting figure is Figure 2.19 that shows a histological section of a pig skin, it is quite clear from that figure that small vessels have good perfusion once you have penetrated the dermis layer. These figures indicate that there is possibility of receiving a low perfusion signal if LEDs are directed towards

the ribs. But they also indicate that there might be a possibility to receive the PPG signal from LEDs shining towards the skin rather then towards the ribs. This can only be concluded with *in vivo* measurements.

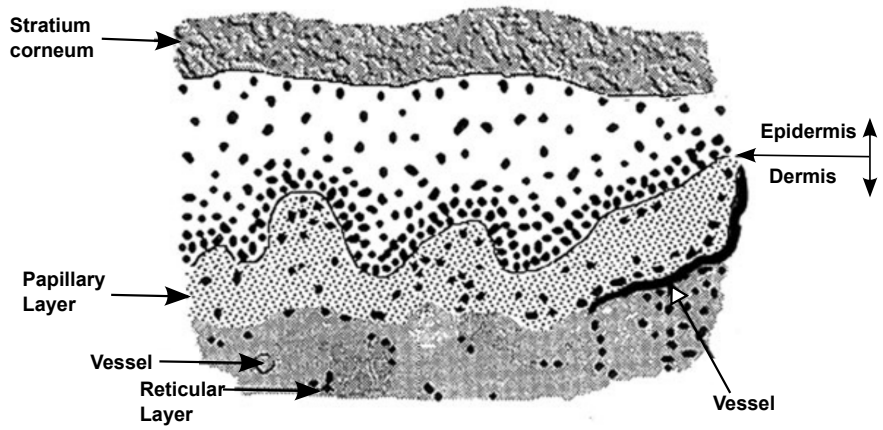

Figure 2.18: *The figure shows the layers of tissue in a human shoulder, the black dots indicate perfusion of the tissue. Figure is adapted from [27].*

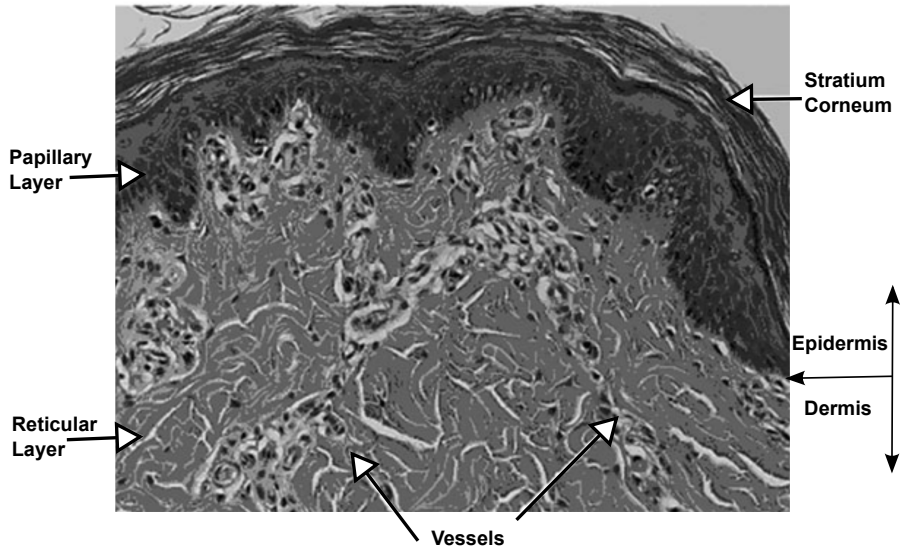

Figure 2.19: *The figure shows a histological section of pig skin. Figure is adapted from [27].*

2.5 Coating materials

As stated earlier the device has to be coated or sealed to fulfil its biocompatible requirements set by the FDA [79]. Biocompatability is according to definition "The

property of being biologically compatible by not producing a toxic, injurious, or immunological response in living tissue" [80]. Previous implants in the Remowel project have had a hybrid type of coating, consisting of both Parylene-C and medical grade epoxy [1]. In those implants the whole device apart from the electrodes was sealed with good result. Thus one of the main interest in the thesis is to determine what kind of effect biocompatible encapsulation has on the LEDs and photosensor.

He *et al.* published a paper where a 20 μm layer of Parylene-C was deposited on top of Silicon coated LED of white and red light (λ = 630nm), their result showed that the optical transmittance was more than 95 % of the non coated LED. Example result is 10,4 lm without the coating compared to 10,2 lm where the red LED was coated. They also tested the coated LED in a 1000 hour test where the LED was placed in temperature of 85 °C and humidity of 85 %. It showed no signs of ware compared to the uncoated LED that showed abnormal black residues around the lead as well as silver thermal adhesive after mechanical decapsulation [81].

The biocompatible epoxy that has been used before in Remowel project is EPO-TEK 301-2FL from Epoxy Technology. It is according to the datasheet suitable for LED encapsulation where it has an optical transmittance of over 99 % in the spectral transmission range of 400-1000 nm [82]. There where no studies found on the optimal coating thickness for photodiodes and LEDs or how the thickness of epoxy will effect the reflectance.

The third method possible for coating the LEDs is described in paper currently *In Press* by Lee *et al.*, it uses biocompatible polytetrafluoroethylene (PTFE) also known as Teflon to coat a Gan-LED. The paper is mostly describing a complete device and does not describe in detail the coating process [83]. This is an alternative that could be researched but is considered out of the scope of this thesis since the author has experience with the other two processes and non with biocompatible teflon.

Another issue regarding biocompatability is the temperature effect the implant has, for external SpO_2 meters the FDA says that "the device should not present a risk due to excessive surface temperature of the applied part" [84] and that further info is given in clause 42 of ISO9919 standard.

2.6 Signal processing of oxygen saturation signals

When discussing signal processing for oxygen saturation signals there are multiple aspects to consider, such as filtering of the signal in analog and digital domain, SpO_2 calculation, volume of individual blood pulsations supplying the tissue and extraction of other parameters such as the HR and blood pressure [55, 30]. Depending on weather you want to calculate the SpO_2 or SvO_2, the DC part of the signal is relevant. In this thesis we are only going to review briefly methods for filtering and SpO_2 calculations that could be done in real-time on the device and

more importantly justify their use, other processing is considered out of the scope of this thesis. Since the device is a prototype meant for measurements that have not been published before it is hard to make any definite statements on how we could process the signal even further.

2.6.1 Analog to digital conversion

Analog to Digital Conversion of the signal is done through an analog-to-digital converter (ADC) where there are namely two things to consider, sampling frequency (f_s) and resolution. The sampling frequency determines the time each sample of data is transformed from analog domain to digital. Nyquist criterion states that if you want to recover or reconstruct a signal of given bandwidth f_B from its digitized version, the f_s must be bigger then two times f_B as shown in equation (2.18) [85].

$$f_s > 2 \cdot f_B \tag{2.18}$$

The resolution of the ADC can be represented as the least significant bit (LSB) voltage, see equation (2.19). This simply means that the full scale voltage range (V_{FSR}) is quantized according to the number of bits (N) the ADC has [85].

$$LSB = \frac{V_{FSR}}{2^N} \tag{2.19}$$

If a circuit has gain the smallest detectable change of a signal is referred to as the sensitivity of the circuit shown in equation (2.20).

$$S = \frac{LSB}{Gain} \tag{2.20}$$

2.6.2 Filtering

By fallowing Nyquist's criterion you eliminate the possibility of any effect do to aliasing, though the PPG signal is a slow one there are number of other factors that affect the signal such as movement artifacts, 50Hz noise from electricity and switching frequency of the LEDs. For our SpO_2 measurements it can be expected that the frequency of movements will be minimal above 0.5 Hz as estimation of the frequency content of the accelerometer from previous implant, shown in Figure 2.20, indicates. Figure 2.20 was created using Welch's method [86] to calculate the power spectral density (PSD). It shows intuitively the first 20min of the signal shown in Figure 2.14 (a) where there is clearly no activity of the animal and the last 20min where there is clearly much activity.

The problem with noise induced by movements is that if we eliminate the DC part of the signal we remove the capability of measuring SpO_2 by the principles of AC/DC

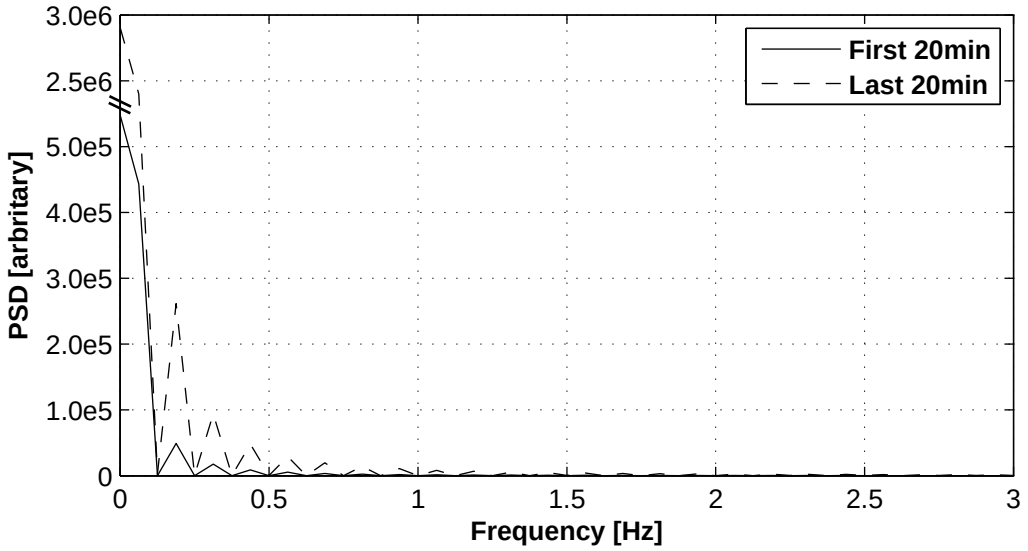

Figure 2.20: *PSD calculation of signal presented in Figure 2.14a showing the first 20min of the signal where there is no activity of the animal and the last 20min where there is much activity. The frequency content is estimated with welch periodogram.*

ratio as well as the option of measuring SvO_2. The switching frequency of the red and IR LEDs is from 100Hz in literature [87], though the standard switching frequency is around 480Hz in most commercial devices [88]. This frequency becomes much higher if certain power saving methods such as pulse-width-modulation (PWM) is utilized.

As was showed in Section 2.3 the HR of the cattle is around 75-100 bpm and even if it goes as high as 120-150 bpm the frequency content is still quite low. Thus a low-pass filter with a pole around 6Hz is sufficient to receive the SpO_2 signal. This filter can be implemented either in analog or digital domain.

2.6.3 SpO_2 calculation

Two main methods are utilized in the calculations of SpO_2 so called *Peak-and-Valley method* and *Derivative method*, both of these methods output what is called Ratio-of-Ratios (R_{OS}) and is simply the variable used to calculate the oxygen saturation [55].

The peak-and-valley method described by Cheung *et al.* [89] extracts simply the un-calibrated SpO_2 value from the minimum and maximum intensities of the red and IR wavelengths, see equation (2.21) and Figure 2.21 for clarification. Empirical calibration curves such as the ones shown in Figure 2.7 are then used to calculate the real saturation value.

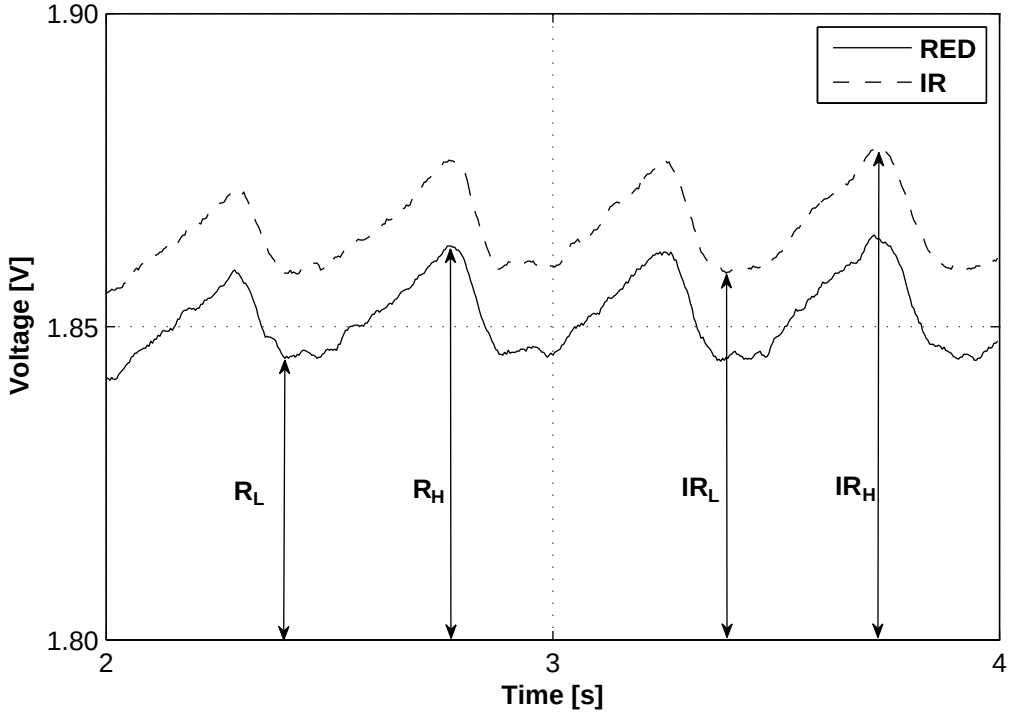

Figure 2.21: *The figure shows graphical interpretation of the values used to calculate R_{OS} in equation (2.21), where the voltage represents the transmitted light intensity. The signal is recorded with non calibrated meter using through finger probe. The figure is adapted from [55] using recorded data from this thesis.*

$$R_{OS1} = \frac{ln\left(\frac{R_L}{R_H}\right)}{ln\left(\frac{IR_L}{IR_H}\right)} \tag{2.21}$$

The derivative method can be explained as a computational simplification to the peak-valley-method since it eliminates the need to calculate the natural logarithm and thus it would suit better for implanted device. A 2-point derivative is calculated between the maximum (t2) and minimum (t1) of the PPG signal of each wavelength, the DC value (t3) is considered to be some point between the two points such as an output from a low-pass filter with a very low cut-off frequency or an average of the signal. Then the R_{OS} can be calculated as shown in equation (2.22) complemented with Figure 2.22 [55].

$$\frac{\frac{dI_{RED}(t)/dt}{I_{RED}}}{\frac{dI_{IR}(t)/dt}{I_{IR}}} \approx \frac{\frac{I_{RED}(t_2)-I_{RED}(t_1)}{I_{RED}(t_3)}}{\frac{I_{IR}(t_2)-I_{IR}(t_1)}{I_{IR}(t_3)}} = \frac{\frac{AC_{RED}}{DC_{RED}}}{\frac{AC_{IR}}{DC_{IR}}} = R_{OS2} \tag{2.22}$$

The medical instrument manufacturer Masimo uses a more advanced pulse oximetry technology to calculate the oxygen saturation that accounts for separation of ve-

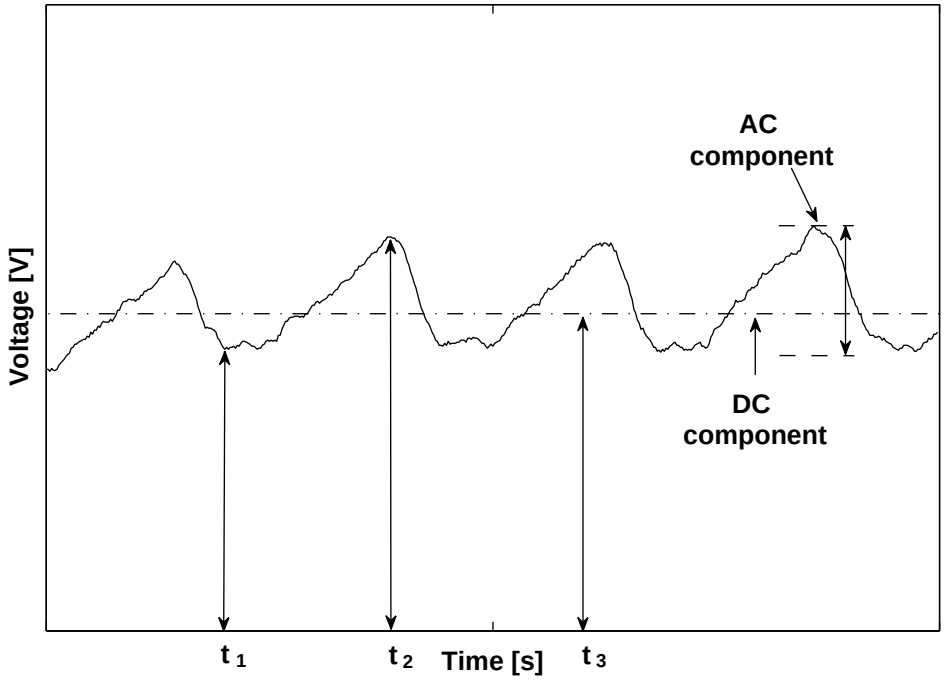

Figure 2.22: *The figure shows a graphical example of a PPG signal where the time positions used for derivative calculation of R_{OS} in equation (2.22) are shown for a single wavelength. The DC and AC components of the signal are also pointed out for further clarification. The signal is recorded with non calibrated meter using through finger probe. The figure is adapted from [55] using recorded data from this thesis.*

nous (non-arterial) blood and arterial or simply the DC and AC part of the signal. Their technology is called Signal Extraction Technology (SET) and it is explained so that the standard ratio technique in equation (2.15) does not account for any pulsatile nature in the DC part that can occur during movements. Instead their model estimates the noise and subtracts it from the PPG signal, further details about the SET method is considered out of the scope of this thesis since it would require significant time to explain but it has shown increased accuracy in estimating the SpO_2 during movement artifacts and moments of low perfusion [90].

Many oximeters output the average of the peak-and-valley such as taking 8 successive maximas and 8 successive minimas to determine the SpO_2 value. In those cases the output is determined as mean-SpO_2 ($mSpO_2$).

2.7 Power consumption

One of the greatest challenges with implantable pulse oximeter is the amount of power it consumes specially the LEDs driving current. Reichelt *et al.* used a driving current of 20mA for the LEDs in their proposed implantable meter [14]. Latest

Table 2.5: *Comparison of power consumption of Tavakoli et al. meter compared to commercial meters manufactured by Nonin. Total Power means only the LED power and processing power excluding the display of the signal. Reconstructed from [87]*

Pulse Oximeter Version	Total Power Consumption	Days in Operation on 4 "AAA" Batteries ($\approx$ 2306mAh)[a]
Tavakoli *et al* chip	4.8mW	60
WristOx®3100	$\approx$ 60mW	5.2
Xpod	60mW	4.8
Ipod	60mW	4.8
Avant®4000	71mW	4
PalmSAT®2500	$\approx$ 80mW	3.6
Onyx®9500	$\approx$ 120mW	2.4
8500 Series	$\approx$ 130mW	2.2

[a]There is no capacity value given in [87] for the AAA batteries they used, but an estimation of 2304 mAh was calculated by assuming a 3.0V supply voltage

implant of the Remowel group [1] used a battery LS14500 by Shaft with capacity of 2600mAh. That would mean only around 130 hours ($\approx$ 5.4 days) of continuous supply current for the LEDs. If we combine that value to the theoretical mean current consumption (2.35mA) of previous implant this value would be even less, only about 4.8 days of continuous measurements.

Tavakoli *et al.* published a paper in 2010 called "An Ultra-Low-Power Pulse Oximeter Implemented With an Energy-Efficient Transimpedance Amplifier" [87]. They introduce a pulse oximeter with a novel transimpedance amplifier, as well as analog domain signal processing methods that save power compared to methods conducted with a digital-signal-processor (DSP). In their paper they made a comparison of processing power between several low-power commercial pulse oximeters manufactured by Nonin Inc. which can be considered one of the leading companies of pulse oximetry devices[91]. Table 2.5 shows the total power consumption (LED power and processing power) of their chip compared to the commercial Nonin Inc. meters. Though there is no value given for the capacity of the batteries used it can be estimated that the supply voltage they use is around 3 V and thus a mean supply current of 1.6mA, this should not be taken literally since it is just an estimation the author of this thesis makes.

Sixty days of continuous measurements makes implantable pulse oximetry become a realistic option for respiratory monitoring and diagnosis in dairy-cattle. Since the application would have to be implanted in the animal ideally for 3-6 months. That recording time could easily be obtained by limiting the sampling periods to for

example ten minute period every one hour increasing the operating time six times. It can still be seen from Tavakoli *et al.* article that the oscillator/LED and switching control makes up 91.5 % of the chip power consumption or 4.48mW. In the appendix of their paper they derive an equation for the total power consumption of the LEDs and photoreceptors (see equation. (2.23)) and explain how much less they could theoretically reduce the power consumption of their meter.

$$P'_{TOT}(x) \backsimeq P'_{LED} + P'_{PR} = (4.4mW)x^{-1} + (80\mu W)x^{2/3} \tag{2.23}$$

Where P'_{LED} is the LED power and P'_{PR} is the power consumption of the photoreceptors. From Equation. 2.23 there is a optimum point where the total power consumption (P_{TOT}) is minimum, namely when $x = 14.1$. This indicated that either the gain of the chip could be increased by a factor of 14.1 or the LED power could be decreased by 14.1. Both options would reduce the total power consumption from $P_{TOT} = 4.48mW$ to $P'_{TOT} = 780\mu W$ or a reducing factor of 5.7. Tavakoli suggests that decreasing the duty cycle of the chopped LED pulses or the LEDs drive current is the only true option since increasing the gain of their amplifier would not help because the photoreceptor power would exceed the LED power. The minimum LED generated photo-current applicable would then be 3.5nA compared to the 50nA typical value of their oximeter [87]. According to Tavakoli *et al.* when such a low photo-current is generated the sensor becomes more sensitive to mainly two factors, that are 1) ambient light and 2) minimum detectable contrast. By implanting the sensor, it is easy to imagine that ambient light will be eliminated quite easily since the skin of the cattle is hairy and quite thick. Tavakoli also showed that at 3.5nA photocurrent the minimum detectable contrast is 0.1% which is lower than the lowest typical value of AC/DC contrast. As stated earlier in section 2.2.2, Reichelt *et al.* proposed implantable ring probe shown in Figure 2.12 showed a contrast of 20%-40% AC/DC level contrast but their probe was attached to the artery directly.

Another power limiting factor to the implantable system is the power consumption of the ADC, Sharpeshkar states that several ADC have a power consumption that can be described by the law presented in equation (2.25) [92]. This is simply a trade-off between the resolution of the ADC and the sampling frequency.

$$P_{ADC} \propto f_s \cdot 2^N \tag{2.24}$$

$$P_{ADC} = E_q \cdot f_s \cdot 2^N \tag{2.25}$$

Where E_q is a relative constant that represents the energy per quantization level and is often referred to as figure of merit (FOM) [92].

3. METHODS

In this chapter we will describe the oxygen saturation meter system developed for this thesis as well as describe the testing procedure and setup. Several prototypes where developed for this thesis, starting from acquiring a basic PPG signal with a LED and a phototransistor. The device described in section 3.1 is the final prototype developed for raw signal measurements. The section justifies the circuit design and component use. Section 3.2 reviews the design/integration of the probe and biocompatability issues towards the design, such as the coating process. Section 3.3 explain the signal processing implementation used in to acquire the results presented in Chapter 4. Finally Section 3.4 introduces the experimental setups used to determine the functionality of different components of the oximeter.

3.1 Device : design and components selection

The implantable oxygen saturation meter developed has two main requirements to fulfil, first it has to be biocompatible since any non-biocompatible material is rejected by the body causing inflammation and other side effects. Secondly it has to be able to acquire sufficiently high SNR to measure the signal. It is thus important that the measurement device has an adaptive LED current control. Adaptive element such as these are often called Automatic-Gain-Control (AGC) feedback systems. A block diagram of the measurement device is shown in Figure 3.1. It is made out of three functional blocks as seen on the figure:

1. **Probe** : Includes the Red and IR LEDs as well as the photosensor.
2. **Analog Circuit** : Incorporates the transimpedance amplifier, switching circuit the AGC as well as analog filters and amplification.
3. **Microcontroller Unit (MCU) / DSP** : Creates the square wave that drives the switching circuit of the LEDs and it also samples and stores the signal data.

The functional blocks where designed so that is is easy to change and test certain parts of the system individually. Most of the prototypes where run with a 555 timer instead of a MCU and both reflectance probes and a through tissue probe was developed to ease the testing.

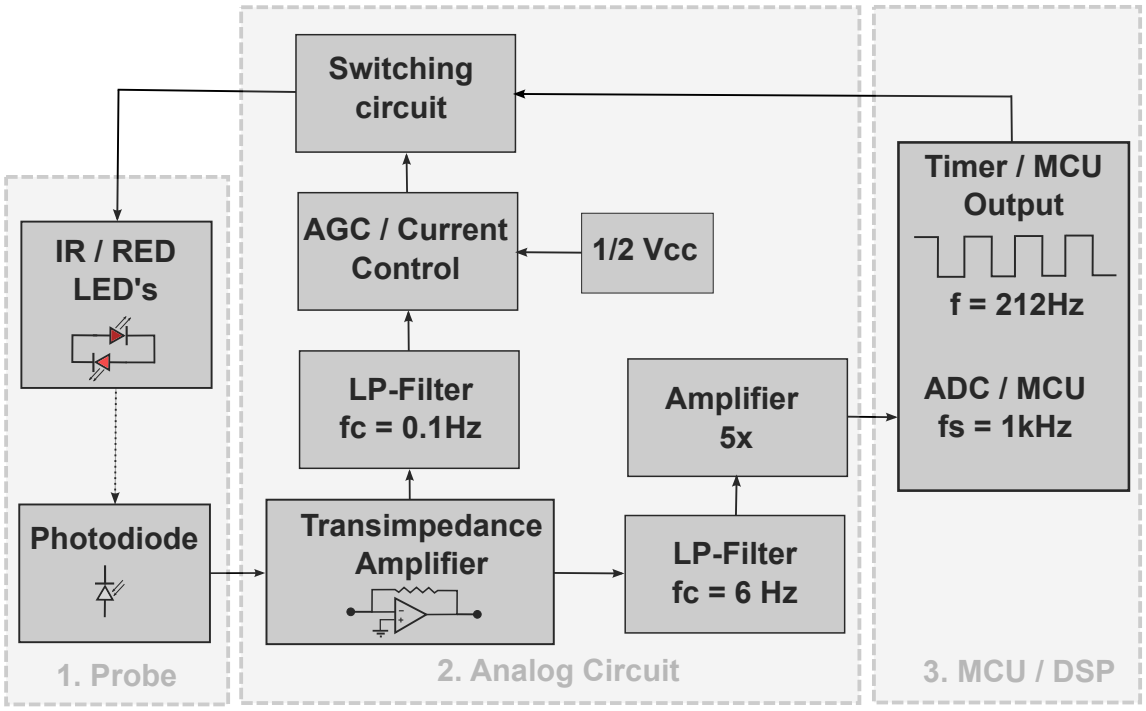

Figure 3.1: *Block diagram of the measurement device*

3.1.1 Transimpedance amplifier

The most important part of the analog circuit is the transimpedance amplifier. Our device utilizes the classic approach of using a linear transimpedance amplifier, the OPA380 from texas instruments. Figure 3.2 shows a linear transimpedance photoreceptor. The OPA380 is a high-performance transimpedance amplifier that is able to operate with a supply voltage of +2.7V to +5.5V and it also has a very low 1/f noise, low input bias current, low input voltage and wide bandwidth [93]. The version of the device presented in this thesis has a transimpedance gain of 120 dB (V/A), meaning that a photo-current of 10nA generates a 10mV output. The major downside to the transimpedance amplifier used is the quite high quiescent current of $\approx$ 6mA. One solution to that problem would be to utilize a transimpedance amplifier proposed by Tavakoli *et al.* in [87]. The current consumption of two transimpedance amplifiers that Tavakoli used was only $80\mu W$. Their amplifier is described in detail in [31] and [87] but its manufacturing was considered too complex for the scope of this thesis. Tavakoli *et al.* amplifier also utilizes a logarithmic response transimpedance amplifier, see Figure 3.3 for basic operation principles. It utilizes an NMOS transistor in the feedback loop of the amplifier and operates in subthreshold regime of operation because the photocurrent is so small and thus it exhibits an exponential I-V characteristics. This would be ideal for most SpO_2 measurement systems, but since there is quite much uncertainty with our measurement signal we don't want to limit our option of measuring the SvO_2 since it is the only signal

that has been retrieved from clinically tested implantable meters utilizing the pulse oximetry principles as stated in Section 2.2.2.

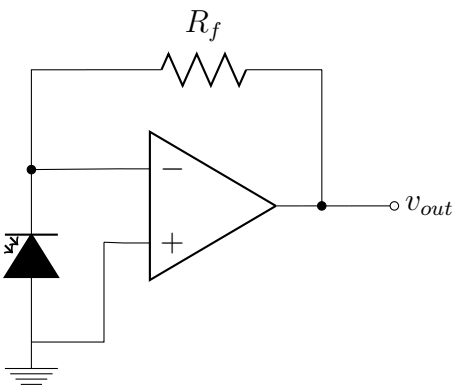

Figure 3.2: *Linear transimpedance amplifier [94].*

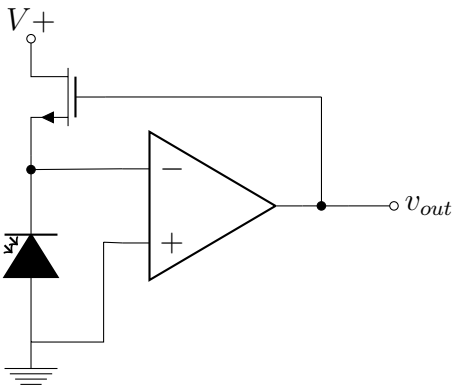

Figure 3.3: *Logarithmic transimpedance amplifier [87].*

3.1.2 Filters

The PPG signal used to determine the oxygen saturation is a slow varying signal as can be seen from Figure 2.21. A high bandwidth photoreceptor is important so that the photoreceptor is able to settle down during the short pulse from the LED. We can then easily filter the signal with a low pass filter at 5-10Hz to retrieve the PPG signal as seen from the block diagram in Figure 3.1. This filter also serves as a antialiasing filter for the ADC, its performance on attenuating higher frequencies such as switching frequency and 50Hz noise should be considered. The other filter we utilize in the feedback loop is to acquire the DC part of the signal. Both filters in the prototypes are standard passive 1st degree filters see Figure 3.4 and the frequency response in Figure 3.5. The choice of filtering method is justified with its simplicity and the easy of changing components to acquire different frequency response, that can be set with equation (3.1).

$$f_c = \frac{1}{2\pi \cdot R \cdot C} \tag{3.1}$$

3.1.3 AGC and switching circuit

The switching circuit utilizes a simple npn-transistor circuit that switches between the red and IR LEDs (see Figure 3.6), depending on a square wave created with the MCU of the measurement device. That is the transistor is utilized as a switch that is turned on when voltage to base (B) is high relative to emitter (E), Figure 3.7 shows a standard representation of an npn transistor [94]. The switching circuit is driven with a voltage coming from the photoreceptor where the DC part is first

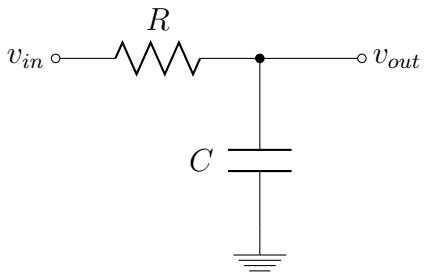

Figure 3.4: *Standard passive 1st-degree low-pass filter [94].*

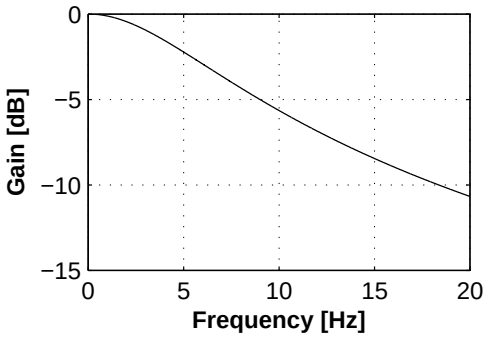

Figure 3.5: *Frequency response of a 1st degree low pass filter with cut-off frequency 6Hz. Created from [95].*

acquired with a Low-Pass filter and then an integrator is used to drive the voltage to an optimized level, this level has to be determined experimentally according to the amplitude of the AC/DC part expected from the signal. In this thesis it was set to 1/2 Vcc. The AGC regulation supplies the LEDs with a current determined by the output voltage of the AGC over the LED resistors, in this thesis we refer to this as LED drive current or LED supply current, it can be determined with equation based on Ohm's law, equation (3.2).

$$I_{LED\ Supply} = \frac{(V_{AGC} - V_f)}{R_{LED\ Supply}} \tag{3.2}$$

Where the value of the supply resistor determines the supply current range determined by the voltage $(V_{AGC} - V_f)$ where (V_f) is the forward voltage of the photodiode. The final stage amplification has to be determined experimentally to avoid saturation of the output, but an amplification of five was used in this thesis. The circuit schematics are shown in Appendix B.

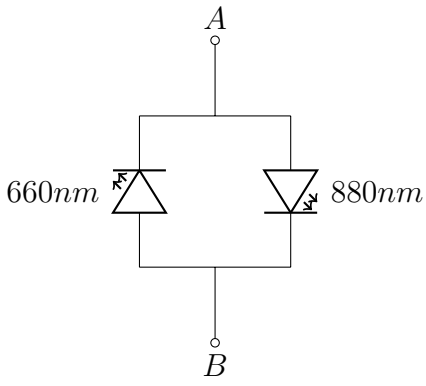

Figure 3.6: *Circuit schematic of Advanced Photonics dual LED chip E838 [96].*

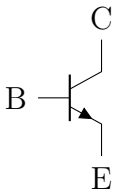

Figure 3.7: *Standard representation of an NPN transistor. Collector(C) (n-type), Base (B) (p-type), and emitter (E) (n-type) [94].*

3.2 Probe design

A major part in the design of the implantable pulse oximeter is the probe since there are two issues that have to be taken into consideration that are not a big factor in normal external SpO_2 measurements. Namely bio-compatibility of the probe as well as temperature effect of the LEDs on internal tissue. The probe includes a photodiode as well as red and IR LEDs. Both components are not available commercially in bio-compatible form, thus they have to be sealed or coated before implantation. A image of the uncoated probe is presented in Figure 3.8.

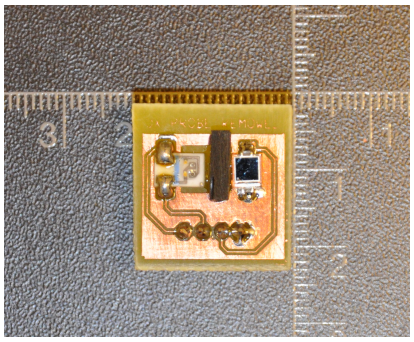

Figure 3.8: *A photograph of un-coated transreflectance probe developed for this thesis. It consists of PDI-E838 dual LED chip, a barrier made out of black Polyoxymethylene (POM) plastic and a BPW34S photodiode. The scale of the figure is in cm.*

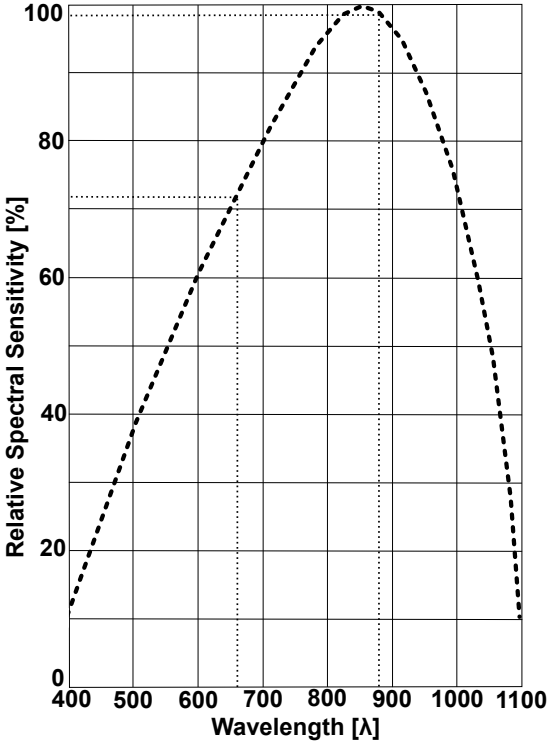

Figure 3.9: *Relative Spectral Sensitivity as a function of wavelength for the photodiode BPW34 [97].*

The LEDs it uses is a dual chip manufactured by Advanced Photonics with red (λ = 660nm) and IR (λ = 880nm) LEDs, called PDI-E838. Figure 3.6 shows a circuit schematic of the chip, it comes in a small plastic surface mount technology (SMT) package with dimensions 4.24mm x 6.35mm [96]. The choice of the IR λ = 880nm, was justified from Medtronics 4327A pacing lead that was the only implantable oxygen saturation system tested clinically. It measured SvO_2 [49] as explained earlier in Section 2.2.2. More commonly used wavelengths for the IR LED are 900nm and 940nm , they are used in most commercial devices and usually justified from the extinction coefficient as shown in Figure 2.3 [98]. Since we are concerned about the fat tissue surrounding the implant 880nm has lower μ_a then

940nm according to Figure 2.17 which is another reason to justify the choice. The photodiode used was an Osram BPW34S that has good relative spectral sensitivity for the wavelengths we are using see Figure 3.9, it has $V_f = 1.3$ V [97].

3.2.1 Coating process

The two methods used for the coating of the device are very different. EPO-TEK 301-2FL epoxy is a thermosetting polymer made out of two components having a specific gravity of $SG_A = 1.06$ and $SG_B = 0.89$. The datasheet of the material provides the ratio of mixing by weight as 100:35, then once the two materials are mixed their curing time is 3 hours at 80 °C or 3 days at 23 °C [82]. The epoxy is pourable liquid when mixed so the use of a cast is required. Figure 3.10 shows a photo of the cast that was manufactured to coat the probe. The cast is made out of Teflon where four stainless steel spikes have been placed to hold the probe and determine the thickness of the epoxy layer, the spikes can be moved to change the thickness of the layer if further coating tests are needed.

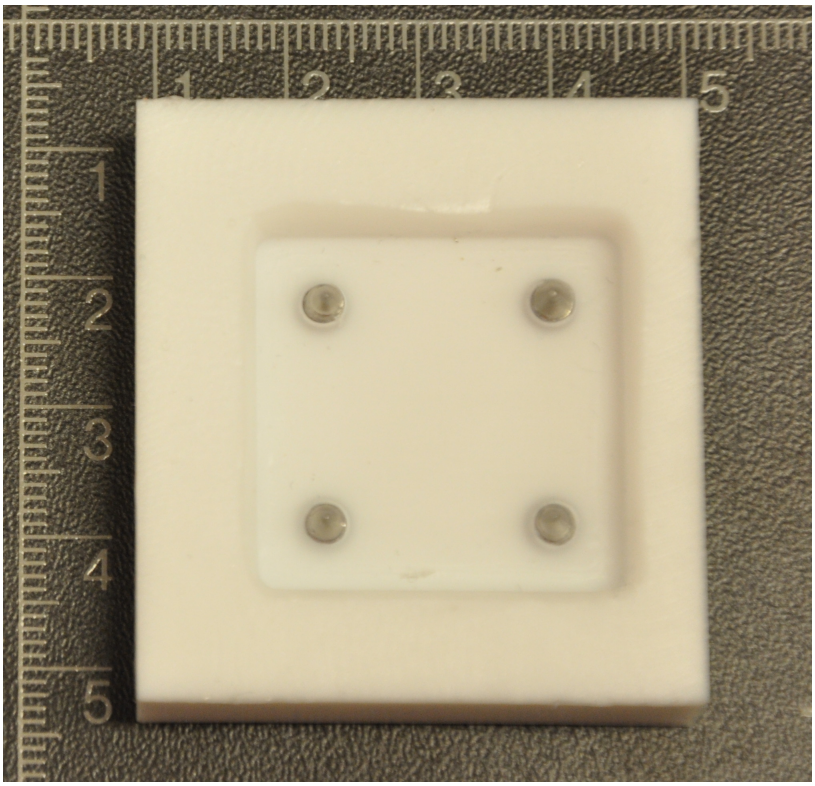

Figure 3.10: *Figure shows the cast manufactured for the epoxy coating, it is made out of Teflon with stainless steel spikes that can be varied in hight and thus it is possible to change the thickness of the epoxy layer. The scale in the figure is in cm.*

Figure 3.11 shows a cross-sectional view of the probe. To utilize the optical properties of the epoxy it is important to empty all air bubbles from the mixed material before curing starts, that can be done in a vacuum chamber. The thickness

of the epoxy was set to be 3.5mm from the PCB board, this was done to test the coating effect with thick layer of coating but not for any optimization purposes.

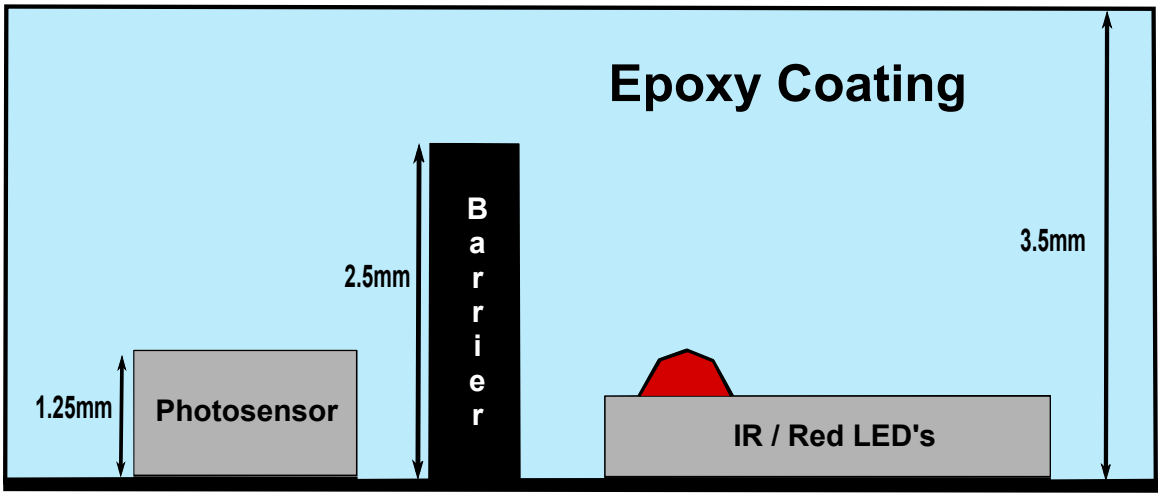

Figure 3.11: *Cross-sectional image of the probe showing different components as well as the thickness of the epoxy coating.*

Parylene-C coating has different and more complex coating procedure compared to epoxy. Figure 3.12 shows the block diagram of the processing method, which can be explained in three steps according to parylenengineering [99] :

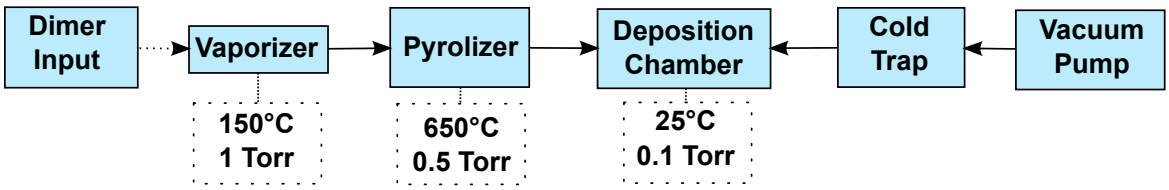

Figure 3.12: *Block diagram of the processing method for Parylene-C coating according to parylenengineering [99].*

1. A dimer called *di-para-xylene* is a chemical precursor to Parylene-C coating. It is in the form of granular white powder. When it is heated to $\approx 150\,^{\circ}\mathrm{C}$ at 1 Torr, it converts to a gaseous state.

2. The vapor is then fed into a pyrolizer at $650\,^{\circ}\mathrm{C}$ at 0.5 Torr, that forms a gaseous monomer.

3. The monomer is then fed into a coating chamber at room temperature (25 °C) at 0.1 Torr. The monomer gas condenses equally on all surfaces and then polymerizes to a product with high degree of crystallinity.

The cold trap is a steel thimble that is cooled with liquid nitrogen. The thimble condenses the Parylene-C process by-products and prevents any contamination to the vacuum pump that maintains the vacuum in the system [100]. Before the Parylene-C process the printed circuit board (PCB) is cleaned, first with Isopropanol for 15 minutes then with a mixture of Saline, de-ionized water and Isopropanol for 30 minutes and again for 15 minutes with Isopropanol. This cleans the PCB so that the Parylene-C coating attaches better to the surface. Figure 3.13 shows how the Parylene-C layer is distributed over the probe.

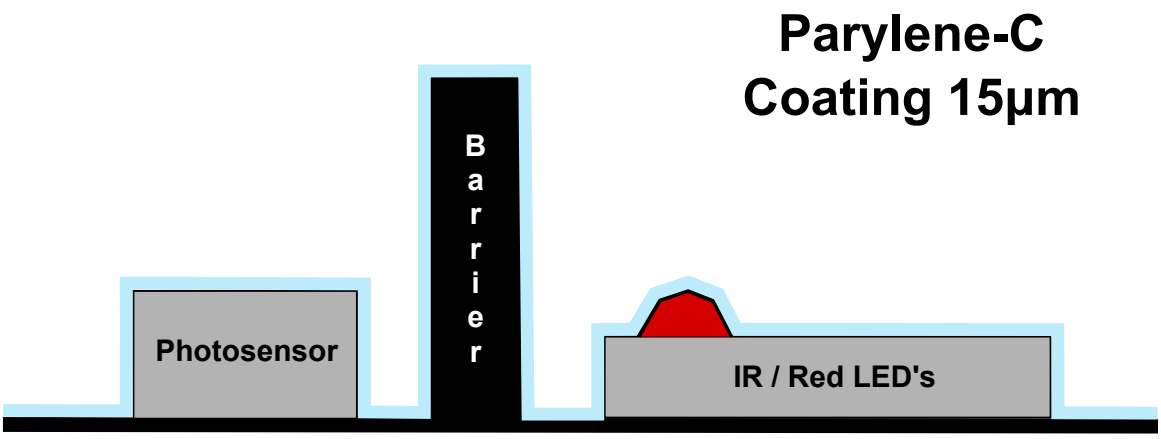

Figure 3.13: *Cross-sectional image of the probe showing different components as well as the thickness of the Parylene-C coating.*

3.2.2 Temperature effect

When discussing temperature effect the main concern is thermal radiation from the LEDs and how it might have destructing effects on the internal tissue when it is absorbed. Another thing is how increased temperature in the implant might effect the temperature sensor in the existing implant. This has to be measured and concluded as well as to measure how the coating of the implant effects this thermal radiation.

3.3 Signal processing implementation

To acquire the oxygen saturation value a post processing script was written in MATLAB. A flow chart of the processing method is presented in Figure 3.14, where the raw signal is acquired from the ADC. The peak detection blocks utilize a function written by Eli Billauer for peak detection in noise, it is distributed without any copyright and for public use [101]. The function fits perfectly to our use and enables us to extract all info without any pre or post filtering. The first peak detection block is used to find the maxima and minima of the raw signal, this enables us to separate the red and IR signal in separate vectors.

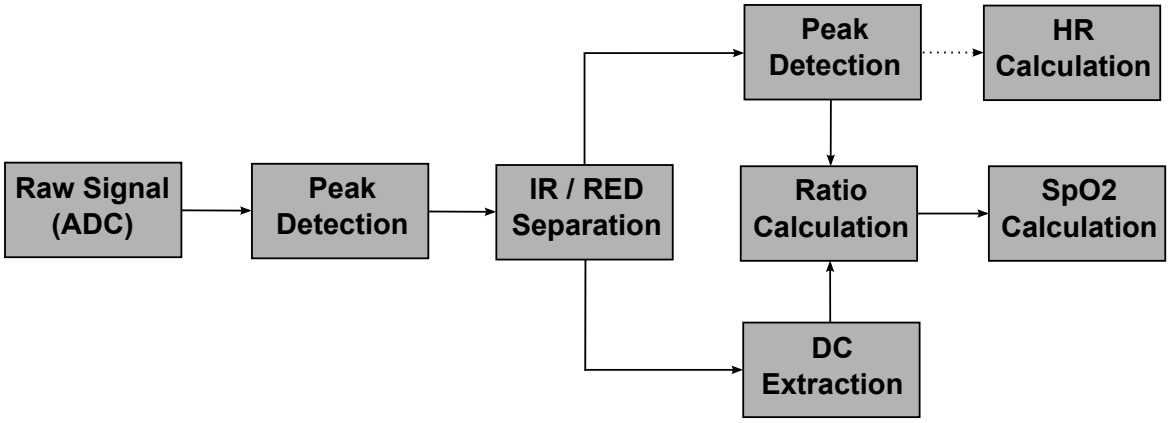

Figure 3.14: *Flow chart of the signal processing for equation (2.22), HR can be easily extracted though it is not our main objective and methods for HR extraction are not presented in this thesis.*

The flowchart of Figure 3.14 is for SpO_2 calculation from equation (2.22), this means that we need to extract the DC part of each signal. Since there is no baseline drift in the test measurements we do this simply by taking the average of each signal. The second peak detection block then extracts the minima and maxima of the signals (peaks-and-valley), Figure 3.15 shows how these two peak detection blocks work in extracting the information from the signal. The ratio calculation block uses equation (2.22) to calculate the the ratio. Then the final block uses equation (2.16) to calculate the SpO_2. This algorithm calculates un-calibrated SpO_2 as stated earlier in Section 2.6.3, but it gives a comparison value between different measurement setup. The same flow chart also applies to equation (2.21) the only difference is the DC extraction block is not needed.

In Chapter 4 the ratio was calculated with the peak-to-valley method, presented with equation (2.21) from Section 2.6.3. It is not convenient method for DSP use

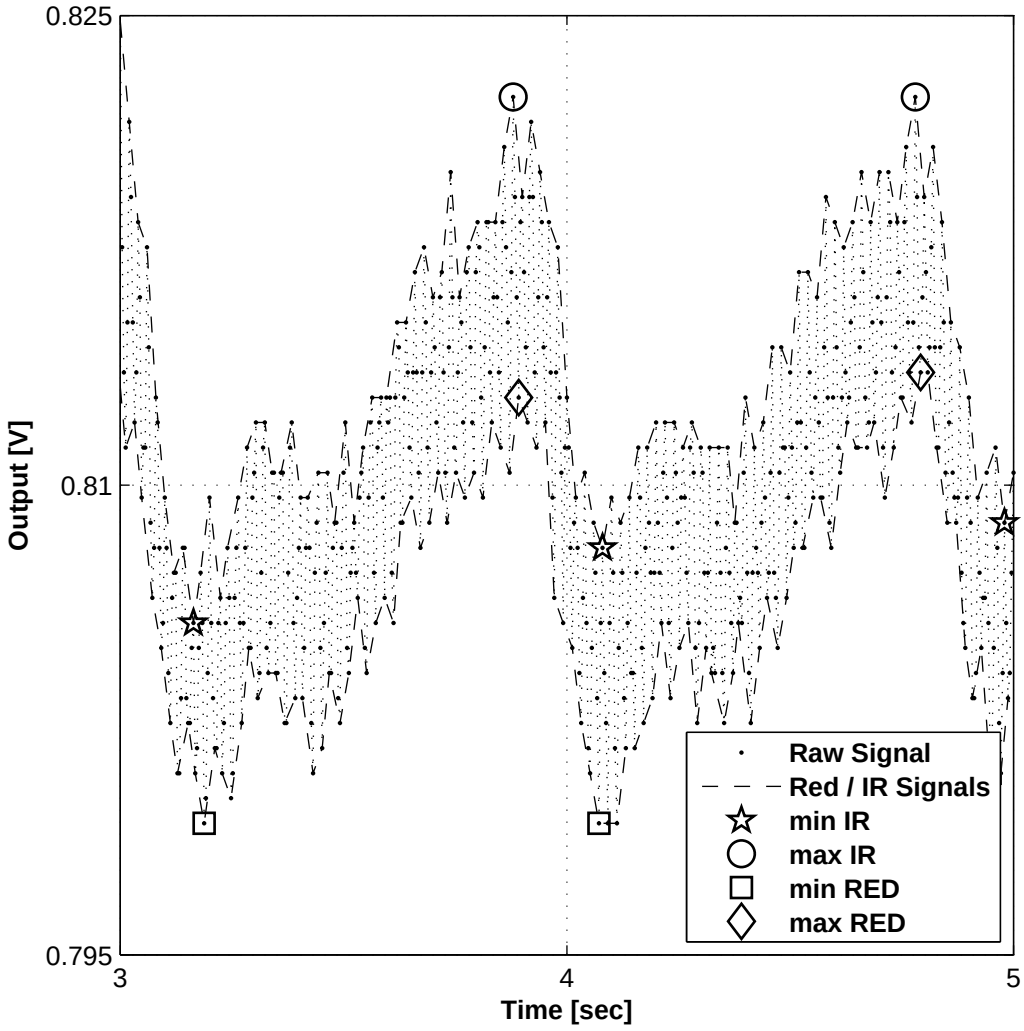

Figure 3.15: *Figure shows the raw signal data, the IR and red data as well as the minima and maxima of each signal used to calculate the ratio with equation (2.21) or (2.22).*

since it uses natural logarithm for calculations, but since our algorithm utilizes MATLAB it is a slightly more accurate method. The ratio computations are presented in all relevant measurements derived from 5-8 minima and maxima and presented as mR_{OS1} for mean values. Since the signal is unambiguous it is not possible to acquire the noise derivation from the mean, so called root-mean-square (RMS) value and thus a single numerical value for the SNR is also not possible. This thesis thus focuses on presenting the mR_{OS} values with the standard deviation (σ) as presented in equation (3.3).

$$\sigma = \sqrt{\left(\frac{1}{n-1}\sum_{i=1}^{n}(x_i - \bar{x})^2\right)} \tag{3.3}$$

Appendix A shows the MATLAB algorithm used to generate the result of all mR_{OS} calculations in Chapter 4, it presents methods for calculating the SpO_2 with both equation (2.21) and (2.22). Depending on the signal acquired some manual threshold changes might be needed to ensure the accuracy of the algorithm.

A common filter method used to smooth the data is to use a moving average filter on the extracted IR and red signal and then find the maxima and minima. The 4-point moving average filter used in some calculations of Chapter 4 can be described with the difference equation (3.4). Figure 3.16 shows a graphical interpretation of this 4-point and 8-point moving average filter on a IR, PPG signal. It is clear from the figure that it smooths out the data considerably thus lowering the σ of the signal.

$$y(n) = \frac{1}{4}x(n) + \frac{1}{4}x(n-1) + \frac{1}{4}x(n-2) + \frac{1}{4}x(n-3) \tag{3.4}$$

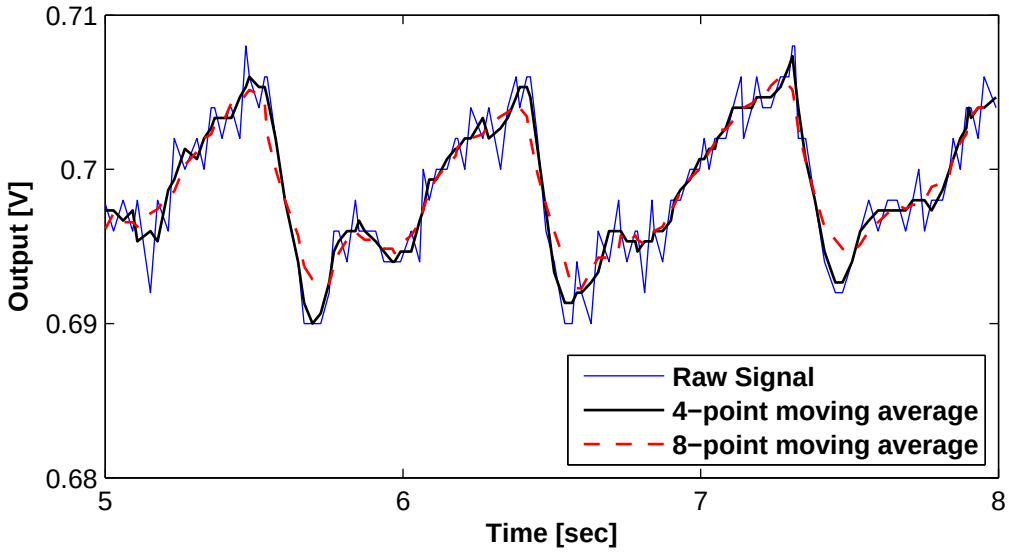

Figure 3.16: *Raw signal showed in comparison with signal filtered with a 4-point moving average filter shown in equation (3.4) and an extended 8-point moving average filter.*

3.4 Experimental testing of the device

There are numeral tests that where performed on the device, listed below:

1. Base testing with constant current
2. AGC testing on final version of device

3. Absorption due to epoxy coating

4. Absorption due to Parylene-C coating

5. Thermal radiation/effect of LEDs

6. Absorption of cattle fat tissue

Two measurement systems where used to acquire the measurement results. The first one (Oxmeter 1) is composed of three separate units, a 555 timer running at 715Hz combined with switching circuit, separate analog circuitry with a transimpedance amplifier, low-pass filter and non-inverting amplifier. The last part is an Tektronix TPS2014 oscilloscope with ADC. Oxmeter 1 has no AGC regulation and thus supplies constant current to the LEDs. The reason why the system was developed in separate units is the ease of changing the design, frequency of the timer and sampling frequency and resolution of the AGC. It thus has a convenient testing mechanism and it is possible to receive experimental data that can further improve the design of the final device. Oxmeter 1 was used for test measurements nr.1 and 3 to 6 with a constant LED drive current of 1mA, since the final system has to be low power the LED drive current was decided from initial tests and it was determined that a sufficiently good signal could be acquired with 1mA drive current.

For the base testing of the device main concern was to utilize the transreflectance probe, a signal was recorded with every finger of a single subjects hand. The signal was extracted so that about 10 minima and maxima were recorded when the subjects finger was sill and minimal motion artifacts or baseline drift where effecting the signal acquisition. Then the mR_{OS1} value where calculated with equation (2.21), $mSpO_2$, standard deviation and the difference from mean value where calculated.

The second system (Oxmeter 2) is a individual system that has a microprocessor protoboard (MSP430F1611) connected to a analog circuit, it is connected through RS232 serial-to-usb converter with a laptop that utilizes MATLAB to acquire the signal and process it. The block diagram of Figure 3.1 describes Oxmeter 2 accurately. It has a AGC feedback that enables it to change the LED drive current from 1.3mA to 2mA, this resolution can be further modified and increased by changing a set of resistors. The results for test measurements nr.1-2 are presented in Section 4.1.

Each probe is measured with same set of basic tests, as described above, before coating and after coating. That gives an estimate on both the intensity changes caused by coating as well as changes in mR_{OS1} values that are used to compute the $mSpO_2$. A single thickness of coating was manufactured with each coating method due to fabrication cost of the probe. The results from measurements nr.2 and 3 are presented in Section 4.3.

The temperature effect of the LEDs was tested with a constant supply current of 1mA and 7mA. A dual output, Fluke 52II temperature meter was used where the environmental temperature was measured with one thermocouple probe and the other thermocouple was placed directly on top of the PDI-E838 to measure the thermal radiation or surface temperature. The Fluke 52II model has an accuracy of $\pm 0.3\,^{\circ}\mathrm{C}$ [102]. The results from these measurements are presented in Section 4.2.

It was stated earlier in Section 2.1.1 that light can penetrate several millimetres in tissue and the associated scattered light several centimetres, it has also been stated in Section 2.4.2 that previous implantation places have included considerable amount of fat tissue. Yet another statement previously concluded in Section 2.1.3 that it is very hard to model the absorption and scattering of the composition of different tissue. The effect of fat tissue was measured by using similar measurement setup as previously, placing fat layers of different thickness on top of the probe and placing the thumb on top of that layer. Then the thickness of layers where varied from 0.5mm to 4mm, the results from this test measurement (nr. 5) are presented in Section 4.4.

4. RESULTS

Section 4.1 starts the chapter by presenting the measurement systems and a simple technical performance measurement that where conducted on the devices. The following sections then present different measurement result. Section 4.2 presents results from thermal radiation measurements. Section 4.3 presents the results from different coatings on the probe and Section 4.4 presents results from adipose tissue measurements.

4.1 Measurement system

As described earlier in Section 3.4, two devices where developed for the thesis and they where named Oxmeter 1 and Oxmeter 2. Figure 4.1 shows the MSP430 protoboard and PCB of Oxmeter 2. The boards are connected together with four wires, namely square wave output of processor to input on the oximeter, amplifier output to ADC input, supply voltage and ground. The main difference between the prototypes is difference in supply voltage, square wave frequency, sampling frequency and resolution of the ADC, but they utilize the same analog circuit and probe.

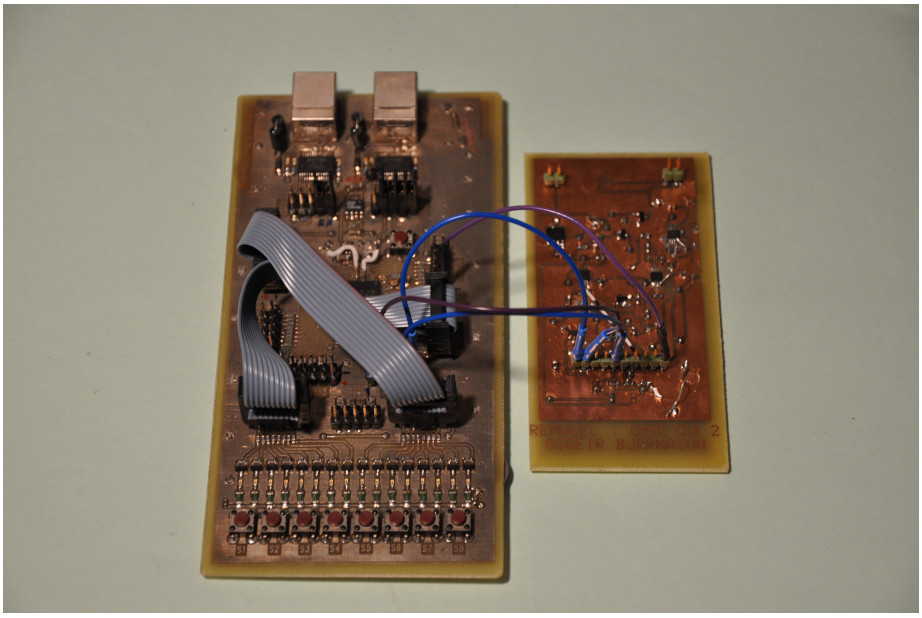

Figure 4.1: *The figure shows MSP430F1611 protoboard connected with the Oxmeter 2 PCB.*

Table 4.1 shows the technical specifications of both systems. The most interesting

parameters are the AGC in Oxmeter 2 that enables a LED drive current of 1.3-2mA and a slightly lower value of LSB that effects the resolution of the ADC.

Table 4.1: *Table showing the technical specifications of both measurement systems, Oxmeter 1 and Oxmeter 2.*

	Oxmeter 1	Oxmeter 2
Supply Voltage	4.5V	3.3V
LED drive current	$\approx$ 1mA	1.3-2mA
Sampling Rate	250Hz	$\approx$ 1kHz
Square Wave Frequency	716Hz	$\approx$ 200Hz
LSB	78 μV	0.61 mV

The ADC of the MSP430F1611 is 12-bit and it uses a reference voltage of 2.5V to have as high resolution as possible, hence the LSB is 0.61mV [103]. The sensitivity of the amplifier can be increased with amplification as shown earlier with equation (2.20). The TPS2014 oscilloscope utilizes 8-bit vertical resolution for the ADC [104], meaning that the window size used to view the signal is important. In this thesis all signals where acquired with 20mV resolution per window.

The relationship between the 2.5V reference voltage of the AGC and the 3.3V supply voltage of Oxmeter 2 works so that an integrator in the AGC feedback is fed with a certain reference voltage (for example 1/2 Vcc) and the LEDs are then controlled by the output of the integrator. If the DC level from the photosensor is less then 1/2 Vcc the output of the integrator will rise linearly until it reaches 1/2 Vcc and the opposite goes if the DC level is higher. A good design technique is to include amplification in the integrator circuit so that it matches the gain of the output amplifier, in our case 5. This changes the behaviour of the integrator from linear to charging behaviour set by the time constant of the integrator circuit. The complete circuit schematic can be seen in Appendix B.

Increasing LED supply current increases both the DC and the AC part of the signal amplitude. Figure 4.2a shows a signal acquired with 1mA supply current to the LEDs and Figure 4.2b shows a signal acquired with 7mA supply current to the LEDs. It is evident from those figures that the amplitude of both AC and DC level increases with higher LED supply current, in the case of Figure 4.2 the values almost double.

As stated earlier in Section 3.3 the signal is unambiguous and thus we can not find the SNR, we thus present the R_{OS1} with the standard deviation to give some estimate of the error. Table 4.2 shows the measurement result for Oxmeter 1. The table shows the R_{OS1} with standard deviation, as well as uncalibrated SpO_2 value derived with equation (2.16) and finally the difference between average SpO_2 measurement and each measurement spot. It is shown in Table 4.2 that the average σ is around 8%, that is a quite high value and indicates that a moving average filtering should be

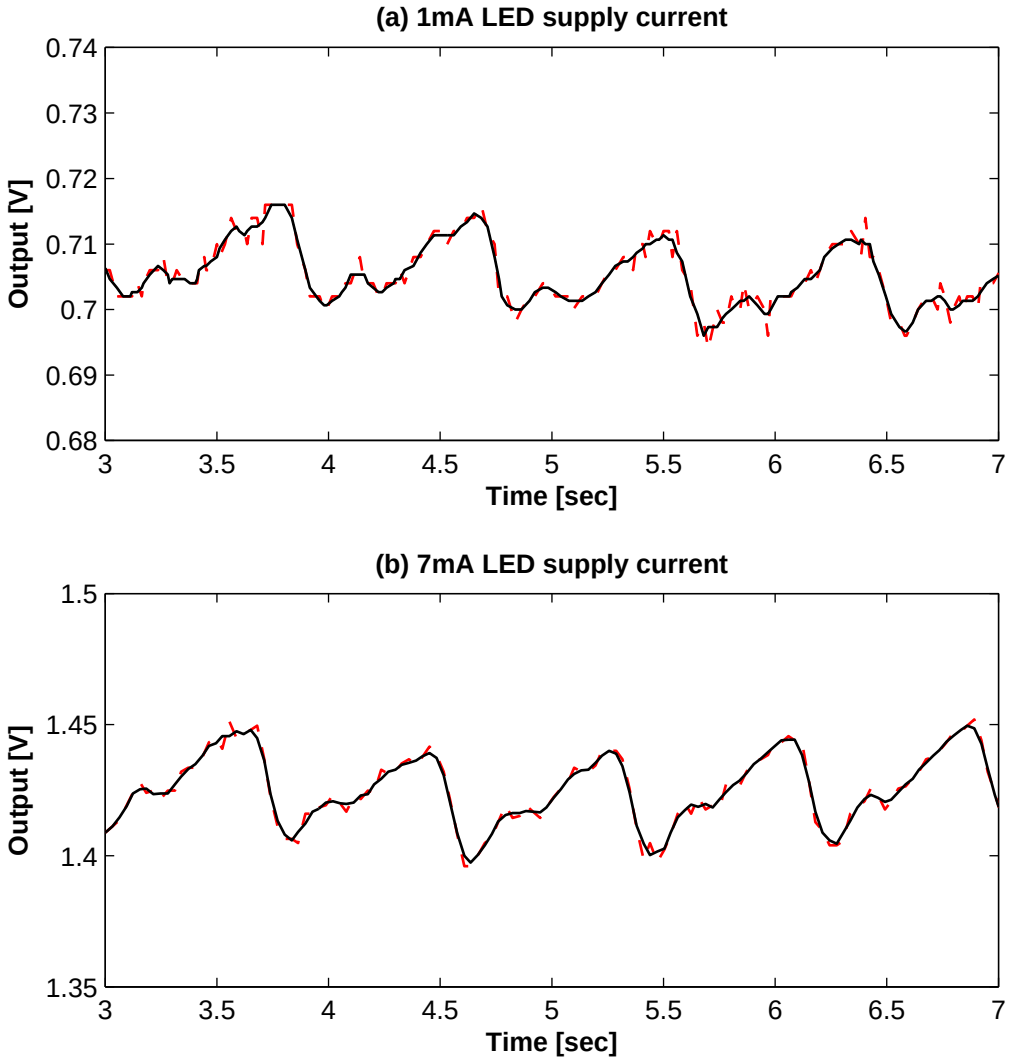

Figure 4.2: *The figure shows two IR signals extracted from measurements done with (a) 1mA LED supply current and (b) 7mA LED supply current. The raw signal is shown with red cut line while the black line shows the filtered signal, filtered with a 4-point moving average filter presented in equation (3.4).*

applied on the signal prior to ratio calculation such as shown in Figure 3.16.

Table 4.3 shows the same results as Table 4.2 but for Oxmeter 2, that the average σ presented is around 9% which is quite much higher than for Oxmeter 1. The variation between the average of calculated $mSpO_2$ and each measurement spot is only around 1%.

The data of Oxmeter 2 where also used to see how the moving average filter presented with equation (3.4) effects the σ of the measurements. The results can be seen in Table 4.4, it is evident from that result that changes in R_{OS1} are minimal but the σ is effected greatly since noise is reduced. The average σ for 4-point moving

Table 4.2: *Oxmeter 1 data showing the mR_{OS1} calculated from eight minimas and maximas with equation (2.21). Standard deviation (σ) as described by equation (3.3), uncalibrated $mSpO_2$ derived with equation (2.16) and the difference (Δ) between average $mSpO_2$ of all fingers and $mSpO_2$ of each finger.*

Finger	mR_{OS1}	σ	$mSpO_2$ [%]	Δ
#1	1.07	± 0.10	72.05	-2.49
#2	0.99	± 0.05	74.66	+0.12
#3	0.96	± 0.06	75.73	+1.19
#4	1.02	± 0.04	73.83	-0.71
#5	0.97	± 0.07	75.44	+0.90
#6	1.01	± 0.07	74.19	-0.35
#7	0.99	± 0.10	74.64	+0.10
#8	1.05	± 0.14	72.87	-1.67
#9	0.96	± 0.08	75.64	+1.10
#10	0.996	± 0.08	76.35	+1.81
Average	0.996	± 0.08	74.54	

Table 4.3: *Oxmeter 2 data showing the mR_{OS1} calculated from eight minimas and maximas with equation (2.21). Standard deviation (σ)as described by equation (3.3), uncalibrated $mSpO_2$ derived with equation (2.16) and the difference (Δ) between average $mSpO_2$ of all fingers and $mSpO_2$ of each finger.*

Finger	mR_{OS1}	σ	$mSpO_2$ [%]	Δ
#1	0.98	± 0.13	75.24	+1.62
#2	1.02	± 0.05	73.74	+0.12
#3	1.05	± 0.10	72.70	-0.92
#4	1.05	± 0.06	72.64	-0.98
#5	0.99	± 0.06	74.72	+1.10
#6	1.03	± 0.06	73.32	-0.30
#7	1.04	± 0.10	73.18	-0.44
#8	1.06	± 0.15	72.67	-0.95
#9	1.01	± 0.05	74.14	+0.52
#10	1.02	± 0.17	73.81	+0.19
Average	1.03	± 0.09	73.62	

average filter is only around 3.9% and for the 8-point moving average filter it is around 2.7%. It is important to limit the number of sample points used in a moving average filter since it creates a delay when processed with a DSP as well as reducing the amplitude of the signal. A optimal ratio between the length of a moving average filter and the sampling frequency was not determined in this thesis.

Table 4.4: *The table shows measurements conducted with Oxmeter 2 and presented earlier in Table 4.3, where the IR and red signals where filtered with both 4-point and 8-point moving average filter presented earlier with equation (3.4). The R_{OS1} and σ values are given for every finger measured.*

Finger	mR_{OS1} 4-point	σ 4-point	mR_{OS1} 8-point	σ 8-point
#1	0.96	± 0.033	0.96	± 0.016
#2	1.01	± 0.047	1.00	± 0.041
#3	1.02	± 0.033	1.00	± 0.028
#4	1.00	± 0.011	1.01	± 0.031
#5	1.01	± 0.015	1.00	± 0.010
#6	0.98	± 0.036	1.00	± 0.015
#7	0.99	± 0.042	0.97	± 0.024
#8	1.06	± 0.070	1.01	± 0.065
#9	1.00	± 0.039	1.00	± 0.042
#10	0.94	± 0.063	0.95	± 0.021
Average	1.00	0.039	1.09	0.029

4.2 Measurement of the thermal radiation of probe and coating

Temperature measurements where conducted by placing a double wired thermocouple directly on top of the LEDs and keeping it in place with a plastic clip, another thermocouple was placed freely measuring room air temperature at the same time. The temperature was measured with LED supply current of 1mA which was the supply current used in most experiments and with a LED supply current of 7mA. Table 4.5 shows the average temperature of the probe as well as the difference between environmental temperature and the thermocouple that is placed on top of the LEDs. As stated earlier in Section 3.4 the accuracy of the thermometer used is ±0.3 °C. Difference of measurements between environmental and probe was only around 0.05 °C for a LED supply current of 1mA, and it was inside the accuracy limit for 7mA LED supply current.

Table 4.5: *Temperature measurement of probe where thermocouple was placed directly on top of the LEDs and the temperature measured for 15 minutes every 20 seconds. Measurements where done with constant LED driving current of 1mA and 7mA. The average temperature is presented as well as the average difference (Δ) between environmental temperature and LEDs temperature.*

LED Drive - Current	Average Temperature [°C]	Δ [°C]
1mA	21.64 ± 0.09	0.35
9mA	24.02 ± 0.51	0.10

According to Walsh [105] it is possible to calculate the temperature rise for a short pulse of light following the principle that heating of a material with light is dependent upon absorption. Equation (4.1) shows this relationship where H_e is the surface radiant exposure given in units (Jcm^{-2}), ρ is the density and c is the heat capacity. Walsh gives a reasonable estimate for ρc in tissue as $\rho c \approx 4.2\ Jcm^{-3}\,^{\circ}\mathrm{C}$ and $\mu_a = 50\ cm^{-1}$.

$$\Delta T = \frac{\mu_a \cdot H_e}{\rho \cdot c} \tag{4.1}$$

In the datasheet of our LEDs we are given the radiant flux (P_O) = 2.4 mW at λ = 660nm and P_O = 1.8 mW at λ = 880nm for a supply current of 20mA [96]. We can relate this value to H_e by presenting equation (4.2) where E_e is the irradiance or the P_O incident on a surface. This means the temperature rise in tissue depends on the surface area exposed and the time it is exposed. Equation (4.3) is an expansion of equation (4.1) and combines this relationship. Where t is time of exposure and A is the surface area light is incident on.

$$H_e = E_e \cdot t = \frac{P_O}{A} \cdot t \tag{4.2}$$

$$\Delta T = \frac{\mu_a \cdot \frac{P_O}{A} \cdot t}{\rho \cdot c} = 2.857 \left[\frac{\mu m^2 \cdot\ ^{\circ}\mathrm{C}}{s}\right] \cdot \frac{t}{A} \tag{4.3}$$

Example is an area of the size 1mm x 1mm = 1 μm^2 and a pulse duration of 0.01 sec, gives $\Delta T = 0.02857\ ^{\circ}\mathrm{C}$.

There are two things equation (4.1) does not account for. First that there is no diffusion during the pulse, this becomes an issue if the duration of the pulse is shorter then the thermal relaxation time defined with equation (4.4). There Walsh gives an estimate of thermal diffusivity in human tissue as $\alpha \approx 1.3 \cdot 10^{-3}\ cm^2 s^{-1}$ and r is defined as the characteristic dimension of the absorbing target [105].

$$\tau_p \approx \frac{r^2}{4\alpha} \tag{4.4}$$

For the thermal relaxation time to be shorter than a pulse of 0.01 sec the surface area has to be larger than $5.2 \cdot 10^{-9} m^2$ or a circular object of diameter $82\mu m$, if not the tissue is cooled with diffusion. Secondly equation (4.1) does not account for any scattering, scattering can cause the local fluence (ψ) to be larger then H_e and thus it should be replaced with (ψ) in equation (4.1). It is quite obvious from these calculations that thermal effect of LEDs inside tissue is minimal and further theoretical accuracy is considered out of the scope of this thesis since it won't be of any value to the measurement system presented in this thesis.

4.3 Measurement of the effect of coating on the probe

The measurements done to estimate the effect of coating on the probe where conducted with three types of coating/probes as stated earlier; non-coated, epoxy-coated and parylene-C coated. The measurements where conducted with constant LED drive current of 1mA and with as similar measurement setup as possible before coating and after coating. The same probe was tested before and after coating, it was not possible to determine the exact amount of ambient light or environmental effect on the measurements other then all lights where turned off and the room kept dark to ensure minimum effect of outside ambient light or ambient light and 50Hz noise from room lights. The epoxy coated probe will be referred to as probe nr.1 and the Parylene-C coated probe will be referred to as probe nr.2 in some occasions.

4.3.1 Epoxy coating

Figure 4.3 shows the probe after being coated with epoxy, due to fabrication techniques the epoxy was slightly matt on the surface. The cast used to fabricate the probe was presented earlier with Figure 3.10 in Section 3.2.1. Table 4.6 shows the measurement data from the epoxy probe prior to coating (No-Coating) and after coating (Epoxy-Coating). The mR_{OS1} values that are given are calculated from equation (2.21) and an average value is calculated from 7 raw signal minimas and maximas.

Table 4.6: *Table shows measurements done on a single subject fingertips. The same probe was measured before and after coating with EPO-TEK 301-2FL medical grade epoxy. mR_{OS1} shows the average of 7 maximas and minimas as calculated with equation (2.21). Δ shows the difference between the coated and un-coated probe.*

Finger	mR_{OS1} No-Coating	mR_{OS1} Epoxy-Coating	Δ
#1	1.04	1.01	0.03
#2	1.00	0.97	0.03
#3	1.02	1.01	0.01
#4	1.02	1.08	-0.06
#5	1.02	1.06	-0.04
#6	1.02	0.97	0.05
#7	0.95	0.99	-0.04
#8	1.04	0.98	0.06
#9	1.04	1.05	-0.01
#10	1.08	1.09	-0.01
Average	1.023	1.021	0.002

It is important for the instrument design to present the difference in signal am-

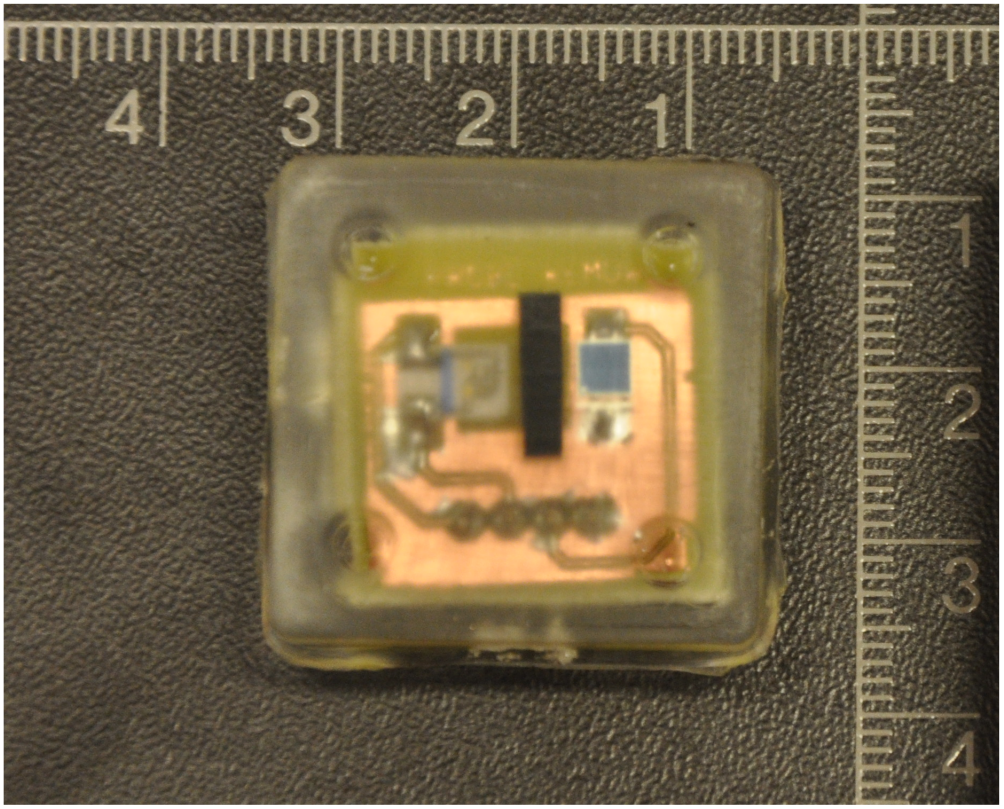

Figure 4.3: *The figure shows a measurement probe after being coated with 3.5mm thick layer of epoxy. The scale of the figure is in cm.*

plitude of the coated and un-coated probe. Figure 4.4 presents a bar chart of the DC level for the IR light measured from probe nr.1 before coating and after coating from a continuous recording of 10 seconds.

Table 4.7 presents the value of both DC and mean AC part of both wavelengths for the same signals as where presented in Figure 4.4 where the AC part is calculated from seven consecutive maximas and minimas. The last result presented for the epoxy coating is a graphical representation of the acquired signal. Figure 4.5 shows the signal before and after coating, the signals are presented as raw and filtered data with a 4-point moving average filter presented in equation (3.4).

Table 4.7: *The table shows amplitude recieved from the separated LEDs with the probe prior to coating and after being coated with epoxy. The DC values are calculated as average from 10sec recording and presented as DC. The mAC part is calculated as the average amplitude between seven maxima and minima.*

Measurement	DC_{IR} [V]	DC_{RED} [V]	mAC_{IR} [V]	mAC_{RED} [V]
No-Coating	0.913	0.905	0.027	0.027
Epoxy-Coating	1.987	1.982	0.015	0.016

As shown previously in Section 4.1 the σ drops significantly when the signal is

Figure 4.4: *The bar chart shows the DC level of IR light measured with probe nr.1 before coating (No-Coating) and after coating (Epoxy-Coating).*

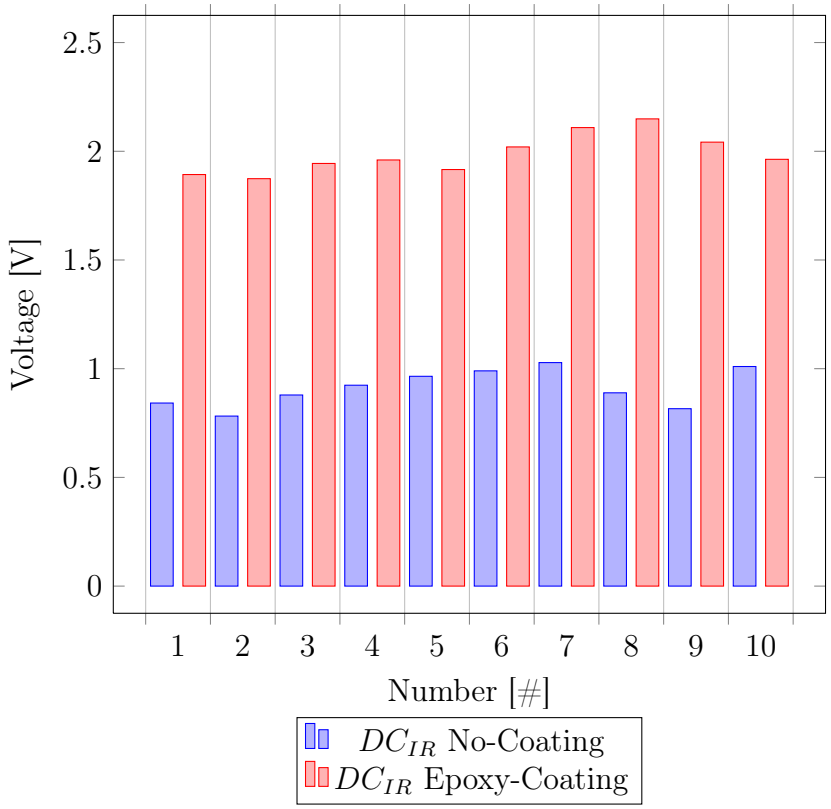

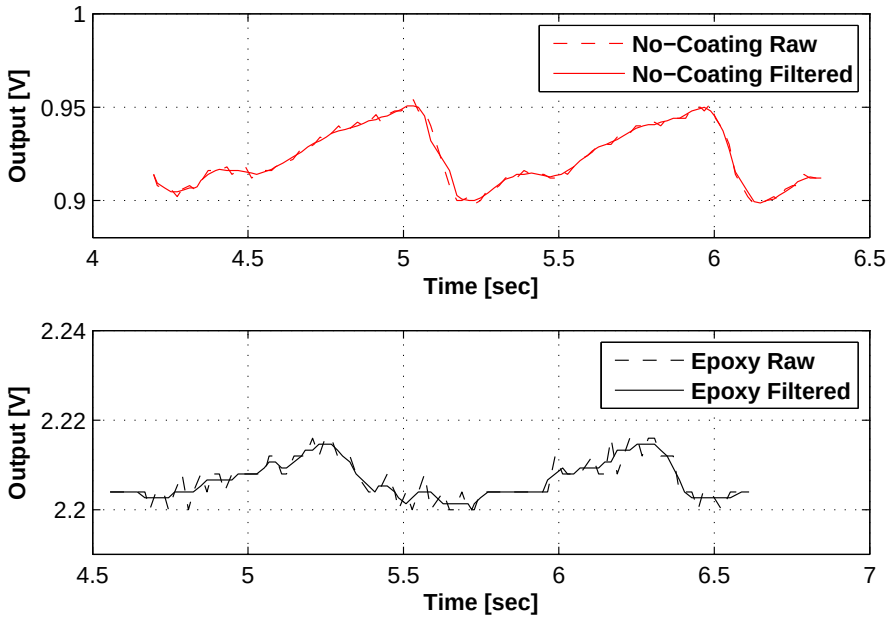

Figure 4.5: *The figure shows the IR signal acquired with probe nr.1 before coating (No-Coating) and after coating (Epoxy). The signals are presented as raw and filtered data with a 4-point moving average filter presented with equation (3.4).*

filtered with a moving average filter. It can be seen graphically from Figure 4.5 that the noise level for the epoxy coated probe is higher after the coating than before coating, this is partially explained by higher DC amplitude and lower mAC amplitude.

4.3.2 Parylene-C coating

The Parylene-C coating is very different from the epoxy coating as shown previously with the processing steps in Section 3.2.1, Figure 4.6 shows the probe after coating. It is evident from the figure that the coating is not visible and it can be hard for the naked eye to determine if a probe has been coated or not. This can easily be tested with a multimeter to see if there is contact in the ground plane.

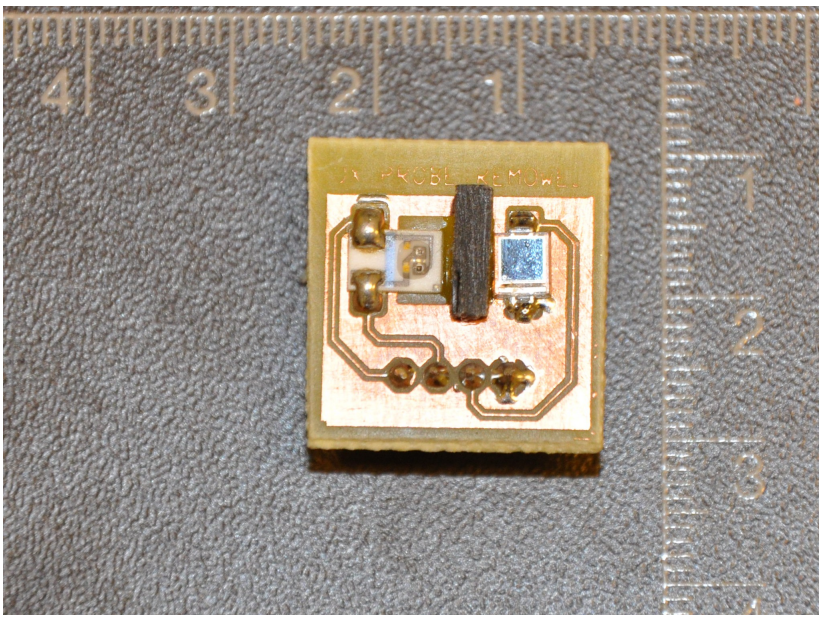

Figure 4.6: *The figure shows a measurement probe after being coated with 15 µm thick layer of Parylene-C. The scale of the figure is in cm.*

The Parylene-C coated probe was tested in the same way as the epoxy coated one, that is before and after coating measurements where conducted with constant LED drive current of 1mA. The results from those measurements can be seen in Table 4.8, where it can be seen that the average change in mR_{OS1} is only 0.004 between the coated and non-coated probe.

We present the same results as earlier for the Epoxy-coated probe, that is a bar graph representing the DC level for the received IR light before and after coating on a ten second recording, see Figure 4.7. From the bar graph it can be seen that the DC level is slightly lower then the DC level of the non-coated probe. Table 4.9 shows the mean value calculated for the DC and AC part of the signals presented in Figure 4.7 where the AC part is calculated from seven consecutive maximas and

Table 4.8: *Table shows measurements done on a single subject fingertips. The same probe was measured before and after coating of Parylene-C. mR_{OS1} shows the average of 7 maximas and minimas as calculated with equation (2.21). Δ shows the difference between the coated and un-coated probe.*

Finger	mR_{OS1} No-Coating	mR_{OS1} Parylene-C Coating	Δ
#1	1.07	0.94	0.13
#2	0.99	0.92	0.07
#3	0.96	1.03	-0.07
#4	1.02	1.11	-0.09
#5	0.97	0.98	-0.01
#6	1.01	1.06	-0.05
#7	0.99	0.92	0.07
#8	1.05	1.07	-0.02
#9	0.96	0.98	0.02
#10	1.00	1.05	0.09
Average	1.002	1.006	0.004

minimas. It can be seen from Table 4.9 that the amplitude of both DC and AC part of the signal is lower after coating.

Table 4.9: *The table shows amplitude recieved from the separated LEDs with the probe prior to coating and after being coated with Parylene-C. The DC values are calculated as average of 10sec recording and presented as mDC, the AC part is calculated as the average amplitude between seven maxima and minima.*

Measurement	mDC_{IR} [V]	mDC_{RED} [V]	mAC_{IR} [V]	mAC_{RED} [V]
No-Coating	0.856	0.852	0.026	0.023
Parylene-Coating	0.629	0.624	0.017	0.017

Just as with the epoxy coated probe a graphical representation of the signals acquired with probe nr.2 before and after coating are shown in Figure 4.8. It can be seen graphically from the figure that the amplitude of DC and AC part of the signal and noise level are similar for the non-coated and Parylene-C coated probe.

4.4 Measurement of the effect of cattle fat tissue

The reason for this test was simply to get a practical experience on how a fat tissue effects the SpO_2 signal that is acquired. The Parylene-C coated probe was used for the measurements and a constant LED supply current of 1mA was used as in previous test measurements. The fat tissue measurements were conducted with a piece of cow fat acquired from local supermarket, see Figure 4.9. Layers from 0.5mm

Figure 4.7: *The bar chart shows the DC level of IR light measured with probe nr.2 before coating (No-Coating) and after coating (Parylene-Coating)*

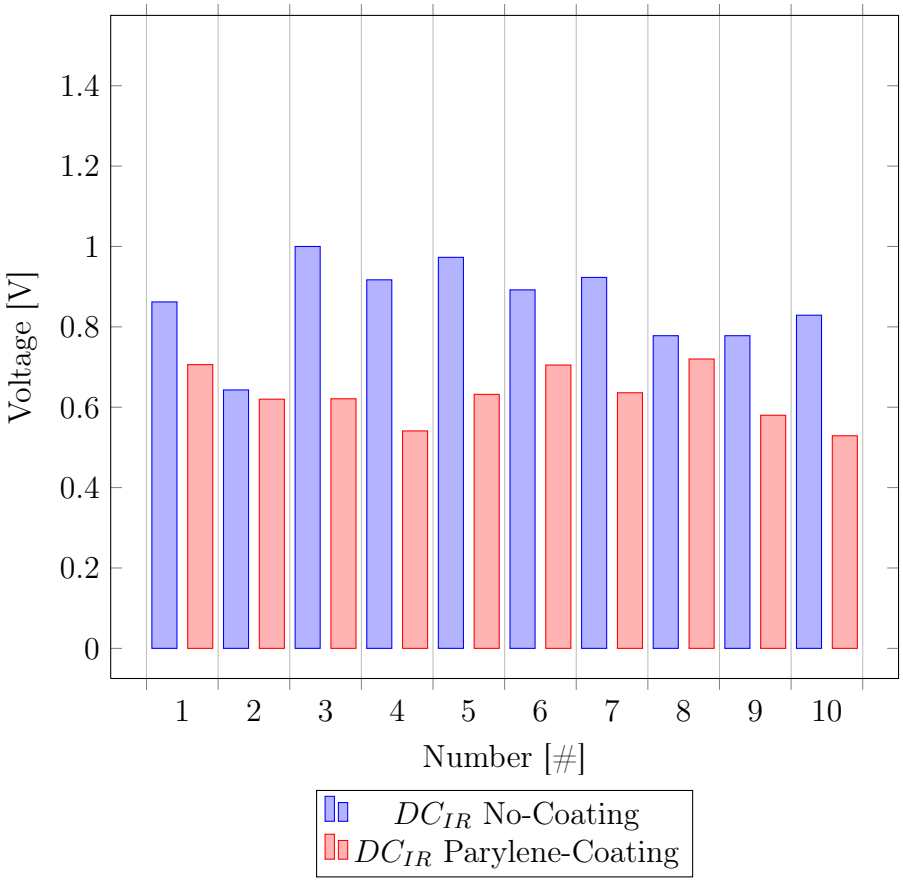

to 4mm were sliced from the original piece and tested by placing them on top of the probe and a finger on top of the fat layer as shown in Figure 4.10. It is not possible to guarantee that the fat is uniform though it is assumed in these measurements. The thickness of the fat is given in approximate value since it is quite elastic and measuring the thickness accurately is hard. In Section 2.4.2 we presented data of absorption coefficient for pig lard, that data gives us an estimate that light should pass quite easily through the cow fat tissue.

The results from the measurements can be seen in Table 4.10, where the m represents mean values that where calculated from six minima to maxima intervals such as the one shown in Figure 3.15. The DC and mAC measurements represent the amplitude and the values of mR_{OS1} are calculated with equation (2.21) and σ with equation (3.3). The Δ represents the difference in R_{OS1} between measurements with no fat tissue on top of the probe and measurements with fat tissue on top of the probe.

The measurements from the $\sim 4mm$ were estimated from a single minima and maxima since the signal strength reduced quite much and that explains why there is no result presented for the $m\sigma$. It has been shown previously that by using a

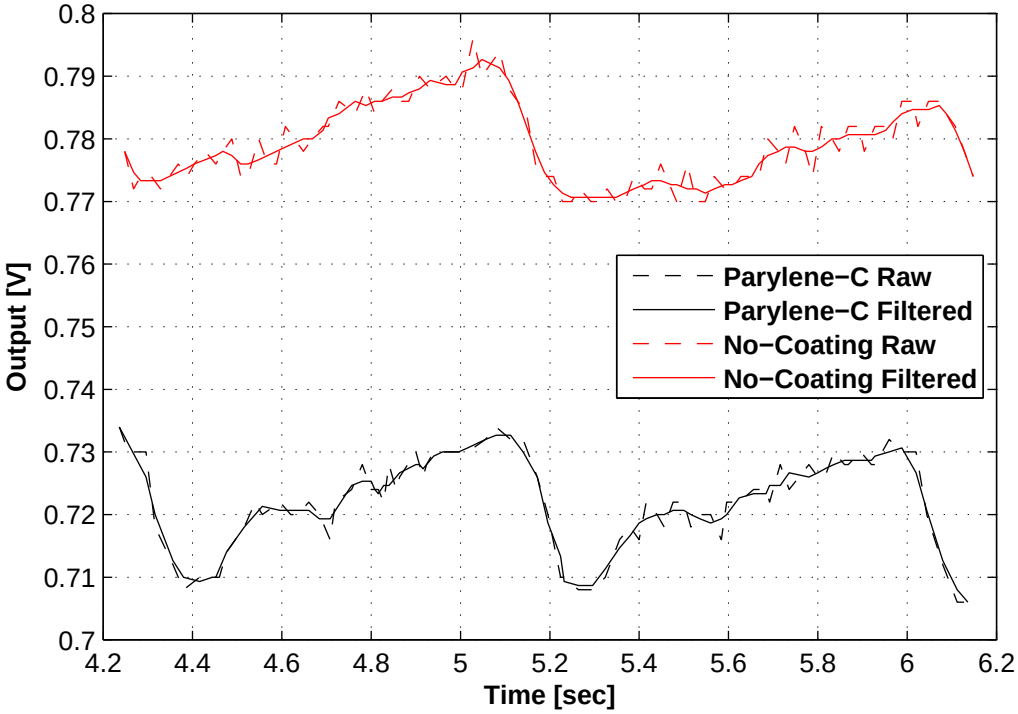

Figure 4.8: *The figure shows the IR signal received from probe nr.2 before coating (No-Coating) and after coating (Parylene-C). The signals are presented as raw data as well as after being filtered with a 4-point moving average filter presented in equation (3.4).*

Figure 4.9: *The figure shows a piece of cow fat acquired from local supermarket, the piece is around one centimetre thick. The scale of the image is in cm.*

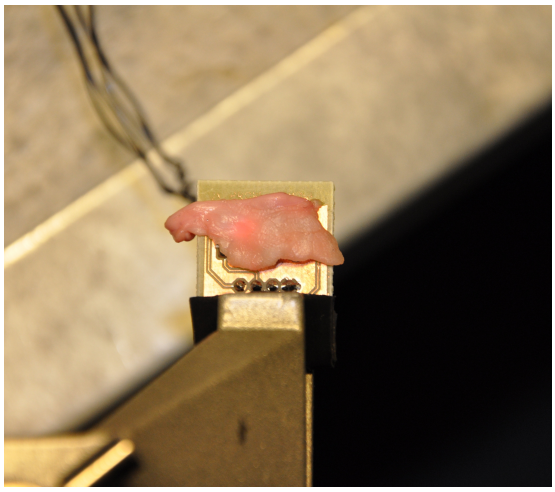

Figure 4.10: *The figure shows one millimetre thick layer of cow fat placed on top of the probe, prior to measurements*

moving average filter it is possible to reduce the noise in the signal significantly. An example of this is Figure 4.11 where the whole piece of fat tissue shown in Figure

Table 4.10: *The table shows number of measurements as a function of fat tissue thickness, the measurement included in the upper part of the table are the DC_{IR}, DC_{RED}, mAC_{IR} and mAC_{RED}. The R_{OS1} is calculated from equation (2.21), the $m\sigma$ is calculated from equation (3.3) and Δ shows the difference between the R_{OS1} for measurement with no-fat and fat tissue. All the measurement except the 4mm thickness are measured from six maximas and minimas.*

Measurement	no-fat	$\sim$ 0.5mm	$\sim$ 1mm	$\sim$ 2mm	$\sim$ 3mm	$\sim$ 4mm
DC_{IR} [V]	0.6935	0.7080	0.6863	0.6678	0.6020	0.3420
DC_{RED} [V]	0.6905	0.6997	0.6791	0.6612	0.5954	0.3380
$mAC_{IR}[V]$	0.0196	0.0196	0.0131	0.0160	0.0129	0.0048
mAC_{RED} [V]	0.0190	0.0191	0.0125	0.0160	0.0134	0.0048
mR_{OS1}	0.9984	0.9750	1.0136	0.9623	1.0529	0.9906
σ	0.0526	0.1580	0.1494	0.0739	0.1718	N/A
Δ	0	-0.0234	0.0152	-0.03607	0.0545	-0.0078

4.9 is placed on top of the probe, the piece is around 1cm thick and has a thin layer of meat on it as well as a tendon between the fat layer and the meat. The raw signal in Figure 4.11 has obviously too much noise for anything to be distinguishable from the raw signal, but after filtering with 8-point moving average filter, it is possible to see the PPG signal.

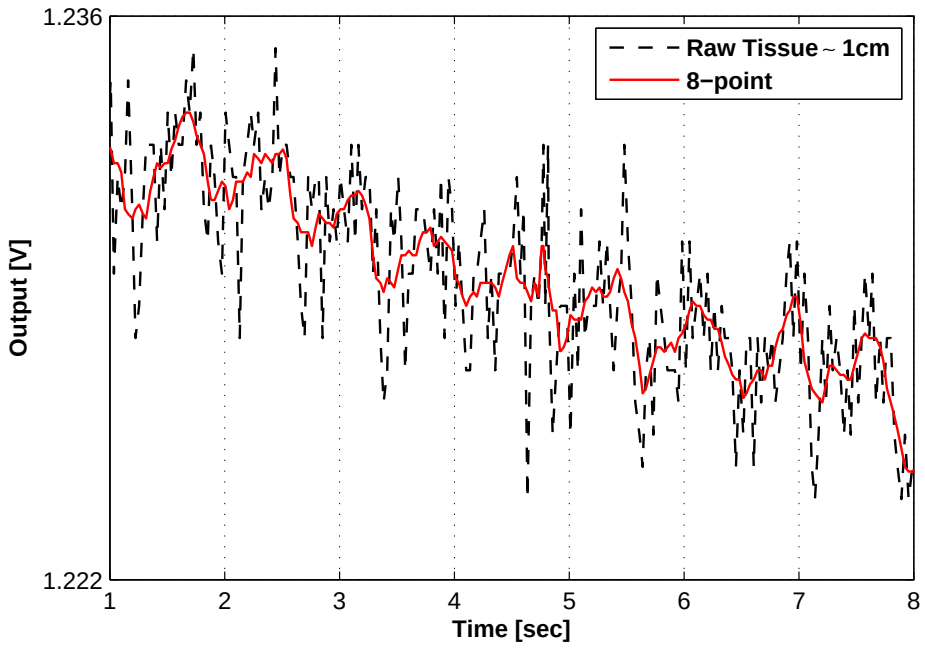

Figure 4.11: *The figure shows a raw signal acquired by placing the piece of tissue shown in Figure 4.9 on top of the probe and a finger on top of that. It is not possible to distinguish the PPG signal from the raw data but when filtered with a 8-point moving average filter the PPG signal becomes visible. The piece of tissue is not uniform fat, it includes a piece of tendon and meat.*

Table 4.10 and Figure 4.12 show that the DC part of the signal drops as the thickness of the fat layer increases. The change is quite small until the $\sim 4mm$ layer is measured. The amplitude of the AC part of the signal changes much less compared to the DC part. There is not a big difference in the mR_{OS1} value between tissues though there is some increase in the mσ meaning the noise level gets slightly higher when increasing the thickness of fat. Figure 4.11 contradicts this since the DC level is around 1.230, the reason for this is probably backscattering from the meat or tendon increasing the DC part of the signal. This clearly shows how different tissues reflect and absorb the light and how problematic it is to model it.

Figure 4.12: *The bar graph shows the DC part of the IR and red LEDs as a function of fat tissue thickness.*

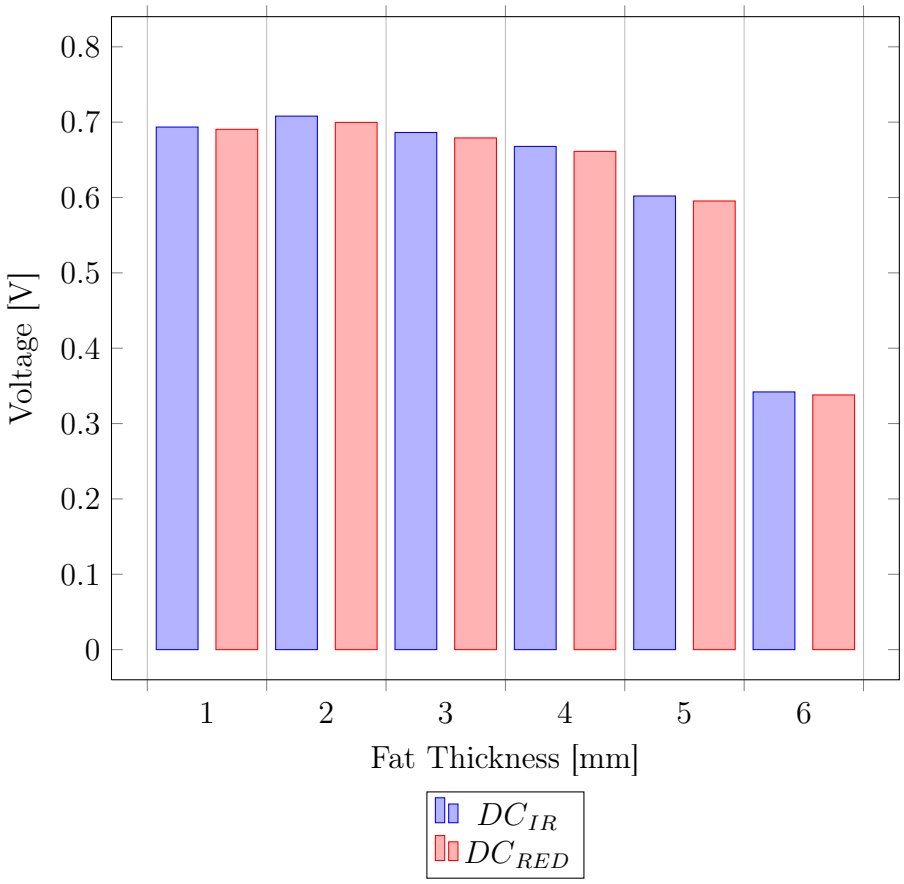

5. DISCUSSION

In this chapter we will discuss the results presented in Chapter 4 as well as other results that can be discussed from this thesis. Section 5.1 discusses the implemented measurement system, how it performed and minor improvements/optimizations that can be made to it. Section 5.2 discusses the test measurements that were performed, such as temperature, coating and fat tissue measurements. Finally Section 5.3 discusses both the future impact of such a device as well as future developments and major improvements that could be made on the current device.

5.1 Measurement system

Two measurement devices have been presented in this thesis, the first one previously discussed as Oxmeter 1 and the improved version Oxmeter 2. Both measurement systems where successful in giving a measurement of uncalibrated oxygen saturation, though calibration of such a meter would be necessary before implantation. When discussing the measurement system it is important to keep in mind that the purpose of the system developed in this thesis is first and foremost to develop and justify a device that is able to make measurements *in vivo*. For the external measurements the R_{OS1} value calculated in most test measurements was quite constant correlating to uncalibrated SpO_2 values of around 75% which in accordance with the theory since human SpO_2 measurements under normal conditions don't variate much from the 96-99 %.

It was shown in Section 4.1 that both systems have quite high σ when measured without any filtering, on average 8% for Oxmeter 1 and 9% for Oxmeter 2, this difference can be partially explained by lower sampling rate and higher resolution of Oxmeter 1 compared to Oxmeter 2 while Oxmeter 2 has higher LED supply current, this explains why the difference is only around 1%. In this thesis the standard deviation (σ) has been used as a measure of noise in the PPG signal acquired. More interesting result was presented in Table 4.4 of Section 4.1 where a 4-point and 8-point moving average filter previously presented with equation (3.4) where used to filter the separated IR and red PPG signals. This filtering lowered the standard deviation of Oxmeter 2 measurements to 3.9% and 2.7%.

The AGC of Oxmeter 2 worked fine even though it drove the the LEDs supply current to its highest possible value in all our measurements. This is explained by

the reason that the integrator is grounded to 1/2 Vcc in the tests, meaning that the DC output of the photosensor has to be higher then 1/2 Vcc. To test the AGC the light in the room was turned on, it saturates the photosensor driving the DC level output to become higher and thus the LEDs supply current controlled with the AGC output voltage lowers. This can be optimized with setting the ground voltage of the integrator or changing the gain of the integrator, if a non inverting amplifier setup is used as an integrator a time constant is created that slows down the response of the integrator. Thus a slower response to DC level changes occur, which is a desired quality for the implantable meter. The reference voltage of the ADC is also important when discussing the gain of the AGC versus the gain of the output amplifier. When a meter would be implanted for test measurement, it would be desirable to have higher interval for the LED supply current, since it was shown in Figure 4.2 that higher supply current creates higher amplitude in signal.

The sampling frequency of Oxmeter 2 can be lowered significantly, since Oxmeter 1 utilized a sampling frequency of 250Hz and the amount of noise was not considered significantly higher. A sampling frequency of around 30Hz should be sufficient to get quality maxima and minima of the PPG signal. The filter response of the output filter of the device should also be redesigned to get a sharper frequency response.

5.2 Interpretation of measurement result

5.2.1 Measurement of the thermal radiation of the probe

In Section 4.2 there are presented results from the temperature measurements of the probe without coating for two LED drive currents, 1mA and 7mA. It is evident from those measurements presented in Table 4.5, that the LEDs do not heat up with such a low drive current. Since our system utilized at the highest a 2mA drive current, it was not considered necessary to do further temperature testing on the coated probe to ensure the FDA standard mentioned in Section 2.5.

A simple theoretical model predicting the temperature increase due to absorption is presented, though it is just a rough estimate and it utilizes slightly higher values for most parameters than the implantable device would have. From that theoretical model presented with equations (4.1), (4.2) and (4.3) we are able to show that the effect of LEDs temperature or radiation on the internal tissue will be very minimal if any. The model does not account for any scattering inside the tissue which would severely complicate the calculations and was considered out of the scope of the thesis. This could be modelled with similar methods as scattering of lasers inside tissue, presented in [26, 78].

5.2.2 Measurement of the effect of coating on the probe

This is the most unique part of the test measurements in the thesis since no coating studies have been conducted on SpO_2 probes in literature. It is crucial for a working implantable SpO_2 meter to have a probe that is biocompatible and functioning correctly *in vivo*. Tables 4.6 and 4.8 show that the difference in the ratio calculation before and after coating of epoxy (probe nr.1) and parylene-C (probe nr.2) is very small. Table 5.1 below summarizes this results, where the No-Coating difference is simply the average mR_{OS1} difference between probe nr.1 and nr.2 prior to coating. This results indicates that coating of the probe with either epoxy or parylene-C has minor effect on the ratio computation compared to the manufacturing difference of the probes. This also shows clearly that each probe manufactured has to be calibrated to get the most accurate result.

Table 5.1: *The table shows comparison values from the coating tests were No-Coating represents the difference between mR_{OS1} for probe nr.1 and probe nr.2 prior to coating. The epoxy and parylene-C are shown as difference in mR_{OS1} before coating and after coating of each probe.*

Coating Type	Δ mR_{OS1}
No-Coating	0.021
Epoxy	0.002
Parylene-C	0.004

Table 5.2 presents comparison result for the amplitudes of Tables 4.7 and 4.9 where the difference between the non-coated probe and coated probe is presented. This summarizes well the data presented in Figures 4.4 and 4.7 where the DC level of the received IR wavelength was presented.

It is clear from this result that the DC level increases $\approx$ 1 V when the probe is coated with epoxy. Even though the optical transmittance of EPO-TEK 301-2FL medical grade epoxy is 99% as stated earlier in Section 2.5, the added thickness on top of the photosensor and LEDs, increase the level of light that hits the sensor without being absorbed by tissue. This is quite visible when the LEDs are turned on the epoxy clearly colors up and radiates pass the POM barrier. This could be studied further and tested with different epoxy thickness and probe designs, this thesis is limited to a single probe and coating due to fabrication cost of each probe.

The Parylene-C coating on the other hand reduces the DC-level of $\approx$ 0.230 V, this is lower than expected since previous studies with a layer of 20 μm showed optical transmittance of 95 % as stated in Section 2.5. Studies measuring the effect of Parylene-C coating on photosensors were not found in literature and could be studied in more detail. The difference of amplitude in the AC part of the epoxy coated probe was lower than for the Parylene-C coated one as presented in Table

Table 5.2: *The table shows a comparison result from Tables 4.7 and 4.9 where DC and the average AC values of the amplitude is compared before and after coating of epoxy and parylene-C.*

Coating Type	$\Delta\ DC_{IR}$ [V]	$\Delta\ DC_{RED}$ [V]	$\Delta\ mAC_{IR}$ [V]	$\Delta\ mAC_{RED}$ [V]
Epoxy	+1.075	+1.077	-0.012	-0.011
Parylene-C	-0.231	-0.228	-0.006	-0.006

5.2, where it is around 12mV compared to 6mV for the Parylene-C coated probe. The AC amplitude of the Parylene-C coated probe complies pretty well with the DC amplitud as presented in Table 4.7 where it is degraded around $\approx 73\%$.

5.2.3 Measurement of the effect of cattle fat tissue

The measurement of fat tissue effect was shown in Section 4.4, it was mainly done to get some practical experience on how the light might propagate through the fat tissue since there is no perfusion in the fat layer. Figure 2.17 in Section 2.4.2 had already shown that the absorption coefficient of pig fat is very low compared to other tissue and water as shown in Figure 2.5 and in Table 2.2. In our measurements layers from 0.5mm to 4mm where placed on top of the probe and the R_{OS1} measured without any filtering. The result presented in Table 4.10 shows mainly two things, the first is that the amplitude of the DC or AC part is not affected greatly until 4mm thick layer of fat, Figure 4.12 shows this in an intuitive way that can be compared to Figures 4.4 and 4.7. When the figures are compared it is clear that the coating process has more constant effect while the effect of fat depends on how uniform thickness it has.

Secondly the data in Table 4.10 shows that there is not much change in the average R_{OS1} measurements as shown with Δ, but the $m\sigma$ is slightly higher in most cases. This indicates that noise increases in relationship with thickness of fat. It should be emphasized that this test was quite unscientific and the effect of fat absorption and scattering from this measurement should not be taken literally. The test still indicated that SpO_2 meter could function in an environment with some millimeters of fat surrounding it. When filtered with a moving average filter as Figure 4.11 shows, the thickness of tissue can be up to one cm without having any perfusion, as long as light will get in contact with well perfused tissue.

5.3 Future considerations

This thesis has focused on developing a device that could be used for prototype measurements of implantable SpO_2 signal. It has focused on problems that have little or no publications instead of copying classic SpO_2 meter approaches. This

leaves room for many improvements that can be done on the device. This also creates a foundation for a discussion on the future impact of an implantable SpO_2 meter.

5.3.1 Future developments and improvements

There are many minor and major improvements that can be done on the current system. Few of the minor ones listed in previous sections and chapters are to improve the low-pass filter of the output amplifier, optimizing the AGC regulation, explore more in depth the effect of coating on both LEDs as well as photosensors and to develop further the fabrication method of the epoxy coating.

The major improvements are mostly related to the power consumption of the device, this thesis focused mostly on the LEDs power consumption since literature review reveled it as major part of the power consumption, see Section 2.7. In Oxmeter 2 the most power consuming component is the transimpedance amplifier OPA380 with a quiescent current $\approx$ 6.2mA at 3.3V Vcc. As stated previously in Section 2.7 Sarpeshkar *et al.* [31, 87] have designed an ultra-low power transimpedance amplifier that has a logarithmic response thus amplifying the AC part of the signal much more than the DC part. It has been stated previously several times that in implantable SpO_2 measurements there is a possibility of low perfused signal, Sarpeshkar transimpedance amplifier would thus fit perfectly to our need.

Another major development is the pulsing of the LEDs, we utilize a simple square wave from the MCU but more common in SpO_2 measurements is to have switching circuit that first lights the red LED then there is a timing interval during which there is no light and then the IR LED is lighted on. This gives a measurement of the ambient light that is effecting the meter, it can thus be removed from both the red and IR PPG signals. This was considered unnecessary since it increases the complexity of the circuit and ambient light measured *in vivo* is expected to be minimal. Yet another improvement on the pulsing of the LEDs would be to utilize PWM as stated previously in Section 2.6, then it is possible to reduce the duty cycle of the LEDs supply current and thus reducing the overall current consumption by turning the same LED on and off multiple times with a high frequency before switching to the other LED.

The calibration of the meter is something that would have to be done to validate the measurements. Calibrating an SpO_2 meter is becoming a standard procedure but quite expensive since it utilizes a CO-oximeter or intravenous meter and the oxygen percentage of the subject has to be varied for full accuracy. As stated earlier in Section 2.1.3, theoretical methods have failed to give an universal calibration equation. According to Moyle many research groups are currently working on calibration methods that utilize human blood in artificial circulation [24].

Further Signal Processing methods can as well be developed, both in analog and digital domain. An optimizing point on how much work is there worth doing on the MCU or DSP that is utilized in the final device. The algorithm presented in this thesis is mainly for post processing in MATLAB, it would be possible to modify it to run on a DSP but some kind of adaptive thresholding method would have to be written for that. Another interesting processing point is the separation of red and IR PPG signals and to even separate the DC and AC parts to acquire the highest SNR by amplifying only the AC part. The moving average filter presented earlier can be implemented easily on a MCU or a DSP once the separation of the PPG signals have been done. These signal processing implementations have to be less power consuming then recording the whole signal. Since the PPG signal is a quite slow varying one, that might not be optimal.

The final development listed here is about the implantation procedure, we have suggested placing the implant near the ribs of the cow in a similar position as previous implants thus we are able to acquire backscatter as well as internal scatter from tissue. This should be discussed with the veterinarians from previous implants in the Remowel project.

Another interesting thing to develop would be to have some kind of porous biopolymer on each side of the implants surface that cells could grow in, thus keeping the implant more still, since we know from literature and own experience that movement of probe to tissue creates big motion artifacts as shown in Figure 2.13.

5.3.2 Future impact

There does not exist an implantable SpO_2 meter on the market and papers previously published on the topic have focused on human measurements and applications. Respiratory diseases and specially BRD are the most common family of diseases that effect both feedlot- and dairy-cattle as stated previously in Section 2.4.1. Since external SpO_2 measurements on cattle are time consuming, mostly because shaving is needed and the thick skin and fur of the cattle it is not a standard procedure when diagnosing respiratory problems. The diagnoses more commonly used are respiratory rate counted over one minute, breathing noise and body temperature of the cow [67]. Those methods fail to detect diseases in their earliest stages and thus they are easily transmitted between cattle. An implantable SpO_2 meter could help in those situations and a complete device measuring SpO_2, respiratory rate and body temperature would be ideal.

Those kind of application are mostly considered as a research tool for scientists since implantations are still quite rare and expensive and not standardized procedure in stables. In last years serious respiratory diseases have spread across the world such as the H1N1 and H5N1 more commonly know as "swine flu" and "bird flu".

They have spread in animals and humans, an implantable SpO_2 meter could be used in drug development studies for such diseases. This device could also be utilized for other animals, we have stated previously in Section 2.3 that cattle move less than other domesticated animals and is thus an ideal candidate to test such a device. Another application is SpO_2 meters that are already used externally for rats and mice in toxicology and drug development studies, an implantable SpO_2 meter could be used in such measurements. A more futuristic approach would be incorporate respiratory monitor in race horses that would measure both respiratory rate and SpO_2 for optimized training purposes. If the implantation procedure is simple and cheap enough such as in the case of radio-frequency identification tags (RFID) tags the possibilities are even greater, with the possibility of utilizing an implantable SpO_2 meter for monitoring purposes.

6. CONCLUSION

This thesis presented a novel device for implantable SpO_2 measurements, that can help to diagnose respiratory diseases not only in dairy-cattle but as well other animals. The benefit of this diagnosing method is mainly thought to help in the detection of BRD which is the main cause of mortality and morbidity in both feedlot- and dairy-cattle. It presents an application that can be used as a monitoring device for outbreaks, for drug response monitoring and to be incorporated in the well-being monitoring device previously developed at TUT for the Remowel project.

The thesis covers wide scope of topics related to the thesis title, where the main focus was on developing a prototype device that could work *in vivo*. No implantable commercial device exists that records SpO_2 and only handful of publications exist on the topic that cover mostly basic approach to SpO_2 measurements. The first approach was to solve a number of minor problems regarding the device design and development, such as the circuit design and components selection, power consumptions of LEDs, AGC control of LEDs, noise filtering of the signal, and processing of the data.

When the prototype device had been developed the author of this thesis decided to focus more on topics where little or no publications had been done. Those topics are related to the biocompatability of the probe which include coating of the probe and thermal effect on tissue from the probe. Another topic is related to the effect that fat tissue, surrounding the probe, will have on the signal acquisition.

Two types of coatings where conducted on a set of special probes designed and manufactured for the thesis, the coating types included epoxy coating with medical grade epoxy and Parylene-C coating. Both types of coatings differ in texture and processing methods, where Parylene-C had a more complex processing method but with lesser effect on the signal. The thesis points out an opportunity to research the effect of coating on both LEDs as well as photosensors, since there is a lack of publications focusing on this topic. The thermal effects of the probe on the tissue was considered minimal from measurements and theoretical calculations. It is possible to study the thermal effects in a greater aspect with an active field of human tissue modelling existing. A practical test was conducted with cow fat acquired from local supermarket. Although the test can not be taken literally it gives an estimation of the effect that fat tissue has on SpO_2 measurements where there is no perfusion.

With some minor signal processing methods it was possible to acquire signal through 1cm thick tissue that had no perfusion.

Implantation is an expensive procedure and it is the author's believe that the main complications for implantable SpO_2 measurements have been solved in this thesis. The main output of the work starts with a novel prototype of a SpO_2 meter optimized for implants in both functionality and number of components used, and it is followed by new research on coating and fat tissue effects, which is crucial information prior to implantation. Analyses of the noise that would possibly affect the signal were conducted from data of previous implants from the Removel group. Those analyses pointed out that the dairy-cow is an ideal candidate to test such a device since it moves less and slower than other domesticated animals. It is thus proposed that further development of the device would need some measurement data from *in vivo* measurements, only then possible applications for other animals could be developed.

REFERENCES

[1] J. Riistama and T. Vuorela. Implantable measurement device to assist in determining the psycophysiological well-being of a dairy cattle. Technical report, Tampere University of Technology, 2010.

[2] J. Riistama, J. Väisänen, S. Heinisuo, J. Lekkala, and J. Kaihilahti. Evaluation of an implantable ECG monitoring device in vitro and in vivo. *Proceedings of the 29th Annual International Conference of the IEEE EMBS Engineering in Medicine and Biology Society in conjunction with the Biennial Conference of the French Society of Biological and Medical Engineering (SFGBM), Lyon, France*, pages 5703–5706, 2007.

[3] J. Riistama, J. Väisänen, S. Heinisuo, H. Harjunpää, S. Arra, K. Kokko, M. Mäntylä, J. Kaihilahti, P. Heino, M. Kellomäki, O. Vainio, J. Vanhala, J. Lekkala, and J. Hyttinen. Wireless and inductively powered implant for measuring electrocardiogram. *Medical and Biological Engineering and Computing*, 45:1163–1174, 2007.

[4] J.B. Ruchala. Applications of pulse oximetry. In J. G. Webster, editor, *Design of Pulse Oximeter*, chapter 13, pages 214–233. IOP Publishing Ltd, 1997.

[5] H. Härtel, S. Nikunen, E. Neuvonen, R. Tanskanen, S-L. Kivelä, P. Aho, T. Soveri, and H. Saloniemi. Viral and bacterial pathogens in bovine respiratory disease in finland. *Acta vet. scand.*, 45:193–200, 2004.

[6] C.V. Bagley. Animal health fact sheet : Bovine respiratory diseases. Technical report, Utah State University, 1997.

[7] J. TB Moyle. *Pulse Oximetry*, chapter 3, pages 15–35. BMJ Books, 2002.

[8] R. Brinkman and W.G. Zijlstra. Determination and continuous registration of the percentage of the percentage oxygen saturation in small amounts of blood. *Arch. Chir. Neerl.*, 1:177–183, 1949.

[9] W.G. Zijlstra and G.A. Mook. Medical reflection photometry. *V.Gorcum Ltd.*, 1962.

[10] A. Cohen and N. Wadsworth. A light emitting diode skin reflectance pulse oximeter. *Med. & biol. Engng*, 10:385–391, 1972.

[11] Y. Enson, W.A. Briscoe, M.L. Polanyi, and A. Courand. In vivo studies with an intravascular and intracardiac reflection oximeter. *J. appl. Physiol.*, 17:552–558, 1962.

[12] M.L. Polanyi and R.M. Hehir. In vivo oximeter with fast dynamic response. *Rev. Sci. Instrum.*, 33:1050–1054, 1962.

[13] C.P. Lau, Y.T. Tai, W.H. Leung, S.K. Leung, J.P. Li, and C.K. Wong. Rate adaptive cardiac pacing using right ventricular venous oxygen saturation: quantification of chronotropic behavior during daily activities and maximal exercise. *Pacing Clin Electrophysiol*, 17:2236–2246, 1994.

[14] S. Reichelt, J. Fiala, A. Werber, K. Förster, C. Heilmann, R. Klemm, and H. Zappe. Development of an implantable pulse oximeter. *IEEE Trans. on Biomed. Eng.*, 55:581–589, 2008.

[15] K. Kuwana, T. Dohi, Y. Hashimoto, K. Matsumoto, and I. Shimoyama. Implantable telemetry capsule for monitoring arterial oxygen saturation and heartbeat. *30th Annual International IEEE EMBS Conference*, pages 3024–3027, 2008.

[16] D.A. Grosenbaugh, J.O. Alben, and W.W. Muir. Absorbance spectra of interspecies hemoglobins in the visible and near infrared regions. *Acta vet. scand.*, 45:193–200, 2004.

[17] F.H. Martini and J.L. Nath. *Fundamentals of Anatomy and Physiology*. Pearson Education, Inc., 2009.

[18] Pdefer at en.wikipedia. A diagram of the alveoli, both in cross section and externally. [WWW], 2011, [cited on 20. Nov, 2011], Available: `http://upload.wikimedia.org/wikipedia/commons/d/db/Alveoli_diagram.png`.

[19] helix84 at en.wikipedia. Gaseous exchange in the lung. [WWW], 2011, [cited on 20. Nov, 2011], Available: `http://upload.wikimedia.org/wikipedia/commons/8/8b/Alveoli.svg`.

[20] S.A. Clark. Normal oxygen transport. In J. G. Webster, editor, *Design of Pulse Oximeter*, chapter 1, pages 1–12. IOP Publishing Ltd, 1997.

[21] O. Wieben. Light absorbance in pulse oximetry. In J. G. Webster, editor, *Design of Pulse Oximeter*, chapter 4, pages 40–55. IOP Publishing Ltd, 1997.

[22] W.G. Zijlstra, A. Buursma, and M. van der Roest. Absorption spectra of human fetal and adult oxyhemoglobin, de-oxyhemoglobin, carboxyhemoglobin, and methemoglobin. *Clin. Chem.*, 37:1633–1638, 1993.

[23] J. TB Moyle. *Pulse Oximetry*, chapter 2, pages 7–14. BMJ Books, 2002.

[24] J. TB Moyle. *Pulse Oximetry*, chapter 4, pages 35–51. BMJ Books, 2002.

[25] Edwards Lifesciences. Understanding continuous mixed venous oxygen saturation (SvO_2 monitoring with the swan-ganz oximetry td system. [WWW], 2002, [cited on 21. Sept, 2011], Available: `www.edwards.com/products/pacatheters/Pages/svo2edbookpdf.aspx`.

[26] A. Vogel and V. Venugopalan. Mechanisms of pulsed laser ablation of biological tissues. *Chem. Rev.*, 103:577–644, 2003.

[27] A.J. Welch, M.J.C. van Gemert, and W.M. Star. Definitions and overview of tissue optics. In A.J. Welch and M.J.C. van Gemert, editors, *Optical-Thermal Response of Laser-Irradiated Tissue 2nd Edition*, chapter 3, pages 27–64. Springer Science + Business Media B.V., 2011.

[28] A.J. Welch and M.J.C. van Gemert. Definitions and overview of tissue optics. In A.J. Welch and M.J.C. van Gemert, editors, *Optical-Thermal Response of Laser-Irradiated Tissue 2nd Edition*, chapter 1, pages 3–13. Springer Science + Business Media B.V., 2011.

[29] A. Kim and B. C. Wilson. Measurement of ex vivo and in vivo tissue optical properties: Methods and theories. In A.J. Welch and M.J.C. van Gemert, editors, *Optical-Thermal Response of Laser-Irradiated Tissue 2nd Edition*, chapter 8, pages 267–319. Springer Science + Business Media B.V., 2011.

[30] K.H. Shelly. Photoplethysmography: Beyond the calculation of arterial oxygen saturation and heart rate. *Anesthesia and Analgesia*, 105:31–36, 2007.

[31] R. Sarpeshkar. *Ultra Low Power Bioelectronics*, chapter 20, pages 597–601. Cambridge University Press, 2010.

[32] Jeffrie Thomas Fox. Reflectance pulse oximetry sensor for the electronic patch. Master's thesis, Kansas State University, 2008.

[33] J.M. Steinke and A.P Shepherd. Role of light scattering in whole blood oximetry. *IEEE Transaction on Biomedical Engineering*, 33:294–301, 1986.

[34] B. Majaron and J.S. Nelson. Laser treatment of port wine stanes. In A.J. Welch and M.J.C. van Gemert, editors, *Optical-Thermal Response of Laser-Irradiated Tissue 2nd Edition*, chapter 23, pages 859–915. Springer Science + Business Media B.V., 2011.

[35] Y. Mendelson and B.D. Ochs. Noninvasive pulse oximetry utilizing skin reflectance photoplethysmography. *IEEE Trans. on Biomed. Eng.*, 35:798–805, 1988.

[36] J. TB Moyle. *Pulse Oximetry*, chapter 1, pages 1–6. BMJ Books, 2002.

[37] Nellcor veterinarian. [WWW], [cited on 20. Sept, 2011], Available: `http://www.nellcorvet.com/index.html`.

[38] Nonin. Veterinarian solutions. [WWW], 2011, [cited on 20. Sept, 2011], Available: `http://www.nonin.com/Veterinary`.

[39] Smiths Medical. Surgivet. [WWW], 2009, [cited on 20. Sept, 2011], Available: `http://www.surgivet.com/`.

[40] Starr Life Sciences Inc. Mouseox: Non-invasive vital signs monitor for anesthetized and conscious small lab animals. [WWW], 2011, [cited on 20. Sept, 2011], Available at: `http://www.starrlifesciences.com/`.

[41] Kent Scientific. Mousestat:pulse oximeter for mice and rats. [WWW], 2011, [cited on 20. Sept, 2011], Available: `http://www.kentscientific.com/products/productView.asp?productID=6384&Mouse_Rat=Respiratory&Products=MouseSTAT+Pulse+Oximeter+for+Mice+and+Rats`.

[42] Med Associates Inc. Canl-425sv-a standalone pulse oximeter. [WWW], January 3. 2011, [cited on 20. Sept, 2011], Available: `http://www.med-associates.com/pulseOx/oximeter.htm`.

[43] Smiths Medical. Surgivet equipment catalogue (veterinary) 2011. [WWW], 2011, [cited on 20. Sept, 2011], Available: `http://www.surgivet.com/Upload/products/PDF/EQUIPMENT_CATALOG.pdf`.

[44] N.S. Matthews, S. Hartke, and J.C. Allen Jr. An evaluation of pulse oximeters in dogs, cats and horses. *Vet. Anaesthesia and Analgesia*, 30:3–14, 2003.

[45] M.K. Chaffin, N.S. Matthews, and N. Cohen. Evaluation of pulse oximetry and anaesthetised foals using mulitple combinations of transducer type and transducer attachment site. *Eq. Vet. Jrnl.*, 28:437–445, 1996.

[46] B. McGorum, N.E. Robinson, J. Schumacher, and P. Dixon. *Equine Respiratory Medicine and Surgery.* Saunders–Elsevier, Philadelphia–USA, 2007.

[47] J. Coghe, Ch. Uystepruyst, F. Bureau, and R. Lekeux. Non-invasive assessment of arterial haemoglobin oxygen saturation in cattle by pulse oximetry. *Vet. Rec.*, 145:666–669, 1999.

[48] Ch. Uystepruyst, J. Coghe, F. Bureau, and R. Lekeux. Evaluation of accuracy of pulse oximetry in newborn calves. *The Vet. Jrnl.*, 159:71–76, 2000.

[49] C.P. Lau, Y.T. Tai, I.S.F Lee, M. Erickson, and C. Yerich. Utility of an implantable right ventricular oxygen saturation-sensing pacemaker for ambulatory cardiopulmonary monitoring. *Chest*, 107:1089–1094, 1995.

[50] B. Kjellströ, C. Linde, T. Bennett, A. Ohlsson, and L. Ryden. Six years follow-up of an implanted SvO_2 sensor in the right ventricle. *Eur. Jrnl. of Hear. Fail.*, 6:627–634, 2004.

[51] Barbro Kjellström. *The usefulness of continuous hemodynamic monitoring to guide therapy in patients with cardiopulmonary disease*. PhD thesis, Karolinska Institutet, Department of Medicine Cardiology Unit, Karolinska University Hospital, Stockholm , Sweden, 2007.

[52] J.O. Gardosi, M. Carter, and T. Becket. Continous intrapartum monitoring of fetal oxygen saturation. *Lancet*, (Letter):692–693, 1989.

[53] F. Karin, P. Kirkinen, V. König, A. Huch, and R. Huch. Intrapartum reflectance pulse oximetry: effects of sensor location and fixation duration on oxygen saturation readings. *Jrnl. of Clin. Mont.*, 13:299–302, 1997.

[54] FDA. Oxifirst fetal oxygen saturation monitoring system, May 2000.

[55] S. Palreddy. Signal processing algorithms. In J. G. Webster, editor, *Design of Pulse Oximeter*, chapter 9, pages 124–158. IOP Publishing Ltd, 1997.

[56] A. Jubran. Pulse oximetry. *Critical Care*, 3(2):11–17, 1999.

[57] N.S. Trivedi, A.F. Ghouri, N.K. Shah, E. Lai, and S.J.Barker. Effects of motion, ambient light and hypoperfusion on pulse oximeter function. *J. Clin. Anesth.*, 9:179–183, 1997.

[58] A.C.M. Dassel, R. Graaff, M. Sikkema, A. Meijer, W.G. Zijlstra, and J.G. Aarnoudse. Reflectance pulse oximetry at the forehead improves by pressure on the probe. *J. Clin. Monit.*, 11:237–244, 1995.

[59] J.F. Kelleher and R.H. Ruff. Vasomotion-dependent pulse oximeter artifact due to probe malposition. *Anesthesiology*, 71:787–791, 1989.

[60] W.M. Schramm, A. Bartunek, and H. Gilly. Effect of local limb temperature on pulse oximetry and the plethysmographic pulse wave. *Int. J. Clin. Monit. Comput.*, 14:17–22, 1997.

[61] P. Talke and C. Stapelfeldt. Effect of peripheral vasoconstriction on pulse oximetry. *J. Clin. Monit. Comput.*, 20:305–309, 2006.

[62] K.A. Reddy. *Novel Methods for Performance Enhancement of Pulse Oximeters*. PhD thesis, Department of Electrical Engineering, Indian Institute of Technology Madras, India, 2008.

[63] R.R. Fluck Jr., C. Schroeder, G. Frani, B. Kropf, and B. Enbretson. Does ambient light affect the accuracy of pulse oximetry? *Respiratory Care*, 48:677–680, 2003.

[64] T.L. Rusch, R. Sankar, and J.E. Scharf. Signal processing methods for pulse oximetry. *Comput. Biol. Med*, 26:143–159, 1996.

[65] Rasmus G. Haahr. Near infrared spectroscopy : A potential method to detect undifferentiated bovine respiratory disease. Master's thesis, Technical University of Denmark, 2006.

[66] H.J. Brooks and J.S. Hughes. The hemoglobin content of the blood of dairy cattle. *The Journal of Nutrition*, 5:35–58, 1931.

[67] T.J. Divers and S.F. Peek. *Rebhun's Diseases of Dairy Cattle*. Saunders–Elsevier, Missouri–USA, 2008.

[68] R.A. Smith. Impact of disease on feedlot performance: A review. *J. Anim. Sci.*, 76:272–274, 1998.

[69] D. Griffin. Economic impact associated with respiratory disease in beef cattle. *Vet. Clin. of N. Am. Food Anim. Pract.*, 13:367–377, 1997.

[70] NADIS. Knowledge transfer to farmers : Respiratory disease in cattle. [WWW], 2009, [cited on 26. Sept, 2011], Available: `http://www.nadis.org.uk/EEDA/Respiratory%20Disease%20%20in%20Dairy%20and%20Beef%20Rearer%20Units(EEDA).pdf`.

[71] H. Härtel, S. Nikunen, E. Neuvonen, R. Tanskanen, S-L. Kivel, P. Aho, T. Soveri, and H. Saloniemi. Viral and bacterial pathogens in bovine respiratory disease in finland. *The Jrnl. of Vet. Emer. and Crit. Care*, 7:36–42, 1997.

[72] R. Faber, N. Hartwig, W.D. Busby, and R. BreDahl. The costs and predictive factors of bovine respiratory disease in standardized steer tests. A. S. Leaflet R1648. Iowa State Univ. Beef Res. Rep., Abes, IA, 1999.

[73] M.J. Schneider, R.G. Tait Jr., W.D. Busby, and J.M. Reecy. An evalution of bovine respiratory disease complex in feedlot cattle: Impact on performance and carcass traits using treatment records and lung lesion scores. *J. Anim. Sci.*, 87:1821–1827, 2009.

[74] The Dairy Site. Merck introduce BRD prevention treatment. [WWW], 2011, [cited on 27. Sept, 2011], Available: http://www.thedairysite.com/news/35809/merck-introduce-brd-prevention-treatment.

[75] F. V. Theobald. Agricultural zoology , figure 250 (p481). [WWW], 2009, [cited on 27. Sept, 2011], Available: http://www.stirfrycentral.com/line_drawings/theobald_agricultural_zoology/cow_skeleton.html.

[76] R.L.P. van Veen, H.J.C.M. Sterenborg, A. Pifferi, A. Torricelli, and R. Cubeddu. Determination of vis- nir absorption coefficients of mammalian fat, with time- and spatially resolved diffuse reflectance and transmission spectroscopy. *Optical Society of America*, X:X–X, 2000.

[77] R.L.P. van Veen, H.J.C.M. Sterenborg, A. Pifferi, A. Torricelli, and R. Cubeddu. Optical absorption of fat. [WWW], 2011, [cited on 30. Nov, 2011], Available: http://omlc.ogi.edu/spectra/fat/.

[78] A.J. Welch and M.J.C. van Gemert. *Optical-Thermal Response of Laser-Irradiated Tissue 2nd Edition*. Springer Science + Business Media B.V., 2011.

[79] FDA U.S. Food and Drug Administration. Use of international standard iso-10993, 'biological evaluation of medical devices part 1: Evaluation and testing'. [WWW], 2011, [cited on 7. Dec, 2011], Available: http://www.fda.gov/MedicalDevices/DeviceRegulationandGuidance/GuidanceDocuments/ucm080735.htm.

[80] Farlex Inc. The free dictionary : Biocompatability. [WWW], 2011, [cited on 7. Dec, 2011], Available: http://www.thefreedictionary.com/biocompatibility.

[81] X. He, F. Zhang, and X. Zhang. Effects of parylene c layer on high power light emitting diodes. *Applied Surface Science*, 256:6–11, 2009.

[82] Epoxy Technology. Epo-tek 301-2fl technical data sheet. [WWW], 2011, [cited on 24. Oct, 2011], Available: www.epotek.com/sscdocs/datasheets/301-2FL.PDF.

[83] S.Y. Lee, K-I. Park, C. Huh, M. Koo, H.G. Yoo, S. Kim, C.S. Ah, G.Y. Sung, and K.J. Lee. Water-resistant flexible gan led on a liquid crystal polymer substrate for implantable biomedical applications. *Nano Energy*, In Press:X–X, 2011.

[84] FDA U.S. Food and Drug Administration. Draft guidance for industry and fda staff - pulse oximeters - premarket notification submissions [510(k)s]. [WWW], 2011, [cited on 7. Dec, 2011], Available: http://www.fda.gov/MedicalDevices/DeviceRegulationandGuidance/GuidanceDocuments/ucm071361.htm#10c.

[85] S. Franco. *Design with Operational Amplifiers and Analog Integrated Circuits 3rd Ed.* MacGraw-Hill , New York, 2002.

[86] L. Sörnmo and P. Laguna. *Bioelectrical Signal Processing in Cardiac and Neurological Applications.* Elsevier Academic Press, 2005.

[87] M. Tavakoli, L. Turicchia, and R. Sarpeshkar. An ultra-low-power pulse oximeter implemented with an energy-efficient transimpedance amplifier. *IEEE Trans. On Biomed. Circ. and Sys.*, 4:27–38, 2010.

[88] K.S. Paranjape. Electronic instrument control. In J. G. Webster, editor, *Design of Pulse Oximeter*, chapter 8, pages 97–122. IOP Publishing Ltd, 1997.

[89] P.W. Cheung, K. Gauglitz, L.R. Mason, S.J. Prosser, R.E. Smith, D.O. Wagner, and S.W. Hunsaker. Feedback-controlled method and apparatus for processing signals used in oximetry. US patent 4,819,646.

[90] J.M. Goldman, M.T. Petterson, R.J. Kopotic, and S.J. Barker. Masimo signal extraction pulse oximetry. *J. Clin. Monit.*, 16:475–483, 2000.

[91] Nonin. Official homepage. [WWW], 2011, [cited on 27. Sept, 2011], Available: http://www.nonin.com/.

[92] R. Sarpeshkar. *Ultra Low Power Bioelectronics*, chapter 15, pages 385–418. Cambridge University Press, 2010.

[93] Texas Instruments : Burr-Brown. Opa380 : Precision, high-speed transimpedance amplifier. [WWW], 2011, [cited on 20. Oct, 2011], Available: http://www.ti.com/lit/gpn/opa380.

[94] A.S. Sedra and K.C. Smith. *Microelectronic Circuits.* Oxford University Press , New York, 2004.

[95] P. Horowitz and W. Hill. *The Art of Electronics.* Cambridge University Press, 1989.

[96] Advanced Photonics Inc [API]. Gaaias high power ir led emitters (660nm/880nm). [WWW], 2011, [cited on 23. Oct, 2011], Available: http://www.advancedphotonix.com/ap_products/pdfs/PDI-E813.pdf.

[97] Osram. Silicon pin photodiode: in smt and as reverse gullwing [bpw 34, bpw 34 s, bpw 34 s(r18r)]. [WWW], 2011, [cited on 23. Oct, 2011], Available: http://www.farnell.com/datasheets/45577.pdf.

[98] P.D. Mannheimer, J.R. Casciani, M.E. Fein, and S.L. Nierlich. Wavelength selection for low-saturation pulse oximetry. *IEEE Transaction on Biomedical Engineering*, 44:148–158, 1997.

[99] Parylene Engineering. The parylene coating process. [WWW], 2011, [cited on 3. Nov, 2011], Available: http://www.paryleneengineering.com/properties.html.

[100] Marvell Nanofabrication Laboratory. 6.22 parylene deposition system 2010 labcoter 2. [WWW], 2011, [cited on 3. Nov, 2011], Available: http://nanolab.berkeley.edu/labmanual/chap6/6.22parylene.pdf.

[101] Elli Billauer. peakdet: Peak detection using matlab. [WWW], 2011, [cited on 1. Nov, 2011], Available: http://billauer.co.il/peakdet.html.

[102] Fluke Corporation. Fluke 50 series thermometer : Specifications. [WWW], 2011, [cited on 1. Nov, 2011], Available: http://www.fluke.com/Fluke/usen/Electrical-Testers/Thermometers/Fluke-50-Series-II.htm?PID=56085.

[103] Texas Instruments. Msp430f15x, msp430f16x, msp430f161x mixed signal microcontroller datasheet. [WWW], 2011, [cited on 28. Nov, 2011], Available: www.ti.com/lit/ds/symlink/msp430f1611.pdf.

[104] Tektronics. Tps2012, tps2014, tps2024 digital storage oscilloscopes datasheet. [WWW], 2011, [cited on 28. Nov, 2011], Available: http://datasheet.octopart.com/TPS2014-Tektronix-datasheet-19308.pdf.

[105] J.T. Walsh. Basic interactions of light with tissue. In A.J. Welch and M.J.C. van Gemert, editors, *Optical-Thermal Response of Laser-Irradiated Tissue 2nd Edition*, chapter 2, pages 13–26. Springer Science + Business Media B.V., 2011.

A. APPENDIX: MATLAB CODE

Code A.1: *SpO2_algorithm.m*

```
clear all

%load the wanted signal
load signal_1.mat

%clean up the signal, manual decition of which part of the signal we want
%to process, 8 minimas-and-maximas preferred.
y = y(501:2500);
x = x(501:2500);

%Separation of wavelengths, IR and RED are double vectors that show the
%local maxima and minima with indices. You need to set the threshold manually
manual_threshold_1 = 0.001;
[IR,RED] = peakdet(y,manual_threshold_1,x);

%peak and valley (max and min) of each wavelength, again you need to set the
%threshold manually
manual_threshold_2 = 0.01;
[maxIR,minIR] = peakdet(IR(:,2),manual_threshold_2,RED(:,1));
[maxRED,minRED] = peakdet(RED(:,2),manual_threshold_2,RED(:,1));

%partial ratio calculation for equations (2.16) and (2.17)
for n = 1:length(maxIR)-1
    R_IR(n,1) = minIR(n,2)/maxIR(n+1,2); %(2.16)
    R_IR_2(n,1) = maxIR(n+1,2)-minIR(n,2); %(2.17)
end

for n = 1:length(maxRED)-1
    R_RED(n,1) = minRED(n,2)/maxRED(n+1,2); %(2.16)
    R_RED_2(n,1) = maxRED(n+1,2)-minRED(n,2); %(2.17)
end

%equation (2.16)
ROS1 = log(R_RED)./log(R_IR);
%equation (2.13)
SpO2_ROS1 = (0.81-0.20.*ROS1)./(0.73+0.09.*ROS1);
%mean equation (2.13) (8 peaks-and-valley)
mSpO2_ROS1 = mean(SpO2_ROS1)
%standard deviation of equation (2.13)
std_ROS1 = std(SpO2_ROS1)

%DC extraction
DC_IR = mean(IR(:,2));
DC_RED = mean(RED(:,2));
```

```
%ratio calculation according to equation (2.17)
ROS2 = (R_RED_2./DC_RED)./(R_IR_2./DC_RED);
%equation (2.13)
SpO2_ROS2 =  (0.81-0.20.*ROS2)./(0.73+0.09.*ROS2);
%mean estimation (2.13) (8 peaks-and-valley)
mSpO2_ROS2 = mean(SpO2_ROS2)
%standard deviation of equation (2.13)
std_ROS2 = std(SpO2_ROS2)
```

Code A.2: *peakdet.m*

```
function [maxtab, mintab]=peakdet(v, delta, x)
%PEAKDET Detect peaks in a vector
%        [MAXTAB, MINTAB] = PEAKDET(V, DELTA) finds the local
%        maxima and minima ("peaks") in the vector V.
%        MAXTAB and MINTAB consists of two columns. Column 1
%        contains indices in V, and column 2 the found values.
%
%        With [MAXTAB, MINTAB] = PEAKDET(V, DELTA, X) the indices
%        in MAXTAB and MINTAB are replaced with the corresponding
%        X-values.
%
%        A point is considered a maximum peak if it has the maximal
%        value, and was preceded (to the left) by a value lower by
%        DELTA.

% Eli Billauer, 3.4.05 (Explicitly not copyrighted).
% This function is released to the public domain; Any use is allowed.

maxtab = [];
mintab = [];

v = v(:); % Just in case this wasn't a proper vector

if nargin < 3
  x = (1:length(v))';
else
  x = x(:);
  if length(v)~= length(x)
    error('Input vectors v and x must have same length');
  end
end

if (length(delta(:)))>1
  error('Input argument DELTA must be a scalar');
end

if delta <= 0
  error('Input argument DELTA must be positive');
end

mn = Inf; mx = -Inf;
mnpos = NaN; mxpos = NaN;

lookformax = 1;

for i=1:length(v)
```

```
  this = v(i);
  if this > mx, mx = this; mxpos = x(i); end
  if this < mn, mn = this; mnpos = x(i); end

  if lookformax
    if this < mx-delta
      maxtab = [maxtab ; mxpos mx];
      mn = this; mnpos = x(i);
      lookformax = 0;
    end
  else
    if this > mn+delta
      mintab = [mintab ; mnpos mn];
      mx = this; mxpos = x(i);
      lookformax = 1;
    end
  end
end
```

B. APPENDIX: SCHEMATICS OF THE DEVICE